Development and Investigation of Optical Frequency Combs for Photonic Communication Systems

Maria Deseada Gutierrez Pascual

B.Eng., M.Eng.

A dissertation submitted in fulfilment of the
requirements for the award of
Doctor of Philosophy (Ph.D.)

School of Electronic Engineering

Faculty of Engineering and Computing

Dublin City University

Supervisor: Prof. Liam P. Barry

External Supervisor: Dr. Frank Smyth

September 2017

Declaration

I hereby certify that this material, which I now submit for assessment on the programme of study leading to the award of Doctor of Philosophy is entirely my own work, and that I have exercised reasonable care to ensure that the work is original, and does not to the best of my knowledge breach any law of copyright, and has not been taken from the work of others save and to the extent that such work has been cited and acknowledged within the text of my work.

Signed:

ID No.: 13210743

Date:

To my parents, sister

and Juan.

The most difficult thing is the decision to act, the rest is merely tenacity. –Amelia Earhart

Acknowledgements

I would like to use this opportunity to express my gratitude to everyone who contributed and helped me throughout the last four years of this research. Without their precious support it would not have been possible to conduct this research. Firstly, I would like to thank my supervisor Prof. Liam Barry for giving me the opportunity to pursue a PhD in his research group and for his expert knowledge and continuous suggestions. His valuable kindness and guidance helped me so much in all the time of research and writing of this thesis.

I would like to thank Professor Camille Sophie-Bres and Dr. Conor Brennan for the affable conversation during the defence and for their knowledgeable reviews and comments that have substantially improved this work.

I will be always indebted to Pilot Photonics, where I have the pleasure of working, and specially to Dr. Philip Perry and Dr. Frank Smyth who first hired me and helped me at the early stages of my professional career. My deepest appreciation goes to Dr. Frank Smyth who has been an exceptional mentor in many aspects of my life. His inspiring enthusiasm, loving understanding, trust and advices have encouraged me even during the most challenging parts of the industrial PhD. Jules Braddell deserves my sincere gratitude for his insightful knowledge and ideas. He has deeply contributed to this work with novel device designs and by teaching me outstanding research skills, which made possible a big part of the research outcomes. I would also like to acknowledge Gaurav Jain and other colleagues for the precious time and support.

A special thanks and dedication goes to Dr. Prince Anandarajah for his immense help and support through the Viva preparation and for his friendship, constant help and encouragement since the first day I walked into the lab. Thanks to Dr. Rui Zhou for his patient guidance, lab mentorship and training, and time for scientific and non-scientific discussions alike; My appreciation also extends to Dr. Vidak Vujicic for his kind help, and valuable time and assistance in experiments, who made the last part of this research so enjoyable, and to Dr. Sean O'Duill for the help provided and theoretical discussions during the Viva preparation. I would also like to thank other colleagues, past and present, from the Radio and Optical Communications Lab, who made the lab such a fantastic place to work and with whom I shared so many laughs over a couple of pints: Fernando, Colm, Eamonn, Arsalan, Aravind, Tam, Tong, Sepideh, Anthony, Jingyan, Regan, John and Kai.

Thanks to all friends I met in Dublin and my loved ones in Malaga, Anita, Silvi, Fran and Samu, who gave me so much needed great social reunions, trips and parties, and always were there helping me to keep a perspective on things.

I would like to express my heart-felt gratitude this work to my parents and sister for their love and encouragement throughout my entire life and for their effort in facilitating my education. They always believed in me and my decisions and without them, none of this would indeed be possible. Lastly, I would like to thank Juan, my partner and best friend, for your unconditional support and love when it is most needed. I cannot wait to see what the future holds for us.

This PhD could not have been possible without you, I'll always be thankful to all.

Contents

Development and Investigation of Optical Frequency Combs for Photonic Communication Systems

Maria Deseada Gutierrez Pascual

Abstract

Data traffic has dramatically increased over the last decades driven by emerging media-rich applications and services, essential for the modern information society. Wavelength Division Multiplexing (WDM) effectively enabled a continual scaling of fibre optical network capacities. Nevertheless, the relentless global traffic growth shows no sign of abating, and forces optical transport networks to evolve towards higher capacities, performance and flexibility to keep meeting the demand for bandwidth.

Advanced modulation formats and multicarrier modulation techniques, such as Nyquist WDM and all optical Orthogonal Frequency Division Multiplexing (OFDM), allow capacity scaling and improved spectral efficiency by encoding information in the optical carrier amplitude, phase and polarization and by minimizing spectral guards between neighbouring channels. The implementation of these techniques, however, imposes stringent requirements on the multi-carrier optical sources in the transmitters, in terms of wavelength stability, good noise properties and cost efficiency. Optical frequency comb sources are key candidates that simultaneously generate multiple phase correlated optical carriers with a stable and constant frequency separation.

This thesis is focused on externally injected gain switched optical frequency comb sources (GS-OFCS). Several advances on the state of the art of these GS-OFCS are presented that further enhance their potential for network deployment. Firstly, a highly flexible GS-OFCS that can be software reconfigured is proposed and fully characterized for flexible optical networks. Secondly, two novel configurations are experimentally demonstrated for broadband GS-OFCS generation, thus, expanding their bandwidth coverage. Thirdly, this work also studies the need for the de-multiplexing of comb sources and, in order to yield further compactness and cost-efficiency, a detailed characterization of two photonic integrated devices for GS-OFCS generation and de-multiplexing is reported. Finally, the integrated GS-OFCS is implemented into two spectrally efficient transmission systems employing multi-level amplitude and phase modulation formats, which prove the quality and relevancy of these integrated devices for future optical networks.

List of Figures

List of Acronyms

AMZI	Asymmetric Mach-Zehnder interferometers
ASE	Amplified Spontaneous Emission
AWG	Arrayed Waveguide Grating
B2B	Back-To-Back
BER	Bit Error Rate
CBCPW	Conductor-Backed Coplanar Waveguide
CW	Continuous Wave
DAC	Digital-to-Analog-Converter
DMLD	Discrete Mode Laser Diodes
DSF	Dispersion-Shifted Fibres
DSH	Delayed Self-Heterodyne
DWDM	Dense WDM
ECL	External Cavity Laser
EDFA	Erbium Doped Fibre Amplifier
ESA	Electrical Spectrum Analyzer
EVM	Error-Vector Magnitude
FEC	Forward Error Correction
FM	Frequency Modulated
FP	Fabry-Pérot
FSR	Free Spectral Range
FTTX	Fibre-To-The-X
FWHM	Full Width at Half Maximum
FWM	Four-Wave Mixing
GS-OFCS	Gain Switched Optical Frequency Comb Source

HDTV	High Definition Television
HNLF	Highly Non-Linear Fibre
InP	Indium Phosphide
ISI	inter-symbol interference
ISO	isolator
ITU	International Telecommunication Union
LO	Local Oscillator
LPF	Low-Pass Filter
MLLs	Mode-locked lasers
MMI	Multi-Mode Interference
MZM	Mach-Zehnder Modulator
OBPF	Optical Band Pass Filter
OCNR	Optical Carrier to Noise Ratio
OFCS	Optical Frequency Comb Source
OFCSs	Optical Frequency Comb Sources
OFDM	Orthogonal Frequency Division Multiplexing
OOK	On/Off Keying
OSA	Optical Spectrum Analyser
OSNR	Optical Signal-to-Noise Ratio
PAM	Pulse Amplitude Modulation
PC	Polarization Controller
PD	Photodetector
PIC	Photonic Integrated Circuit
PLL	Phase-Locked Loop
PM	Polarization Division Multiplexing
PON	Passive Optical Network
PSK	Phase Shift Keying
QAM	Quadrature Amplitude Modulation
QPSK	Quadrature PSK
RF	Radio frequency

RIN	Relative Intensity Noise
RTO	Real Time Oscilloscope
SMSR	Side-Mode-Suppression Ratio
SOH	Silicon-Organic Hybrid
SSMF	Standard Single Mode Fibre
TEC	Thermoelectric Cooler
TL	Tunable Laser
VOA	Variable Optical Attenuator
WDM	Wavelength Division Multiplexing
WSS	Wavelength Selective Switch

Introduction

Wavelength Division Multiplexing (WDM) has successfully scaled the capacity of commercial optical systems during the last 30 years. However, the demand for optical bandwidth continues to grow at a rapid pace due to the appearance of new bandwidth-hungry services and applications such as cloud storage, high definition video entertainment or online gaming, and with the upcoming *Internet of things*, where a plethora of devices will become inter-connected, the data traffic is only expected to increase exponentially.

As such, high speed optical communication links are evolving towards the use of flexible and highly spectrally efficient techniques to provide increased data throughput, by using available resources more efficiently, and to facilitate network adaptability according to dynamic traffic patterns. These techniques include higher order modulation formats that allows multi-level encoding of the optical carriers, and multicarrier modulation techniques, such as Nyquist WDM and all optical Orthogonal Frequency Division Multiplexing (OFDM) where optical channels are tightly packed and, consequently, the overall bandwidth minimized and spectrally efficiency optimised.

Optical frequency combs sources (OFCS) have recently attracted much interest for next generation spectrally efficient and flexible optical transceivers. OFCS simultaneously generate multiple phase correlated optical carriers offering low complexity by replacing multiple independent lasers with a single subsystem. Therefore, OFCS can enable a superior spectral efficiency as they allow the reduction or elimination of guard bands in advanced multicarrier modulation techniques by featuring fixed frequency spacing between the carriers, avoiding drifts and interferences of the individual wavelengths over time.

Next generation optical networks would substantially benefit from an optical frequency comb technology with potential for photonic integration, that could additionally exhibit good inherent properties such as low optical linewidth and Relative Intensity Noise (RIN), and large Optical Carrier to Noise Ratio (OCNR) for the use of advanced modulation formats, and Free Spectral Range (FSR)

and central wavelength flexibility to accommodate dynamic baud rate adaptation and spectrum allocation according to traffic conditions and network resources.

This thesis studies externally injected gain switched optical frequency combs as they present remarkable simplicity, noise properties and stability. Several key advances in the state of the art of this technology were accomplished with the focus of enhancing the feasibility and practicality of the proposed comb technique in future flexible and spectrally efficient networks.

Main contributions

The main contributions of this work can be outlined as follows:

- The generation and characterisation of a software reconfigurable optical frequency comb prototype based on optical injection and gain switching techniques. The notable advantages of this source include simplicity, stability, low intensity and phase noise, and remarkable flexibility with continuous FSR and central wavelength tunability which can be both dynamically controlled according to traffic and network conditions.
- The investigation of bandwidth expansion techniques for flexible, externally injected gain switched comb sources. The two proposed methods are experimentally demonstrated to generate wider bandwidth optical frequency combs that preserve a strong phase correlation between comb tones, low optical linewidth, and continuous wavelength tunability. Both expansion techniques are compared and a trade-off between complexity and obtained spectral flatness is discussed.
- The testing and performance demonstration of a four-output monolithically integrated comb de-multiplexer, based on the optical injection locking of single mode semiconductor lasers, for phase-correlated comb tone separation. The four outputs from the de-multiplexer select an individual comb tone with a suppression of adjacent comb tones larger than 37 dB. Furthermore, the use of this de-multiplexer does not reduce the comb tone power, avoiding the need for optical amplifiers.
- The comb generation and detailed characterisation of a novel integrated externally injected, gain switched optical frequency comb device. The obtained frequency comb exhibits a flexible FSR ranging from 6 to 10 GHz, with a high OCNR larger than 46 dB. The noise properties of interest for optical communications were characterized, which include a RIN of -125 dB/Hz, an optical linewidth of 1.5 MHz and a strong phase correlation between the comb lines.

- The first demonstrations of the novel photonic integrated gain switched comb source in a 4-level Pulse Amplitude Modulation (PAM), and in a Nyquist-Quadrature Phase Shift Keying (PSK) (QPSK) optical transmission system. Successful experimental transmissions of a 50 Gbit/s PAM-4 signal over 3 km of Standard Single Mode Fibre (SSMF) suitable for intra-datacentre application, and of a 80 Gbit/s Nyquist-QPSK signal over 50 km of SSMF for inter-datecentre scenario, are demonstrated with performances below the 7% Forward Error Correction (FEC) limit for all the sub-channels.

Thesis structure

This thesis is structured as follows:

Chapter 1 describes the evolution of optical communications networks as well as the reasons for their continued growth in capacity today. The challenges that the next generation of optical networks faces are outlined and capacity scaling approaches are discussed, with particular attention to advanced modulation formats, and multicarrier modulation techniques that enable greater network capacities by improving the spectral efficiency. Finally, optical frequency comb sources are introduced as a key enabling technology for future optical communication transmitters and their motivation is discussed.

Chapter 2 provides a detailed overview and comparison of the main technologies for optical frequency comb generation which include mode-locking, Kerr-effect in microresonators, parametric processes, electro-optic modulation and gain switching. The working principle and typical configurations of these comb sources are presented, as well as inherent characteristics of each individual technology (FSR and wavelength tunability, optical linewidth, RIN, OCNR, complexity, power per line, etc.). To conclude, gain switching is chosen as the comb generation technique of study in this thesis.

Chapter 3 introduces the concept of flexible networks and presents the initial experimental outcome of this thesis: the development and generation of a software reconfigurable gain switched optical frequency comb. The flexible features, which include dynamic and continuous configuration of FSR and central wavelength, and noise properties of the source are examined in detail.

Chapter 4 focuses on the bandwidth expansion of gain switched optical frequency combs, which typically offer relatively narrow optical bandwiths compared to other comb generation techniques. This restraint may prevent their use in optical networks and thus, two novel techniques are proposed in this chapter and experimentally demonstrated. The spectral bandwidth, flexibilities, and

noise properties that include optical linewidth and phase correlation of the obtained expanded gain switched combs are analysed.

Chapter 5 examines the importance of photonic integration for future optical networks. Two novel photonic integrated devices for gain switched comb generation and comb de-multiplexing are subject to detailed characterisation which are described in this chapter. The experimental implementation of the integrated comb source in a PAM-4 and in a Nyquist-QPSK transmission system is also demonstrated to analyse the influence of RIN, OCNR and phase noise from the device.

Chapter 6 concludes the thesis with a brief summary of the research and highlights the main contributions of this study. Finally, some future research lines are also proposed and discussed.

Chapter 1

Optical Fiber Communications

Optical fibre communication systems revolutionized the telecommunications industry by enabling true long-haul and high capacity transmissions that facilitated the development of the Internet, and clearly shaped the way we live, work, do business, and interact.

Optical communication systems use lightwave signals (in the THz frequencies) typically generated from semiconductor lasers to carry data and employ optical fibres, which present low attenuation, huge bandwidth and low electromagnetic interference, for transmission. These systems have been successfully implemented in the network since the 1980s, remarkably evolving in capacity growth and cost reduction to keep satisfying the demand for bandwidth.

This chapter gives an introduction to the current status of optical fibre communications networks and systems. It presents a historical overview of the main technological breakthroughs that consolidated their relevance and pushed their expansion. The late challenges that the next generation of optical networks faces due to the ever-increasing traffic demand, are then outlined. Finally, novel spectrally efficient techniques to enable greater network capacities are detailed and the motivation behind optical frequency comb sources is discussed.

1.1 Optical Network Topology

The current optical network is a complicated system consisting of interconnected sub-networks that ensure robust exchange of information throughout the world. The illustration of the general network

topology is illustrated in Figure 1.1. The optical network is usually divided into core (long-haul), metropolitan (metro) and access networks according to their geographical extension, functionality and requirements [1].

Optical fibre communications have certainly dominated the core and metro network segments for a relatively long time, and more recently has started its expansion to the access network segment as well. An incessant growth in traffic is revolutionizing optical communications and forcing a transformation throughout the optical network towards reconfigurability, higher performance and reduced power consumption.

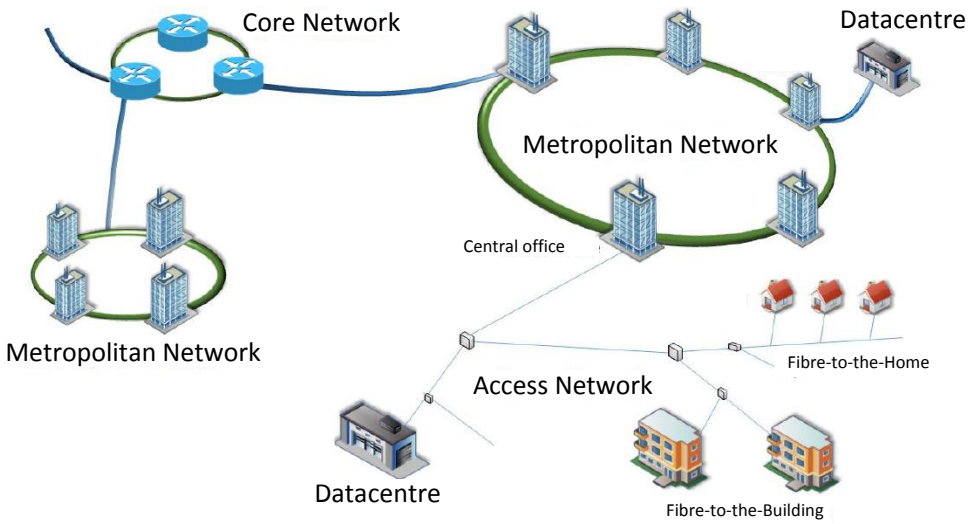

Figure 1.1: Optical Network Topology including core, metropolitan, access and datacentre networks. After: [2]

1.1.1 Core Networks

The core network is the backbone of global communications systems. It connects continents and countries, covering distances of hundreds and thousands of kilometres through terrestrial or submarine fibres. These networks concentrate millions of users and transport large amounts of aggregated data, thus, their long-haul links and systems require reliable technologies that allow ultra-high capacity and robust long distance communications even at a high cost.

1.1.2 Metro Networks

Metro networks interconnect core networks and access networks which connect to the end user. They typically span from tens up to a few hundred of kilometres. As data traffic increases, metro networks must also be upgraded to support the demand for bandwidth from users in the access network. Hence, currently deployed metro networks are evolving towards spectrally efficient 100 Gb/s data rates enabled by coherent reception and will soon require innovative technologies while keeping implementation costs down.

1.1.3 Access Networks

The access network connects the end users to the rest of the network, typically covering distances from a few hundred meters up to a few kilometres. The bit rates involved in access networks are not very high, but they present important technical challenges due to the non-uniform distribution of users. Service providers are currently commercializing the Fibre-To-The-X (FTTX) where *X* refers to the last point where fibre is deployed (cabinet, home, building, etc). Since the access part of the network is costly to deploy, Passive Optical Network (PON) with a cost-efficient tree-like point to multipoint distribution is the dominant approach.

1.1.4 Datacentres

Emerging cloud applications such as mobile devices interconnectivity, with data backup and synchronization, remote desktop, cloud computing, etc. require more traffic being delivered between datacentres.

Lately, significant research efforts are being made in the development of intra-datacentre networks [3]. Datacentres host a number of servers and short fibre links of up to a couple of kilometres are needed. These intra-datacentre systems require high throughput, reduced size of modules, low cost, power consumption and latency. On the other hand, communication links between datacentres, also known as inter-datacentre communications, are performed mainly within metro networks and in some cases, through long haul transport links.

1.2 Evolution of Optical Fibre Communication Systems

During the latter half of the twentieth century, major technological breakthroughs resulted in the development of optical fibre communication systems. The invention of the laser in 1960 [4] followed by the first proposed optical fibre in 1966 [5], primarily drove the research towards low-loss materials for feasible optical fibre transmission. In 1970, Corning Glass Works (now Corning Inc.) achieved and started to manufacture the first optical fibres with an acceptable low-loss of 17 dB/km [6] that, combined with advances in semiconductor laser technology [7], made optical communications practically possible.

Over the next 30 years, there would be extraordinary developments in the manufacturing of optical fibres and lasers that would dramatically boost the transmission capacity and consolidate optical communications as a superior emerging technology over electrical transmission.

1.2.1 Early history

The evolution of optical fibre communications can be divided into several distinct generations that are directly related to these technological innovations and to the resultant increase in the bit rate, B, and transmission distance, L, as illustrated by Figure 1.2.

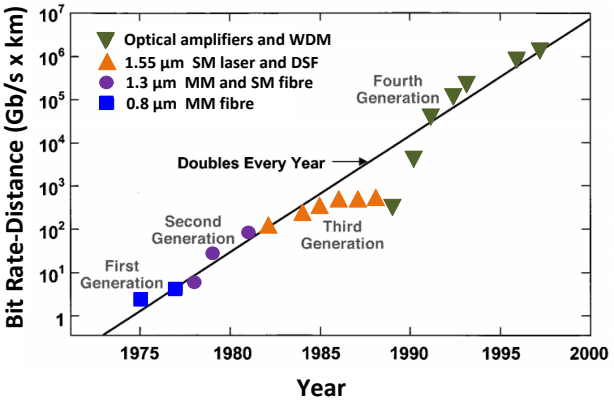

Figure 1.2: Evolution of $B \cdot L$ product over the period 1975 to 2000 through several generations of optical communication links. Each generation with the correspondent technological breakthrough is represented by a symbol. MM: Multi-Mode fibre, SM: Single-Mode fibre, DSF:dispersion-shifted fibre, WDM: Wavelength Division Multiplexing. After: [8]

The first generation of optical systems operated in the 0.8 µm wavelength region and utilized mul-

timode optical fibres. Such systems became commercially available in 1980 [9] and transmitted 45 Mb/s with repeater spacings of up to 10 km, compared to 1 km spacing of the contemporaneous coaxial systems. During the second generation the focus was to increase the $B \cdot L$ product by shifting the operating wavelength towards 1.3 μm where the attenuation in fibres is below 1 dB/km. The first systems were developed in multimode fibres and limited by dispersion. Rapidly, single mode fibres that exhibit minimal dispersion at 1.3 μm were implemented and by 1981, a transmission of 2 Gb/s over 44 km of single mode fibre was demonstrated [10]. Consequently, single mode fibre (at 1.3 μm and later at 1.55 μm wavelength) became the standard fibre for long distance systems where large $B \cdot L$ is required. In 1987, commercial systems at 1.3 μm became available and the first optical transatlantic fibre, TAT-8, was deployed [11]. The third generation intended to use wavelengths around 1.55 μm where the fibre losses are lower, namely 0.2 dB/km. Nevertheless, optical fibres also present a larger dispersion at this wavelength range. Two alternative approaches were developed to overcome the dispersion impediment: the use of single longitudinal mode lasers and Dispersion-Shifted Fibres (DSF), specially designed to have minimum dispersion near 1.55 μm. Transmissions of up to 4 Gb/s over 100 km were first demonstrated in 1985 [12] and commercially deployed in 1990. As illustrated by Figure 1.2, these three generations resulted in a gradual increase of the bit rate and transmission distances.

The major revolution, however, took place during the fourth generation where the capacity of optical communication systems saw explosive growth [13] that resulted in a $B \cdot L$ doubling every year, as depicted in Figure 1.2. This was driven by the emergence of optical amplifiers and a technique defined as Wavelength Division Multiplexing (WDM), explained in detail in the next section due to their importance. These technological developments were mainly driven by the commercial deployment of the Internet and the resultant intensified demand for long-distance transmission capacity. Consequently, optical communications gained enormous attention as a prosperous business and substantially fostered the *Information Age*.

1.2.2 Information Age and Wavelength Division Multiplexing

The introduction of optical amplifiers, specifically the Erbium Doped Fibre Amplifier (EDFA), in the early 1990s resulted in extended all-optical transmission distances [14], [15]. EDFAs compensate for the signal attenuation due to fibre propagation, increasing the spacing between repeaters or, in some systems, their elimination. However, the advent of personal computers and the Internet evolution from a text to a multimedia platform drove a rapid traffic growth that also required higher

bit rates.

WDM was the key technology that facilitated the development of high bandwidth communications by scaling the capacity transmission in frequency. WDM uses multiple wavelengths to transmit data, where each wavelength represents an individual channel. As illustrated in Figure 1.3, each channel comprises a single mode laser source that generates an optical signal where the information is encoded, in this Figure through external modulation. These channels are combined together for transmission over a single optical fibre. The frequency separation between two adjacent wavelengths in WDM is known as the channel spacing and typically accounts for the information bandwidth and guard bands, that are unused parts of the spectrum between channels for the purpose of preventing interference. Current deployed WDM systems typically operate at a 50 GHz grid spacing, standardised by the International Telecommunication Union (ITU) [16] and referred to as Dense WDM (DWDM). During transmission, the multiplexed signal can be amplified via EDFAs, and individual optical channels can be inserted or removed from the network as desired, using optical add-drop multiplexers. At the receiver side, the optical signal is demultiplexed into individual channels, distributed to the intended destination where the optical signal is photodetected and the data recovered.

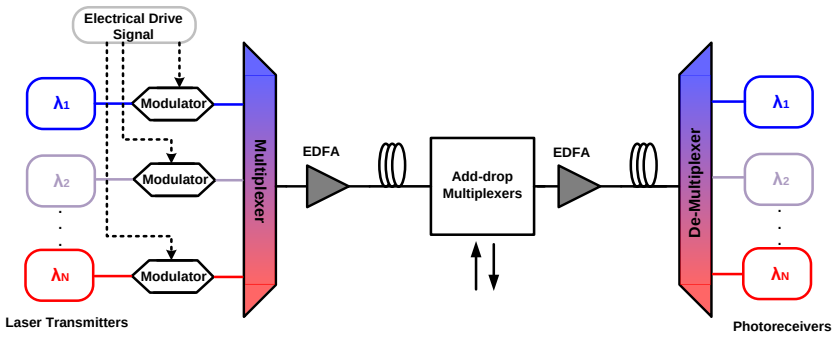

Figure 1.3: Generic WDM architecture.

WDM was mainly enabled by the development of EDFAs that allow simultaneous amplification of all WDM optical channels and compensation for losses in multiplexers, de-multiplexers and during fibre transmission. The utilization of numerous wavelengths, as opposed to the exclusive use of the 1550 nm wavelength, allows bi-directional data transfer through one fibre, and increased system capacities maintaining mature low speed electronics. In 1995 the first commercial WDM system was deployed with a total bandwidth transmission of 20 Gb/s consisting of 8 WDM channels at a bit rate of 2.5 Gb/s [17], and a regenerator span of 360 km. In 1996, research experiments proved

an overall transmission of 1 Tb/s [18] (55 WDM channels at 20 Gb/s) over 150 km [19].

Since the first WDM system implementations, technology developments allowed the channel count and the bit rate per WDM channel to continually increase, from 2.5 to 100 Gb/s per wavelength [18] with a total number of 80 channels (separated by a channel spacing of 50 GHz), thus boosting the overall capacity over a fibre. The combination of both technological breakthroughs, EDFAs and WDM, certainly boosted the $B \cdot L$ product and facilitated long-haul systems with potential for further scalability.

1.2.3 State of the art: Towards 100 Gb/s and Beyond

Figure 1.4 shows the global Internet traffic for 1990-2015 estimated by Cisco Systems [20], along with their forecast for the period between 2016 and 2020 [21]. Although the Internet traffic growth rate has decelerated compared to the previous decade, it remains robust at an intensive 23 % increase per year largely driven by the emergence of smart Internet-connected devices, and bandwidth-hungry services and applications, such as on-demand High Definition Television (HDTV), cloud storage and high quality online games.

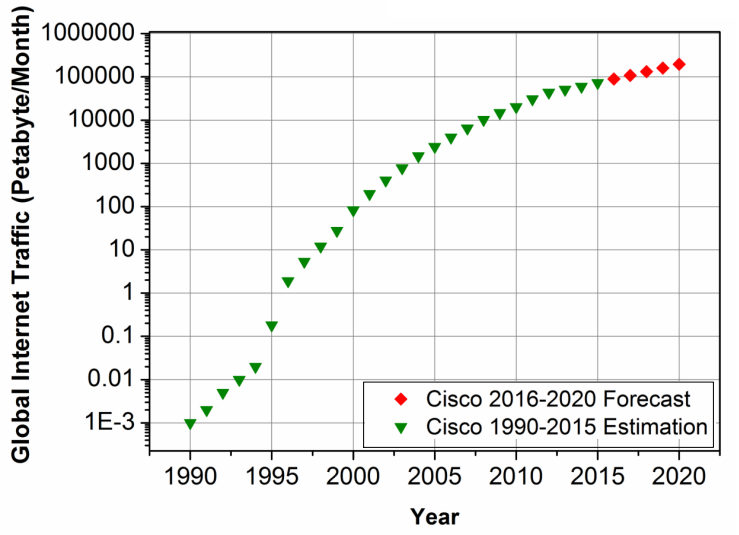

Figure 1.4: Global Internet traffic growth for period 1990-2020.

The capacity growth of commercial optical systems, enabled by WDM, exceeded the requirements of network bandwidth during the first decade. However, as the Internet traffic keeps growing exponentially and the technology matures, it becomes more difficult to increase the systems capac-

ity [22]. In fact, some studies have concluded that the network traffic will grow 10 times faster than current systems capacity over the next decade [23]. In order to satisfy the ever-increasing demand for bandwidth, optical networks must evolve towards higher performance and spectral efficiency, and reduced power consumption [24].

Novel scaling techniques, that are being introduced progressively by the industry, are focusing on improving the spectral efficiency by two main scaling methods: increasing the data rate per optical channel, and reducing the channel spacing which implies a larger number of usable channels. The spectral efficiency is the information rate that can be transmitted over a given bandwidth or channel spacing and it is measured as the ratio *Bit Rate/Channel Spacing* in (bit/s)/Hz. It indicates how efficiently the available fibre bandwidth is being utilised. WDM systems with 10 Gb/s per channel, spaced by 50 GHz, presented a spectral efficiency of 0.2 (bit/s)/Hz.

The first step towards high spectral efficient systems was the implementation of coherent optical communications where higher-order modulation formats are used to increase the data rate per optical channel. Early commercial WDM systems employed, with a high degree of success, a 2 level amplitude modulation format referred to as On/Off Keying (OOK). Even though the possibility of practical implementation of 40 Gb/s OOK systems was demonstrated [25], as data rates are required to exceed 10 Gb/s per channel, this modulation format presents dispersion impairments that can be prohibitive [26] and its spectral efficiency is limited for further scaling. On the other hand, advanced modulation formats, explained in detail in section 1.3, can modulate the amplitude and phase components of both linear polarisations of the optical signal. Therefore, more information can be transmitted when these three parameters are modulated and the spectral efficiency can be at least quadrupled, compared to OOK systems.

The initial introduction of coherent communications allowed 40 Gb/s per channel [27] and a spectral efficiency of 0.8 (bit/s)/Hz. As shown in Figure 1.5, 40 Gb/s has been soon followed in the industry by 100 Gb/s per channel [28] that is able to run at the same 50 GHz channel spacing as 10 Gb/s systems but provides a 10X higher spectral efficiency, namely 2 (bit/s)/Hz.

While commercial coherent 100 Gb/s systems are currently being deployed in long-haul links, research and industry are already moving forward and considering a new spectrally efficient approach for next generation optical transport networks with higher-speed per channel (i.e. 400 Gb/s and 1 Tb/s): the coherent superchannel [29], [30].

A superchannel is an adaptation of DWDM where multiple optical carriers (or sub-channels) are

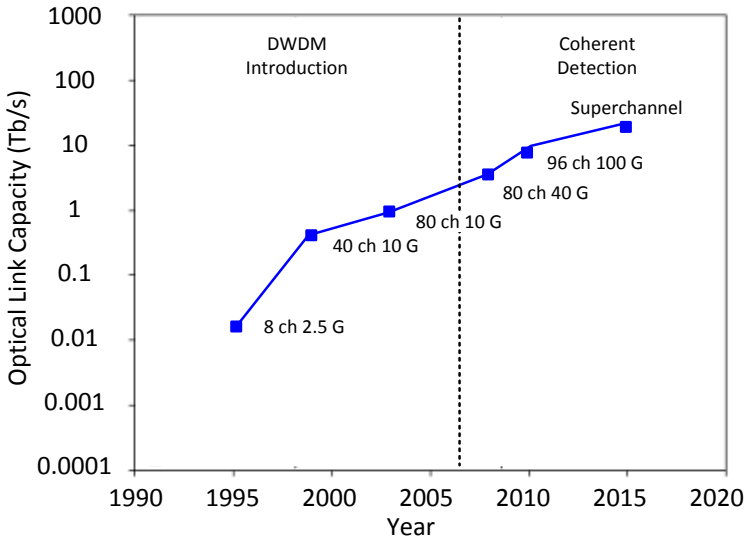

Figure 1.5: Technology roadmap of fibre link capacity in commercial networks. After: [31]

combined to create an aggregated and unified high data rate channel. Therefore, superchannels are multi-wavelength signals that further maximize the spectral efficiency and throughput of installed optical fibres by minimizing the frequency spacing between sub-channels and even eliminating guard bands.

At the time of this writing, research studies have demonstrated superchannel transmissions with spectral efficiencies of up to 8.67 (bit/s)/Hz [32] and claim a possible overall bit rate of 40 Tb/s over 1000 km links when using the total bandwidth of a single optical fibre, which results in a $B \cdot L$ product of 40,000 (Tb/s)·km. Commercial superchannel field trials have also recently started and shown a real-time 2 Tb/s superchannel transport over 727 km [33].

1.3 Advanced Modulation Formats

In optical communications, signal modulation is achieved by imposing the information data on the amplitude, wavelength, phase or polarization of a laser lightwave.

The electric field at the output of a monochromatic laser can be expressed as:

$$E(t) = A(t) \cdot e^{j(w_0 t + \phi(t))} = A(t) \cdot e^{j\phi(t)} \cdot e^{jw_0 t} \tag{1.1}$$

where A is the amplitude, w_0 is the angular frequency and ϕ the phase of the electric field. As observed in Equation 1.1, the amplitude and phase of the complex optical signal could be represented as a phasor. The real and imaginary components of this phasor are also referred to as the In-phase (I) and the Quadrature (Q) components. Thus, amplitude and phase modulations can be represented in an IQ constellation diagram, as depicted in Figure 1.6. The vectorial length from the origin to each of the points of the constellation diagram (symbols) relates to the amplitude of the electric field with the angular component representing the phase. Hence, the IQ plane shows the baseband I and Q signals required to produce the modulated signal.

Conventional optical systems use a remarkably simple and effective 2-level form of intensity modulation: OOK. It consists on turning the laser light on and off to represent a binary 1 or 0, respectively. Due to its simplicity, OOK has been used with data rates up to 10 Gb/s in the entire optical industry for decades. The constellation diagram of OOK presents a symbol at the origin with a zero amplitude, while a second symbol is found at the amplitude of the E-field on the I-axis, indicating that the phase is not changed, as depicted in Figure 1.6 (a). For OOK, the bit rate and symbol rate (or baud rate) are the same since one optical symbol represents only one bit.

Advanced modulation formats allow the number of bits encoded per symbol to be increased. As such, larger information transmissions are achieved with the same symbol (baud) rate, resulting in an enhanced spectral efficiency. The simplest way to do this is to transmit multiple bits per symbol using multilevel amplitude modulation. 4-level Pulse Amplitude Modulation (PAM) is a modulation technique that has been recently attracting a lot of attention whereby 4 distinct pulse amplitudes are used to convey the information. The transmission of four amplitudes allows the encoding of 2 bits of binary data per symbol and thus, PAM-4 enables twice the transmission capacity in comparison to OOK systems. PAM-4 is currently being considered a promising solution for short intra-datacentre links, mainly due to its implementation simplicity, cost-effectiveness and low power consumption [34], [35].

Quadrature Phase Shift Keying (PSK) (QPSK) is a form of phase modulation, where the phase of the laser optical light is used for encoding data. The constellation formed by four symbols is shown in Figure 1.6 (c). Each symbol, or constellation point, corresponds to a discrete phase value that will be imposed on the optical carrier, but maintains the same amplitude. The transmission of four phases also enables the encoding of 2 bits of binary data per symbol. Consequently, QPSK doubles the bit rate transmitted by OOK in the same bandwidth, obtaining a doubling of the spectral efficiency. For any modulation format the relationship between the number of available symbols,

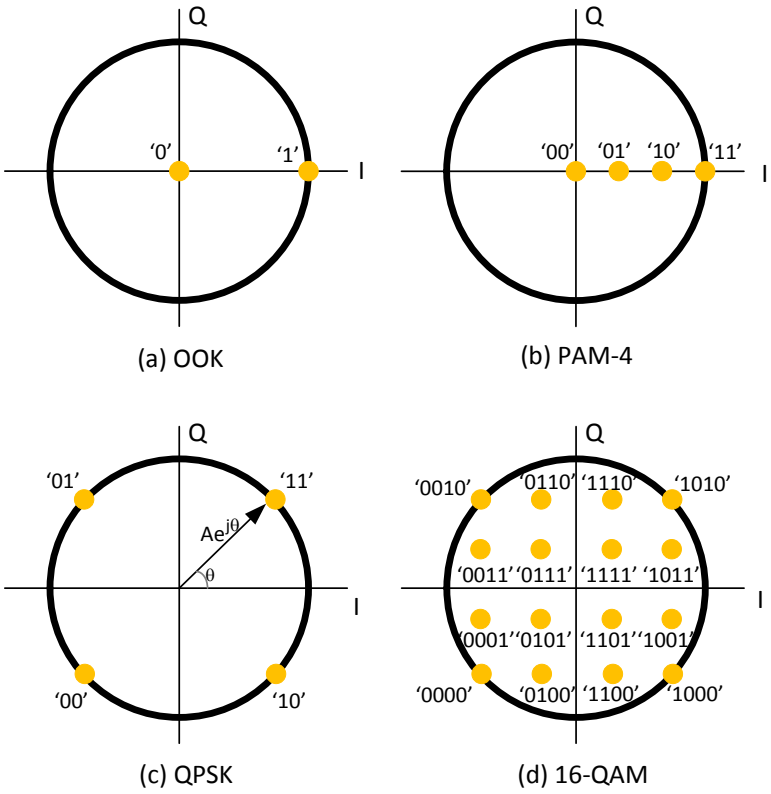

Figure 1.6: Examples of advanced modulation format constellations: (a) OOK, (b) PAM-4, (c) QPSK and (d) 16-QAM.

m, and the number of bits transmitted per symbol, M, is given by:

$$M = \log_2(m) \tag{1.2}$$

It should be noted that higher-order modulation formats also allow the use of lower symbol (baud) rates for a certain overall bit rate. This means that not only the signal spectral width is reduced, but lower cost electronic devices that are commercially available and mature can be used to transmit the same bit rate.

The encoding efficiency can be escalated by employing a combination of phase and multilevel amplitude modulation that extend the number of bits transmitted per symbol. This modulation format is referred to as Quadrature Amplitude Modulation (QAM) and it is often denoted as m-QAM, where m represents the overall number of symbols. The constellation of a 16-QAM is illustrated in Figure 1.6 (d). As it can be seen, each symbol has a unique combination of amplitude and phase and it can convey 4 bits of information, hence the use of 16-QAM quadruples the transmitted bit

rate and the resultant spectral efficiency compared to OOK systems.

Additionally, Polarization Division Multiplexing (PM) is generally used in conjunction with high order PSK or QAM to double the transmitted data by carrying different information in two orthogonal light polarization modes independently, allowing the development of 100 Gb/s in the ITU DWDM standard 50 GHz grid using 25 Gbaud PM-QPSK which has been the preferred format for 100 Gb/s applications by the industry. The major problems with the practical use of PM are continuous drifts and dispersion in the polarization states during fibre-optic transmission. As a result, PM requires digital signal processing at the coherent receiver to estimate and decode the signal, eliminating polarization-related artefacts [36].

The symbol size, and thereby the spectral efficiency, of m-QAM systems can be further increased by using a larger number of amplitude and phase levels, as 32-QAM (5 bits per symbol), 64-QAM (6 bits per symbol) or higher m [37], [38]. However, as the order of modulation continuously increases, the requirement for higher Optical Signal-to-Noise Ratio (OSNR) becomes more stringent and the transmission reach may get limited, which can be prohibitive for some communication systems [39].

The constellations in Figure 1.6 show a black circle that exemplifies the maximum peak power that can be launched into a fibre before optical non-linearities, taking place in the fibre, appear and distort the signal. Therefore, as the modulation order increases, the constellation points are situated closer, making them less distinguishable and hence, more susceptible to noise in transmission systems [40]. This has a direct impact in the reachable transmission distance before dispersion and added noise in the system create interferences that make the symbols non recognizable and decoded erroneously at the receiver. As such, the noise purity of the transmitter optical source (in terms of intensity and phase noise) becomes crucial and a major limiting factor in spectrally efficient coherent systems [36]. This will be further detailed later in this thesis.

In conclusion, advanced modulation formats offer a significant enhancement of the spectral efficiency of optical transmission systems. As such, in some scenarios the signal spectral width is notably reduced, resulting in an inefficient use of the ITU 50 GHz grid. Furthermore, when channel rates above 100 Gb/s are considered, a continual increase of the modulation order might not suffice as the noise requirements and transmission distance penalties may be impracticable. In pursuance of better utilisation of the available bandwidth of a fibre, advanced modulation formats can be combined with the use of superchannels and multicarrier techniques, explained in section 1.4. These methods aim to fit more optical sub-channels and decrease channel spacings and guard bands for

higher performance and throughput.

The following subsections describe in detail the various processes to generate and detect these advanced modulation formats over optical signals.

1.3.1 External modulation

In external modulation, the laser diode bias current is kept constant and thereby, the laser is on a Continuous Wave (CW) operation where its emitting output power is constant. The laser light is then passed through a modulator that manipulates amplitude and/or phase of the light according to an electrical data drive signal, also applied to the modulator. This modulation is isolated from the driving conditions of the laser and thus, the performance, noise properties and behaviour of the laser remain constant. Furthermore, the use of external modulation enables complex modulation formats, such as QPSK or QAM, to be imposed on an optical carrier.

Two main optical modulators are here revised due to their relevance in optical fibre transmission systems: Mach-Zehnder Modulator (MZM) and IQ MZM.

1.3.1.1 Mach-Zehnder Modulator

The schematic of a MZM structure is shown in Figure 1.7. It comprises two couplers and two electro-optic modulators placed in the MZM arms (some MZMs may have only one electro-optic modulator in one arm). The principle of operation of an electro-optic modulator is based on the electro-optic effect, also known as Pockels effect. It consists of a linear variation in the refractive index of a waveguide according to the strength of an applied electric field [45]. As a consequence, the propagation speed of the light travelling through the waveguide is affected and phase delays, proportional to the electric signal, are induced. By controlling the external voltages applied, the phase of the incoming optical field can be modulated and so, such electro-optic modulators are sometimes referred to as phase modulators.

The incoming beam light from a laser diode operating in CW mode is equally divided into the two arms. An independent drive voltage is applied across each phase modulator and so the optical signals in either path are subjected to different changes in phase. The two signals are then recombined. By controlling the relative phase shift between the two arms, the interference between the two signal varies from constructive to destructive and so the output signal can be also modulated in terms

of amplitude. Different configurations of optical modulators exist, but in general they all can be reduced to a combination of phase modulators and/or MZMs. Considering a dual-drive MZM, where

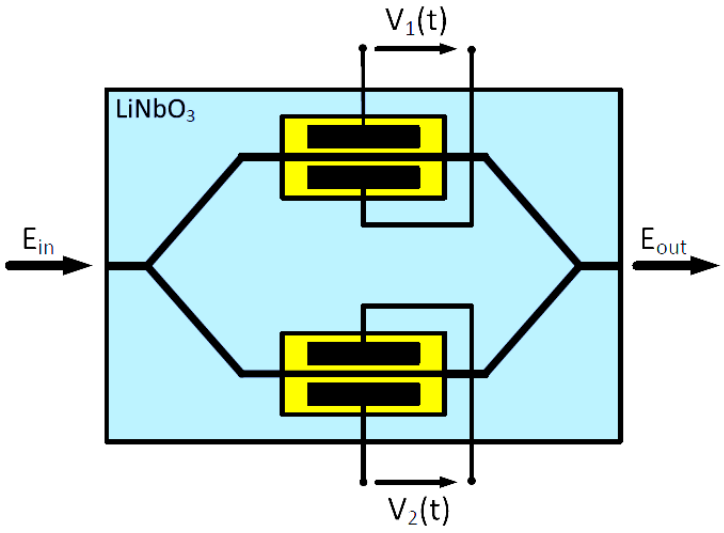

Figure 1.7: Mach-Zehnder Modulator structure.

there is a phase modulator in each arm that can be controlled independently, the optical output is mathematically described as [45]:

$$E_o(t) = \frac{1}{2} \cdot \left(e^{j\phi_1(t)} + e^{j\phi_2(t)} \right) \cdot E_i(t) \tag{1.3}$$

where $E_i(t)$ is the input optical field, $E_o(t)$ is the output optical field and $\phi_1(t)$ and $\phi_2(t)$ are the phase shifts applied to the upper and lower paths of the modulator. Manipulating this equation, it can be observed that the transfer characteristic of a MZM allows amplitude and phase modulation of the input electric field according to $\phi_1(t)$ and $\phi_2(t)$:

$$E_o(t) = E_i(t) \cos\left(\frac{\phi_1(t) - \phi_2(t)}{2} \right) \cdot e^{j\left(\frac{\phi_1(t) + \phi_2(t)}{2} \right)} = A(\phi_1(t), \phi_2(t)) \cdot e^{j(\phi_1(t), \phi_2(t))} \tag{1.4}$$

The voltage difference needed to create a relative phase shift between the two optical paths equal to π is called the half-wave voltage V_π and thus, the phase shifts can be defined as:

$$\phi_{1,2}(t) \approx \frac{\pi \cdot V_{1,2}(t)}{V_\pi} \tag{1.5}$$

where $V_{1,2}(t)$ is the applied voltage composed of a DC voltage, V_b corresponding to the operating

bias of the device, and the AC signal $s(t)$ with the data information to transmit [13]:

$$V(t) = V_b + s(t) \tag{1.6}$$

In the ideal case, a shift of V_π in the voltage difference ΔV between the two arms of the modulator is capable of changing the output optical power from minimum to maximum, as illustrated in Figure 1.8 where the transfer function for the electric field and optical power of the MZM are illustrated. In order to obtain intensity modulation, the operating bias point is set to be in the linear region between minimum and maximum transmission points to achieve a linear relationship between driving voltages and optical output power. This is known as the quadrature bias point. Phase modulation

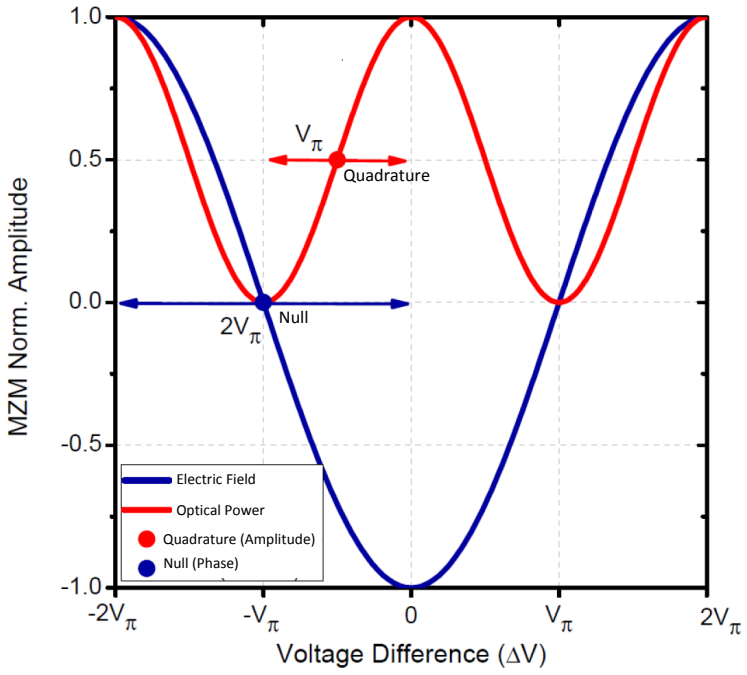

Figure 1.8: Normalised field (blue) and power (red) transfer functions of a dual-drive Mach-Zehnder modulator. Operation bias points for amplitude (quadrature) and phase (null) modulation are also shown. After: [2]

can also be achieved when the operating bias is set to the minimum transmission point, known as the null point. This can be observed visually in Figure 1.8. In this case, a more complicated receiver, capable of detecting phase change, is required as it will be later shown.

Although a single MZM can generate amplitude and phase modulation of the input light by choosing $V_{1,2}$ appropriately, it does not have the capability of modulating I and Q independently.

1.3.1.2 IQ Mach-Zehnder Modulator

An optical complex field modulator, also known as IQ modulator, consists of two nested MZMs with an additional 90° phase shifter in one of the arms as illustrated in Figure 1.9. By choosing the applied voltages appropriately, one can cover the entire complex IQ plane in the constellation diagram and generate higher order modulation formats such as QPSK and 16-QAM that require independent modulation of I and Q components.

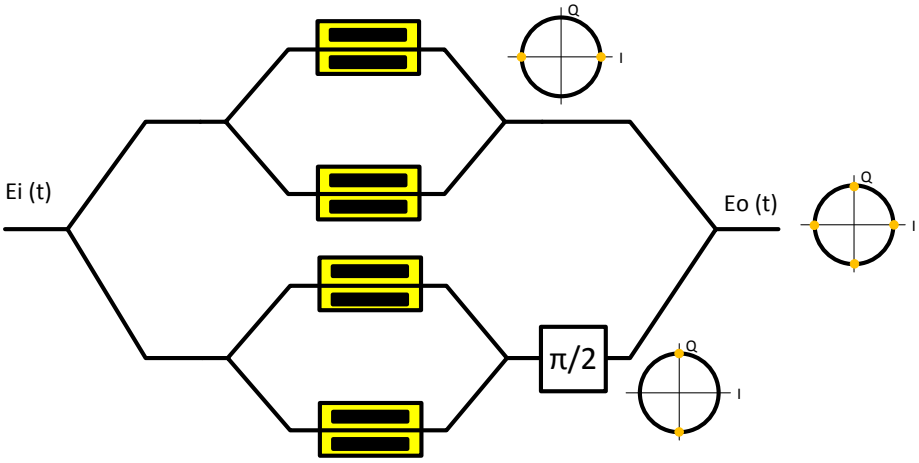

Figure 1.9: Schematic of an IQ MZM. An example of QPSK modulation with the correspondent constellation diagrams is also shown.

As an example, consider a QPSK modulation. Each MZM should be biased at null to generate a binary phase modulation in each of the arms, corresponding to phase shifts of 0 and π. The signal in the lower arm is then phase shifted by $\frac{\pi}{2}$ relative to the other arm. As a result, the two I and Q components are generated.

1.3.2 Direct detection

After fibre transmission, the optical signal needs to be detected and the electrical data information extracted, or de-modulated, from the optical carrier in an optical receiver.

As explained in section 1.3.1 the optical power of a laser lightwave can be modulated to carry information. In a direct detection receiver, the optical signal is detected by a photodiode that generates a photocurrent, proportional to the power of the optical incident signal. Hence, the induced electric current variations correspond to the recovered modulating data [13].

The performance of direct-detection receivers is predominantly affected by intensity noise.

1.3.3 Coherent detection

Direct detection is a simple and cost-efficient optical receiver, however, it allows only amplitude modulated formats to be recovered as the detected average optical power is phase independent.

Modulation formats that use the optical carrier phase to transmit information require more complicated receivers, called coherent detectors. In these, phase variations are converted into intensity changes by coupling the modulated optical signal with a reference signal, known as Local Oscillator (LO), creating constructive or destructive interferences depending on the relative phase differences.

The phase diversity quadrature frontend, depicted in Figure 1.10, comprises a 90° hybrid and a pair of balanced photodetectors allows the amplitude and phase de-modulation of both IQ components [46]. The generated photocurrents are mathematically expressed as [36], [46]:

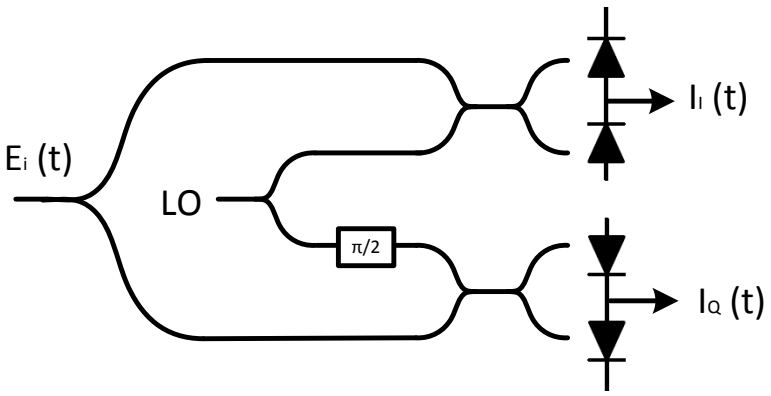

Figure 1.10: Schematic of a phase diversity coherent receiver, formed by a 90° hybrid and two of balanced photodetectors.

$$I_I(t) \approx \frac{R}{2}|E_i||E_{LO}| \cos\Big(w_i(t) - w_{LO}(t) + \phi_i(t) - \phi_{LO}(t)\Big) \tag{1.7}$$

$$I_Q(t) \approx \frac{R}{2}|E_i||E_{LO}| \sin\Big(w_i(t) - w_{LO}(t) + \phi_i(t) - \phi_{LO}(t)\Big) \tag{1.8}$$

where $I_I(t)$ and $I_Q(t)$ represent the photocurrents for the I and Q components respectively, R is the responsivity of the photodetector, $|E_i(t)|$, w_i and ϕ_i are the electric field amplitude, frequency and phase of the modulated optical signal and $|E_{LO}(t)|$, w_{LO} and ϕ_{LO} are the electric field amplitude, frequency and phase of the local oscillator reference. The signal phase ϕ_i contains the phase of the optical carrier and the phase of the encoded data. Therefore, phase modulation and coherent receivers are sensitive to phase noise so future high capacity transmitters and require low noise optical transmitters. Additionally, low phase noise LOs and high-speed digital signal processing are required to perform phase and frequency tracking [46].

1.4 Superchannel

Superchannels have been considered as key enablers for high capacity next generation optical transport networks by both the research community and industry [47]- [53].

Superchannels are formed by multiple combined optical carriers, or sub-channels, typically encoded with high order modulation formats and spectrally close-spaced thereby, fulfilling the bandwidth demands with transmissions of $>$100 Gb/s per channel while keeping pace with the spectral efficiency.

The motivation behind superchannels comes as an evolution of DWDM after the employment of advanced modulation formats. As previously explained, combinations of amplitude, phase and polarization modulations can dramatically increase the network capacity. However, by employing optical carriers spaced by the current DWDM 50 GHz grid, the spectrum is not efficiently used as these high order modulations schemes occupy narrower bandwidths. Superchannels seek to alleviate this spectrum waste and further increase the throughput by decreasing the channel spacings, allowing more channels to be fitted, and by using in conjunction, multicarrier modulation transmission techniques that allow the reduction and even elimination of guard bands, as explained in subsection 1.4.2.

In Figure 1.11 an example of the potential spectrum savings is illustrated. Figure 1.11 (a) shows a 1 Tb/s superchannel formed by using ten optical carriers at 100 Gb/s each employing 12.5 Gbaud polarization multiplexed 16-QAM. The sub-channels are separated by the fixed 50 GHz grid and as a result, the superchannel occupies a bandwidth of 500 GHz. On the other hand, Figure 1.11 (b) shows a spectrally efficient 1 Tb/s superchannel comprised of ten optical carriers with the same modulation format and baud rate, polarization multiplexed 16-QAM. In this case, the sub-channels are placed

contiguously, using a multiplexing technique named Nyquist WDM that allows the reduction of the bandwidth of each sub-channel to 12.5 GHz, and 500 MHz guard bands are in place. Hence, a total bandwidth of 129.5 GHz is needed, obtaining a 74.1 % in spectral usage.

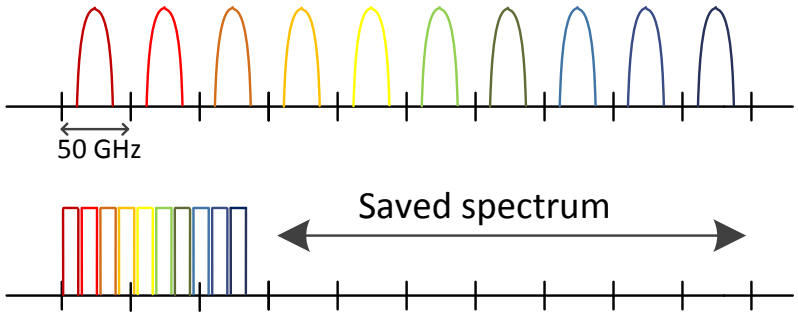

Figure 1.11: 1 Tb/s superchannel illustration. Upper, superchannel in existing 50 GHz grid. Lower, same superchannel employing Nyquist WDM, with 13 GHz of frequency spacing between sub-channels.

Superchannels were first demonstrated by S. Chandrasekhar [47] in 2009. The superchannel consisted on 24 optical carriers with PM-QPSK spaced by 12.5 GHz, where an overall transmission of 1.2-Tb/s over 7200 km was obtained. Numerous research works and field trials by companies such as NEC, Infinera and Alcatel-Lucent soon followed with early commercially available products by 2012. NEC first demonstrated the transmission of 1.15 Tb/s superchannels over 10,000 kilometres of existing transoceanic fibres with 23 optical carriers, each with 12.5 Gbaud PM-QPSK [50] and the first Infinera 500 Gb/s superchannel was brought into market, comprising ten optical carriers modulated with PM-QPSK, in 2012. Since then, superchannels gained a lot of attention and numerous works have successfully proved their suitability for high performance and capacity transmissions [51]- [52]. Currently, Infinera offers commercial products for superchannel transmissions of up to 1.2 Tb/s employing PM-16-QAM [53]. Remarkable recent achievements include a superchannel transmission with 8.67 (bit/s/Hz) of spectral efficiency [32], and the late field trial demonstrations of real-time superchannels of 5.6 Tb/s over 359 km and 2 Tb/s over a live 727 km network by British Telecommunications and Huawei Technologies [33].

1.4.1 Flexible Networks

The fibre bandwidth is currently divided in a 50 GHz grid defined by the ITU standards that, although successfully allowed 100 Gb/s to be commercially deployed, will have difficulties allocating higher bit rates (400 Gb/s, 1Tb/s, etc.). Furthermore, an arbitrary number of smaller frequency slots could allow the creation of bandwidth-fitted superchannels avoiding misuse of the available spectrum, as illustrated by Figure 1.11. Thus, there is a necessity for the grid to evolve towards finer granularities or even gridless [54] and new standards as the *Flexible grid* defined by the ITU-T in the G.694.1 recommendation [55] are emerging to support their deployment. The new flexible grid defines channels having a granularity of 12.5 GHz, combined with the ability to define an aggregate superchannel spectral width of 12.5 GHz multiples.

Flexible optical networks, also referred as elastic networks, make use of these flexible grids and are gaining a lot of attention to allow 400 Gb/s and 1Tb/s superchannels as they additionally enable a superb efficient usage of the available spectrum by dynamically allocating the bandwidth (elastic spectrum allocation) according to temporal traffic demands. Furthermore, an optimized spectral efficiency and performance can be achieved by dynamically adjusting transmission parameters such as sub-channel bandwidths, information rates and modulation formats depending on the unoccupied bandwidth, required capacity, optical link reach or other operating specifications.

1.4.2 Enabling Multicarrier modulation techniques

As previously mentioned, superchannels utilize multicarrier modulation techniques that allow the multiple sub-channels to be closely frequency spaced and reduce the overall transmitted bandwidth. These techniques rely on spectral and temporal shaping of the pulses that carry the data. The initial use of signal shaping techniques [56] in optical communications was motivated by the reduction of inter-symbol interference (ISI), a form of distortion of a signal in which one symbol interferes with subsequent symbols, and improvement of the transmission performance of the signal [40], [49].

In this work, we focus on two specific techniques: Nyquist WDM and all-optical Orthogonal Frequency Division Multiplexing (OFDM).

1.4.2.1 Nyquist WDM

In Nyquist WDM each sub-channel is spectrally shaped to occupy the minimum bandwidth that ensures ISI-free transmission, defined by the *Nyquist ISI criterion* and coincides with the baud rate [57]. Such narrow sub-channels can then be multiplexed very tightly, with minimum guard bands that ensure sub-channel filtering at the receiver without incurring in crosstalk (inter-channel interferences) [58], as observed in the ideal spectrum in Figure 1.12 (a).

These ideal non-overlapping rectangular-shaped sub-channel spectra correspond to an overlapped sinc-shaped response in the time domain [59], as observed in Figure 1.12 (b).

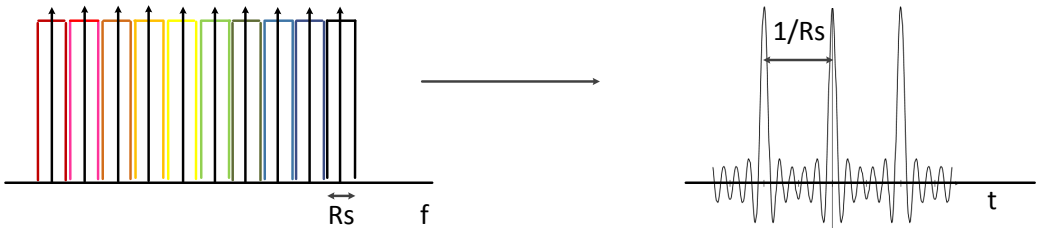

Figure 1.12: Left, a typical spectrum of a Nyquist WDM multicarrier signal. Right, time response of the Nyquist WDM multicarrier signal, with QPSK modulation and where the period corresponds to the baud rate used.

Nyquist WDM, therefore, requires a specific optical spectral rectangular shaping which can be performed at the transmitter using digital, analog electrical or optical filtering. However, perfect rectangular signals (sinc pulses) are not physically realisable and alternatively, practical implementations widely use raised-cosine pulses, illustrated in Figure 1.13, for Nyquist pulse shaping. The sharpness of the spectral filtering is determined by the roll-off factor, β, where $0 < \beta \leq 1$ [60].

Hence, Nyquist WDM reduces the total superchannel bandwidth allowing a better spectral efficiency by tightly packing the sub-channels and minimizing their bandwidth. This poses wavelength stability and low phase noise (that translates into frequency noise) requirements on the optical subcarriers to avoid drift and interference.

1.4.2.2 All optical OFDM

All optical OFDM transmits data on many sub-channels that are spectrally overlapped [57]. Analogous to Nyquist WDM, all optical OFDM involves temporal shaping of the signal and thus, the

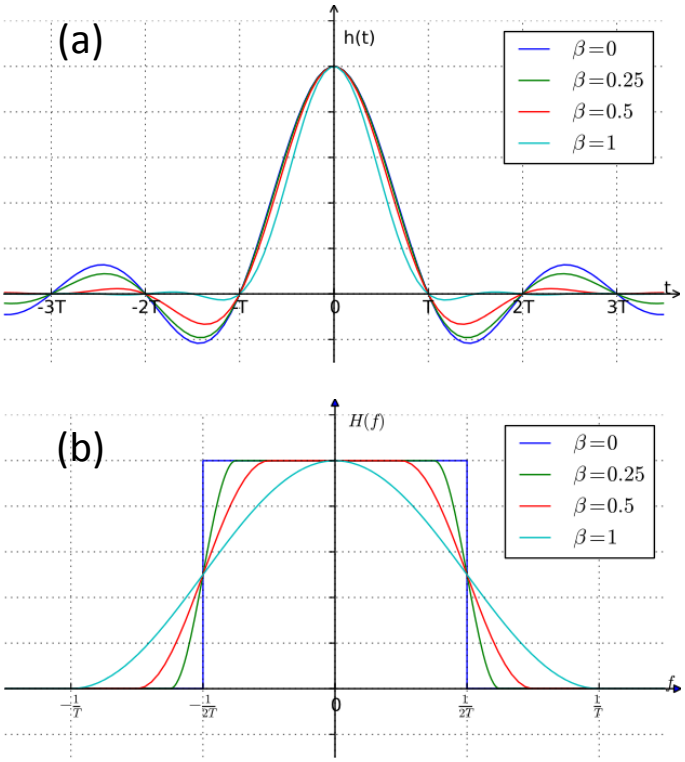

Figure 1.13: (a) Raised-cosine pulse in the time domain (b) Frequency response of raised-cosine pulse. After: [61]

transmitted pulses are ideal rectangular pulses. Therefore, the spectrum of the sub-channels correspond to sinc-shaped functions precisely spaced at multiples of the inverse of the symbol periods. These shaped spectra strongly overlap but are mathematically orthogonal with the peaks of the sub-channel spectra coinciding with the nulls of the spectra from neighbouring sub-channels, as illustrated in Figure 1.14.

In all optical OFDM crosstalk is clearly presented in the spectrum but it can be eliminated at the receiver if the sub-carriers have a strong phase correlation [57], [62], i.e. their phase noises are correlated and can be cancelled out. If, on the contrary, the sub-carriers present arbitrary phase noises that translates into frequency noise, the sub-channels will interfere in an unpredictable way.

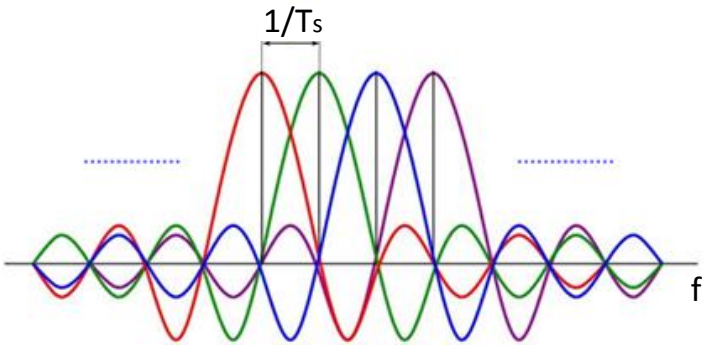

Figure 1.14: All optical OFDM ideal spectrum with overlapped sinc sub-carriers.

1.5 Optical Multicarrier Sources

The generation of superchannels that uses advanced modulation formats and multicarrier modulation techniques, require an optical multi-wavelength transmitter capable of creating multiple, closely frequency spaced and stable optical carriers.

1.5.1 Bank of lasers

A conventional approach to generate optical multicarrier sources is to use a bank of single mode lasers, which can be implemented with discrete lasers or with an integrated laser array [63], [64]. Each laser is adequately set to a certain wavelength to create the desired frequency spacing.

A single Photonic Integrated Circuit (PIC) can host numerous lasers allowing a large number of optical carriers from a single chip. Nevertheless, laser banks struggle to provide a constant frequency spacing between the carriers as each laser emission wavelength can arbitrarily drift over time. Clearly, as the spacing between sub-channels is reduced and guard bands omitted or become very small, this wavelength drift becomes problematic, causing undesired interference between adjacent sub-channels, and therefore, their use limit the achievable spectral efficiency. In order to maintain an acceptable stability each laser needs additional complicated control mechanisms [65], as well as independent biasing circuits which increases the complexity, cost and power consumption. Moreover, modifying the frequency spacing requires all lasers to be precisely tuned individually.

Finally, the independent lasers are not phase correlated to each other, which is an enabling con-

dition for all-optical OFDM modulation technique and an indispensable requirement to reverse the non-linear distortions through fibre transmission, which also enables power above the non-linear barrier to be launched into fibres and consequently, longer record-breaking transmission distances [66].

1.5.2 Optical Frequency Comb Source (OFCS)

OFCSs have shown significant promise for use in wide ranging applications among numerous disciplines, such as millimetre wave and THz signal generation [67], microwave photonics, spectroscopy [68] and, particularly, next generation spectrally efficient optical transceivers [69], [70].

An OFCS simultaneously generates, from a single device or subsystem, a number of precisely spaced and equidistant spectral carriers that share a strong phase correlation. Hence, OFCSs have attracted much interest and have proven to be key components in spectrally-efficient advanced multicarrier modulation techniques, thanks to their inherently precise and stable frequency spacing which enables the reduction or elimination of guard bands. Moreover, a single OFCS can replace multiple independent lasers reducing the power consumption and complexity.

OFCSs may also offer tunable frequency spacing and wavelength that allows a single source to be dynamically and easily adapted to suit the chosen symbol rate and to allocate a superchannel simultaneously to a specific wavelength band, according to traffic demands [70]. Finally, recent research studies have demonstrated that the phase correlation between the optical carriers presented in OFCSs is essential to push the fibre transmission capacity and distance over previous estimated limits [66]. The input power to a fibre is typically limited to a certain power level, beyond that threshold, additional power irreparably creates non-linearities that distort the information travelling through the fibre. The phase correlation between the multiple optical carriers, can be used to cancel these non-linearities and substantially recover the transmitted information. Consequently, the study demonstrated a record 12,000 km transmission [66].

Due to these beneficial characteristics, this thesis is focused on OFCS for next generation optical transmission applications.

The advanced modulation techniques that have been discussed in this Chapter offer a large fibre capacity and throughput enhancement by dramatically improving the spectral efficiency. Depending on the network topology and application, diverse requirements and specifications (such as transmission lengths, overall superchannel bandwidth, modulation formats and complexity) are stipulated.

Additionally, at the time of writing, there are no defined standards for the implementation of these emerging technologies. Therefore, a single compact OFCS with the potential to meet the stringent requirements of various optical networking scenarios, from intra-datacentre to long-haul optical transport, would be highly desirable.

Large number of carriers capable of allocating a superchannel, with good spectral flatness, stability, frequency spacing and wavelength flexibility, low Relative Intensity Noise (RIN), high Optical Carrier to Noise Ratio (OCNR), low phase noise and strong phase correlation between the carriers are all advisable qualities for versatile OFCSs that successfully allow the deployment of advanced modulation formats and superchannels. Furthermore, optical comb sources are expected to reduce component count and power consumption at the optical transmitters, so in order to yield further compactness and cost-efficiency, the photonic integration of these sources has lately become crucial.

A number of OFCS have been proposed, such as Mode-locked lasers (MLLs), electro-optic modulator based, parametric and gain-switched OFCSs that will be reviewed in Chapter 2.

1.6 Conclusions

From the first fibre optic link at Mb/s over several kilometres, optical communications have transformed to a complex high-capacity network spanning the globe that has facilitated the evolution of the Information Age. Modern society relies on inter-connected mobile devices and fast data exchange for communication, entertainment, mobility, education, business operations and health. Numerous emerging services and bandwidth-hungry applications are further contributing to the incessant and relentless traffic growth.

As such, various capacity scaling and spectrally efficient methods have been proposed recently to cope with bandwidth demands. High-order modulation formats, such as QPSK and QAM, improve the spectral efficiency by multi-level encoding of the information in the optical carrier amplitude, phase and polarization while maintaining the bandwidth. Simultaneously, the multicarrier modulation techniques presented, Nyquist WDM and all optical OFDM, reduce the frequency spacing and guard bands between adjacent optical channels, optimizing the bandwidth usage. In conjunction, these techniques will enable spectrally efficient optical superchannels to reach data rates beyond Tb/s. The implementation of these technologies require compact multi-carrier optical sources in the transmitter with wavelength stability, good spectral and noise properties as well as cost efficiency.

Optical frequency comb sources are key candidates that simultaneously generate multiple phase correlated optical carriers with an outstanding stable and equidistant frequency separation.

This work is focused on a specific kind of optical frequency comb sources: externally injected gain switched optical frequency comb sources (GS-OFCS). This thesis investigates novel experimental configurations to enhance their potential for network deployment, with improved flexibility and expanded bandwidth coverage. This work also studies the need for de-multiplexing of these comb sources and, in order to yield further compactness and cost-efficiency, a detailed characterization of two photonic integrated devices for GS-OFCS generation and de-multiplexing is reported. Finally, the integrated GS-OFCS is implemented into two spectrally efficient transmission systems that denote the quality and relevancy of these devices for future optical networks.

References

[1] R. Ramaswami, K. N. Sivarajan, and G. H. Sasaki, "Optical Networks: A Practical Perspective," Morgan Kaufmann, 2010.

[2] V. Vujicic, "Optical multicarrier sources for spectrally efficient optical networks," Thesis, Available: http://doras.dcu.ie/20981/1/Thesis_Vidak_Vujicic_Final_version.pdf

[3] S. J. B. Yoo, Y. Yin and K. Wen, "Intra and inter datacenter networking: The role of optical packet switching and flexible bandwidth optical networking," 16th International Conference on Optical Network Design and Modelling (ONDM), Colchester, 2012, pp. 1-6.

[4] T. H. Maiman, "Stimulated Optical Radiation in Ruby," *Nature*, vol. 187, pp. 493–494, 08/06/print 1960.

[5] K. C. Kao and G. A. Hockham, "Dielectric surface waveguides for optical frequencies," in *Proceedings of the Institution of Electrical Engineers*, vol. 133, pp. 1151–1158, July 1966.

[6] F. P. Kapron, D. B. Keck, and R. D. Maurer, "Radiation losses in glass optical waveguides," *Applied Physics Letters*, vol. 17, pp. 423–425, 1970.

[7] I. Hayashi, M. B. Panish, P. W. Foy, and S. Sumski, "Junction Lasers which Operate Continuously at Room Temerature," *Applied Physics Letters*, vol. 17, pp. 109–111, 1970.

[8] H. Kogelnik, "High-capacity optical communications: personal recollections," *IEEE Journal of Selected Topics in Quantum Electronics*, vol. 6, no. 6, pp. 1279–1286, Nov. 2000.

[9] R. J. Sanferrare, "Terrestrial lightwave systems," *AT&T Technical Journal*, vol. 66, pp. 95–107, 1987.

[10] J. I. Yamada, S. Machida, and T. Kimura, "2 Gbit/s optical transmission experiments at 1.3 um with 44 km single-mode fibre," *Electronics Letters*, vol. 17, pp. 479–480, 1981.

[11] S. Abbott, "Review of 20 years of undersea optical transmission system development and

deployment since TAT-8," in *34th European Conference on Optical Communication*, Brussels, Belgium, 2008, pp. 1-4.

[12] A. H. Gnauck, B. L. Kasper, R. A. Linke, R. W. Dawson, T. L. Koch, T. J. Bridges, E. G. Burkhardt, R. T. Yen, D. P. Wilt, J. C. Campbell, K. C. Nelson, and L. G. Cohen, "4-Gbit/s transmission over 103 km of optical fibre using a novel electronic multiplexer/demultiplexer," *Journal of Lightwave Technology*, vol. 3, pp. 1032–1035, 1985.

[13] G. P. Agrawal, Fiber-Optic Communication Systems, 3rd ed.: Wiley, 2002.

[14] R. J. Mears, L. Reekie, I. M. Jauncey, and D. N. Payne, "High-gain rare-earth-doped amplifier at 1.54 μm," in *Proceedings of Optical Fiber Communication Conference*, Nevada, USA, paper WI2, Jan. 1987.

[15] E. Desurvire, J. Simpson, and P.C. Becker, "High-gain erbium-doped traveling-wave amplifier," *Optics Letters*, vol. 12, No. 11, pp. 888–890, Nov. 1987.

[16] International Telecommunications Union (ITU), "G.694.1 spectral grids for WDM applications: DWDM frequency grid", Series G: Transmission Systems and Media, Digital Systems and Networks, 2012

[17] R. C. Alferness, H. Kogelnik, and T. H. Wood, "The Evolution of optical systems: optics everywhere," *Bell Labs Technical Journal*, vol. 5, pp. 188–202, Mar. 2000.

[18] A. H. Gnauck, R. W. Tkach, A. R. Chraplyvy and T. Li, "High-Capacity Optical Transmission Systems," *Journal of Lightwave Technology*, vol. 26, no. 9, pp. 1032–1045, May, 2008.

[19] H. Onaka, H. Miyata, G. Ishikawa, K. Otsuka, H. Ooi, Y. Kai, S. Kinoshita, M. Seino, H. Nishimoto, and T. Chikama, "1.1 Tb/s WDM transmission over a 150 km 1.3 μm zero-dispersion single-mode ," in *Proceedings of Optical Fiber Communications Conference*, San Jose, California, USA, Paper PD-19, 1996.

[20] Cisco Systems, Available: http://en.wikipedia.org/wiki/Internet_traffic#cite_note-CSCO-15

[21] Cisco Systems, "The Zettabyte Era: Trends and Analysis", White paper, Jun. 2016. Available: http://www.cisco.com/c/en/us/solutions/collateral/service-provider/visual-networking-index-vni/vni-hyperconnectivity-wp.html

[22] E. Desurvire, "Capacity demand and technology challenges for lightwave systems in the next two decades," *Journal of Lightwave Technology*, vol. 24, no. 12, pp. 4697–4710, 2006.

[23] R. Essiambre and R. W. Tkach, "Capacity Trends and Limits of Optical Communication Networks," *Proceedings of the IEEE*, vol. 100, pp. 1035–1055, March 2012.

[24] S. Gringeri, E. B. Basch, and T. J. Xia, "Technical considerations for supporting data rates beyond 100 Gb/s," *IEEE Communications Magazine*, vol. 50, no. 2, pp. 21–30, Feb. 2012.

[25] M. Birk, L. Raddatz, D. A. Fishman, P. Magill, S. Woodward, "Field Trial of End-to-End OC-768 Transmission Using 9 WDM Channels over 1000km of Installed Fiber," in *Proceedings of Optical Fiber Communications Conference*, Atlanta, Georgia, USA, paper TuS4, 2003.

[26] T. Foggi, E. Forestieri, G. Colavolpe, G. Prati, "Maximum-Likelihood Sequence Detection With Closed-Form Metrics in OOK Optical Systems Impaired by GVD and PMD," *Journal of Lightwave Technology*, vol. 24, no. 8, pp. 3073–3087, Aug. 2006.

[27] H. Sun, K.-T. Wu, and K. Roberts, "Real-time measurements of a 40 Gb/s coherent system," *Optics Express*, vol. 16, pp. 873–879, 2008.

[28] P. J. Winzer, G. Raybon, H. Song, A. Adamiecki, S. Corteselli, A. H. Gnauck, D. A. Fishman, C. R. Doerr, S. Chandrasekhar, L. L. Buhl, T. J. Xia, G. Wellbrock, W. Lee, B. Basch, T. Kawanishi, K. Higuma, Y. Painchaud, "100-Gb/s DQPSK Transmission: From Laboratory Experiments to Field Trials," *Journal of Lightwave Technology*, vol. 26, no. 20, pp. 3388–3402, Oct. 2008.

[29] P. J. Winzer, "Beyond 100G Ethernet," *IEEE Communications Magazine*, vol. 48, no. 7, pp. 26–30, July 2010.

[30] Infinera, "Super-channels: DWDM Transmission at 100 Gb/s and Beyond," White Paper, Available: https://www.infinera.com/wp-content/uploads/2015/07/SuperChannel_WhitePaper.pdf

[31] Fiber optic components, "What is the Meaning of 100G Channels Networks to Service Providers", Article, April 2014. Available: http://www.-optic-components.com/what-is-the-meaning-of-100g-channels-networks-to-service-providers.html

[32] A. Nespola, S. Straullu, G. Bosco, A. Carena, J. Yanchao, P. Poggiolini, F. Forghieri, Y. Yamamoto, M. Hirano, T. Sasaki, J. Bauwelinck, and K. Verheyen, "1306–km 20x124.8–Gb/s PM–64QAM Transmission over PSCF with Net SEDP 11,300 (b·km)/s/Hz using 1.15 samp/symb DAC," *Optics Express*, vol. 22, pp. 1796–1805, Jan. 2014.

[33] Y. R. Zhou, K. Smith, S. West, M. Johnston, J. Weatherhead, P. Weir, J. Hammond, a. lord, J. Chen, W. Pan, C. Cao, R. Yang, N. Zhou, and S. Wu, "Field Trial Demonstration of Real-Time

Optical Superchannel Transport up to 5.6Tb/s over 359km and 2Tb/s over a Live 727km Flexible Grid Optical Link using 64GBaud Software Configurable Transponders," *Journal of Lightwave Technology*, vol.PP, no.99, pp.1-1, July 2016.

[34] F. Karinou, C. Prodaniuc, N. Stojanovic, M. Ortsiefer, A. Daly, R. Hohenleitner, B. Kogel, and C. Neumeyr, "Directly PAM-4 modulated 1530-nm VCSEL enabling 56 Gb/s/λ data-center interconnects," *IEEE Photonics Technology Letters*, vol. 27, no. 17, pp. 1872–1875, Sept. 2015.

[35] D. Sadot, G. Dorman, A. Gorshtein, E. Sonkin, and O. Vidal, "Single channel 112 Gbit/sec PAM4 at 56 Gbaud with digital signal processing for data centers applications," *Optics Express*, vol. 23, pp. 991–997, Jan. 2015.

[36] K. Kikuchi, "Coherent Optical Communications: Historical Perspectives and Future Directions," in *High Spectral Density Optical Communication Technologies*, Springer, 2010.

[37] X. Zhou, L. E. Nelson, P. Magill, R. Isaac, B. Zhu, D. W. Peckham, P. I. Borel, K. Carlson, "PDM-Nyquist-32QAM for 450-Gb/s Per-Channel WDM Transmission on the 50 GHz ITU-T Grid," *Journal of Lightwave Technology*, vol. 30, no. 54, pp. 553–559, Feb. 2012.

[38] A. H. Gnauck, P. J. Winzer, A. Konczykowska, F. Jorge, J.-Y. Dupuy, M. Riet, G. Charlet, B. Zhu, D. W. Peckham, "Generation and Transmission of 21.4-Gbaud PDM 64-QAM Using a Novel High-Power DAC Driving a Single I/Q Modulator," *Journal of Lightwave Technology*, vol. 30, no. 4, pp. 532–536, Feb. 2012.

[39] P. J. Winzer, "High-Spectral-Efficiency Optical Modulation Formats," *Journal of Lightwave Technology*, vol. 30, no. 24, pp. 3824–3835, Dec. 2012.

[40] R.-J. Essiambre, G. Kramer, P. J. Winzer, G. J. Foschini, B. Goebel, "Capacity limits of optical fiber networks," *Journal of Lightwave Technology*, vol. 28, no. 4, pp. 662–701, Feb. 2010.

[41] S. Lindgren, H. Ahlfeldt, L. Backlin, L. Forssen, C. Vieider, H. Elderstig, et al., "24-GHz modulation bandwidth and passive alignment of flip-chip mounted DFB laser diodes," *IEEE Photonics Technology Letters*, vol. 9, pp. 306-308, 1997.

[42] Y. Matsui, "55-GHz bandwidth short-cavity distributed reflector laser and its application to 112-Gb/s PAM-4," in *Proceedings of Optical Fibre Communication Conference*, Postdeadline Paper, Th5B.4, 2016.

[43] Y. Matsui, R. Schatz, G. Carey, T. Sudo and C. Roxlo, "Direct modulation laser technology toward 50-GHz bandwidth," *International Semiconductor Laser Conference*, Kobe, Japan, pp.

1–2, 2016.

[44] T. L. Koch and J. E. Bowers, "Nature of wavelength chirping in directly modulated semiconductor lasers," *Electronics Letters*, vol. 20, pp. 1038–1040, 1984.

[45] M. Seimetz, "High–Order modulation for Optical Fiber Transmission Systems," Springer, Atlanta, GA, 2009.

[46] K. Kikuchi, "Fundamentals of Coherent Optical Fiber Communications," *Journal of Lightwave Technology*, vol. 34, no. 1, pp. 157–179, Jan. 2016.

[47] S. Chandrasekhar, X. Liu, B. Zhu, and D. Peckham, "Transmission of a 1.2-Tb/s 24-Carrier No-Guard-Interval Coherent OFDM Superchannel over 7200-km of Ultra-Large-Area Fiber," in *Proceedings of European Conference on Optical Communications*, Vienna, Austria, Post deadline paper PD 2.6, 2009.

[48] G. Bennett, "Superchannels to the rescue!," Lightwave magazine Article. Available: http://www.lightwaveonline.com/articles/print/volume-29/issue-2/features/superchannels-to-the-rescue.html

[49] J. Fischer, M. Nolle, L. Molle, C. Schmidtlanghorst, J. Hilt, R. Ludwig, C. Schubert, "Beyond 100G - high-capacity transport technologies for next generation optical core networks," *Future Network & Mobile Summit*, Berlin, pp. 1–9, 2012.

[50] Y. Huang, M. Huang, D. Qian, Y. Shao, E. Ip, T. Inoue, Y. Inada, T. Ogata, Y. Aoki, and T. Wang, "4 × 1.15-Tb/s DP-QPSK Superchannel Transmission Over 10,181-km of EDFA Amplified Hybrid Large-Core/ Ultra Low-Loss Fiber Spans with 2-dB FEC Margin," in *Proceedings of Asia Communications and Photonics Conference and Exhibition (ACP)*, Shanghai, Post-deadline paper, pp. 1-6, 2011.

[51] F. P. Guiomar, S. B. Amado, J. D. Reis, S. M. Rossi, A. Chiuchiarelli, J. R. F. Oliveira, António L. Teixeira and A. N. Pinto, "Ultra-long-haul 400G superchannel transmission with multi-carrier nonlinear equalization," in *Proceedings of European Conference on Optical Communication*, Valencia, pp. 1-3, 2015.

[52] J. Renaudier, R. R. Müller, L. Schmalen, P. Tran, P. Brindel and G. Charlet, "1-Tb/s PDM-32QAM superchannel transmission at 6.7-b/s/Hz over SSMF and 150-GHz-grid ROADMs," in *Proceedings of European Conference on Optical Communication*, Cannes, pp. 1-3, 2014.

[53] Infinera Multi-terabit Product Brochure. Available: https://www.infinera.com/wp-content/

uploads/2015/10/Infinera-BR-DTN-X-Family.pdf

[54] G. Shen and Q. Yang, "From coarse grid to mini-grid to gridless: how much can gridless help contentionless?", in *Proceedings of Optical Fiber Communication Conference/National Fiber Optic Engineers Conference*, paper OTuI3, 2011.

[55] ITU-T Recommendation G.694.1, "Spectral grids for WDM applications: DWDM frequency grid", Available: http://www.itu.int/rec/T-REC-G.694.1/en

[56] J. Leuthold, W. Freude, "Chapter 9: Optical OFDM and Nyquist Multiplexing", Optical Fiber Telecommunications VIB, Academic Press, 2013.

[57] G. Bosco, A. Carena, V. Curri, P. Poggiolini and F. Forghieri, "Performance limits of Nyquist-WDM and CO-OFDM in high-speed PM-QPSK systems," *IEEE Photonics Technology Letters*, vol. 22, no.15, pp. 1129–1131, 2010.

[58] G. Bosco, V. Curri, A. Carena, P. Poggiolini and F. Forghieri, "On the performance of Nyquist-WDM terabit superchannels based on PM-BPSK, PM-QPSK, PM-8QAM or PM-16QAM subcarriers," *Journal of Lightwave Technology*, vol. 29, no.1, pp. 53–61, 2011.

[59] R. Schmogrow, M. Winter, M. Meyer, D. Hillerkuss, S. Wolf, B. Baeuerle, A. Ludwig, B. Nebendahl, S. Ben-Ezra, J. Meyer, M. Dreschmann, M. Huebner, J. Becker, C. Koos, W. Freude, and J. Leuthold, "Real-time Nyquist pulse generation beyond 100 Gbit/s and its relation to OFDM," *Optics Express*, vol. 20, no. 1, pp. 317–337, Jan. 2012.

[60] J. Proakis, and M. Salehi, "Digital Communications, 5th Edition," McGrow Hill, 2007.

[61] Raised-Cosine Filter Article, Wikiwand. Available: http://www.wikiwand.com/en/Raised-cosine_filter

[62] D. Hillerkuss, R. Schmogrow, T. Schellinger, M. Jordan, M. Winter, G. Huber, T. Vallaitis, R. Bonk, P. Kleinow, F. Frey, M. Roeger, S. Koenig, A. Ludwig, A. Marculescu, J. Li, M. Hoh, M. Dreschmann, J. Meyer, S. Ben Ezra, N. Narkiss, B. Nebendahl, F. Parmigiani, P. Petropoulos, B. Resan, A. Oehler, K. Weingarten, T. Ellermeyer, J. Lutz, M. Moeller, M. Huebner, J. Becker, C. Koos, W. Freude, J. Leuthold, "26 Tbit/s line-rate super-channel transmission utilizing all-optical fast Fourier transform processing," *Nature Photonics*, vol. 5, no. 6, pp. 364–371, May 2011.

[63] J.H. Ke, Y. Gao, and J.C. Cartledge, "400 Gbit/s single-carrier and 1 Tbit/s three-carrier super-channel signals using dual polarization 16-QAM with look-up table correction and optical pulse

shaping," *Optics Express*, vol. 22, pp. 71–84, 2014.

[64] Z. Xiao, S. Fu, S. Yao, M. Tang, P. Shum and D. Liu, "ICI Mitigation for Dual-Carrier Superchannel Transmission Based on m-PSK and m-QAM Formats," *Journal of Lightwave Technology*, vol. 34, no. 23, pp. 5526-5533, Dec. 2016.

[65] K. Igarashi, T. Tsuritani, I. Morita, K. Katoh, K. Kikuchi, "Frequency stabilization of multiple semiconductor lasers for Nyquist-WDM transmission systems," in *Proceedings of Optical Fiber Communication Conference/National Fiber Optic Engineers Conference*, Anaheim, CA, USA, paper OTu2I.6, Mar. 2013.

[66] E. Temprana, E. Myslivets, B.P.-P. Kuo, L. Liu, V. Ataie, N. Alic, and S. Radic, "Overcoming Kerr-induced capacity limit in optical fiber transmission," *Science*, vol. 348, no. 6242, pp. 1445–1448, Jun 2015.

[67] T. Shao, H. Shams, P. M. Anandarajah, M. J. Fice, C. C. Renaud, F. van Dijk, A. J. Seeds, and L. P. Barry, "Phase Noise Investigation of Multicarrier Sub-THz Wireless Transmission System Based on an Injection-Locked Gain-Switched Laser," *IEEE Transactions on Terahertz Science and Technology*, vol. 5, no. 4, pp. 590–597, July 2015.

[68] Michael J. Thorpe, David Balslev-Clausen, Matthew S. Kirchner, and Jun Ye, "Cavity-enhanced optical frequency comb spectroscopy: application to human breath analysis," *Optics Express*, vol. 16, pp. 2387–2397, 2008.

[69] V. Vujicic, C. Calo, R. Watts, F. Lelarge, C. Browning, K. Merghem, A. Martinez, A. Ramdane and L. P. Barry, "Quantum Dash Mode-Locked Lasers for Data Centre Applications," *IEEE Journal of Selected Topics in Quantum Electronics*, vol. 21, no. 6, pp. 53–60, Dec. 2015.

[70] P. Zhu, J. Li, L. Niu, Y. Xu, Y. Chen, X. Xie, X. Chen, B. Guo, Z. Chen, and Y. He, "Optical Comb-enabled Cost-effective ROADM Scheme for Elastic Optical Networks," in *Proceedings of Optical Fiber Communication Conference*, San Francisco, CA, paper W3B.5, 2014.

Chapter 2

Generation of Optical Frequency Comb Sources

Research into Optical Frequency Comb Sources (OFCSs) experienced a major breakthrough in 2005, when John L. Hall and Theodor W. Hänsch were jointly awarded the Nobel Prize in physics for their pioneering work into optical frequency combs for spectroscopy applications. Since then, OFCSs have proved to be versatile optical devices with significant promise for use in wide ranging applications among numerous disciplines, such as millimetre wave and terahertz signal generation [1], microwave photonics, spectroscopy [2] and, particularly, next generation spectrally efficient optical transceivers [3], [4].

As introduced in the previous chapter, OFCSs are a key technology in the milestone to high spectrally efficient superchannels and Flexible Networks by ensuring constant and stable frequency spacing between the carriers, which enables the reduction or elimination of guard bands in advanced multicarrier modulation techniques and supports fibre non-linearity compensation. Additionally, OFCSs may also offer free spectral range (FSR) flexibility that allows a single source to be easily adapted to suit different modulation formats and symbol rates [4].

In this chapter, a general review on the key parameters that define the quality of an Optical Frequency Comb Source (OFCS) is first presented. Then, several selected comb generation techniques are described, and their basic characteristics are discussed. The comb generation technologies analysed include mode-locking, Kerr-effect in microresonators, parametric processes, electro-optic modulation and gain switching. The latter technique is explained in more detail as it is the OFCS configuration utilized in the rest of this work.

2.1 Optical Frequency Comb Source Properties

An optical frequency comb provides a number of precisely spaced and equidistant spectral carriers generated by a single device or subsystem. These optical carriers, usually referred to as comb lines, share a strong phase correlation. Therefore, an ideal optical frequency comb spectrum consists of a periodic impulse train in the frequency domain which corresponds to a regular train of impulses in the time domain (through a Fourier transform), where the fixed comb frequency spacing is the inverse of the pulse repetition rate. However, real implementations of pulse trains are not ideal impulse responses but ultrashort pulses with a certain pulse width and thus, the equivalent optical frequency combs are not infinite, but limited in bandwidth, as shown in Figure 2.1 (c). The temporal pulse width is inversely proportional to the comb optical bandwidth and thus, the narrower the pulse, the wider the comb spectrum.

An OFCS should satisfy certain requirements and is generally expected to deliver diverse spectral properties that determine the flexibility, modulation formats and baud rates that can be employed. These parameters will have an impact on the quality and performance over the network and are outlined as follows:

• **Optical bandwidth**. It is the total width of the optical spectrum obtained from the OFCS, also known as frequency span. It can be measured as the number of comb tones for a specific frequency spacing, or by the overall width in frequency (or wavelength) specified at 10 dB or 20 dB from the peak comb tone. This parameter indicates the maximum number of comb tones that can be used, and thus, it determines the transmission capabilities.

• **Spectrum flatness**. The optical power level may differ between comb tones. The spectrum flatness refers to the amplitude deviation of this power distribution. Flat-top optical power distribution among comb lines is desirable in communication applications to avoid equalisation and ensure similar performance between channels.

• **Frequency spacing**. Also known as Free Spectral Range (FSR), refers to the frequency distance between comb lines. Some approaches for comb generation present fixed FSR which may hinder their applicability. A multipurpose OFCS for future high capacity and Flexible Networks would advantageously present FSR tunability to adapt the frequency spacing for different baud rates, allowing reconfigurability, and compatibility with existent networks.

• **Central wavelength** refers to the wavelength of the central comb tone in the OFCS spectrum. Central wavelength tunability is beneficial in terms of network flexibility and desirable for dynamic

spectrum allocation and efficient use of unused bandwidth slots.

• **Relative Intensity Noise (RIN)** is the intensity noise (optical power fluctuations), normalized to the average power level. The optical output of a laser presents fluctuations in its intensity, phase and frequency caused by spontaneous emission in the cavity. Each spontaneously emitted photon adds to the coherent field (established by stimulated emission) a small component with random phase that randomly perturbs both the amplitude and phase, resulting in intensity and phase noise [5]. The relative intensity noise can be statistically described with a power spectral density which depends on the noise frequency. This RIN power spectral density is typically represented in logarithm scale, with units of dB/Hz.

• **Phase Noise and Optical Linewidth**. Phase noise is crucial for advanced modulation formats that convey information in the carrier phase. As previously mentioned, spontaneous emission also produces random phase fluctuations and thus, phase noise. These phase fluctuations are equivalent to frequency variations. Consequently, the spectrum exhibits frequency fluctuations that produce a broadening of the spectral tone. This spectral width is referred to as the optical linewidth. The phase noise can also be statistically described as a power spectral density of the frequency fluctuations, known as the Frequency Modulated (FM)-noise spectrum. In this work, the phase noise is characterized by measuring both linewidth and FM-noise spectrum.

• **Phase Correlation**. It is a signature of how well the phase noise of the comb lines correlate to each other. It is typically measured by detecting the optical comb with a high speed photodiode and observing the linewidth of the obtained Radio frequency (RF) beat tone, which is generated at the frequency that corresponds to the distance between the comb tones. The spectral linewidth of the RF beat tone is composed by the combination of the phase noises of the detected comb tones. If a strong phase correlation exists, these phase noises cancel each other out. Therefore, the spectral linewidth of the RF beat tone reduces as the phase correlation between the tones improves, and ideally a Dirac delta function would be observed.

• **Optical Power per Comb Line**. High power per comb tone eliminates the need for bulky and costly optical amplifiers in transmitters, enabling longer reach without amplification and thus, cost and power consumption reduction.

• **Optical Carrier to Noise Ratio (OCNR)** is the difference between the power and noise level of a comb tone. In this work, it is measured in dB with a high resolution Optical Spectrum Analyser (OSA). The OCNR is a limiting parameter in advanced intensity modulated systems and can be

degraded along system transmission through inclusion of attenuation, losses and optical amplifiers that increase the system noise level.

• **Stability, compactness and manufacturing costs and reproducibility**. These are obvious drivers for commercial deployment. OFCS are required to present long term stability in wavelength, frequency spacing and optical power.

In summary, a large number of carriers with good spectral flatness, FSR and wavelength flexibility, low RIN, high OCNR, narrow optical linewidth, and strong phase correlation are all desirable qualities of a versatile OFCS. Furthermore, optical comb sources are expected to exhibit good stability and reduce component count at the optical transmitters.

2.2 Mode-locked lasers

Mode-locking is a technique, proposed in 1964 [6], that introduces phase correlation between the longitudinal modes in a semiconductor laser cavity [7]. In a conventional semiconductor laser, where no fixed phase relationship exists, each longitudinal mode oscillates independently and phases may vary randomly, as illustrated in Figure 2.1 (a). These longitudinal modes interfere in the cavity and tend to average to a near-constant intensity power, similar to a combined set of independent lasers emitting at different frequencies. When a fixed phase relationship is induced amongst the optical longitudinal modes, they will constructively and periodically interfere, resulting in the emission of a train of ultrashort pulses, as represented in Figure 2.1 (b). The laser is then said to be *phase-locked* or *mode-locked*. Therefore, the optical spectrum of Mode-locked lasers (MLLs) consists of an optical frequency comb with comb tones equally spaced by the frequency spacing between the longitudinal modes, which is determined by the laser cavity length.

Mode-locking can be achieved using lasers with different structures [8] and mode-locking methods can be classified into active, passive and hybrid mode-locking [9], [10]. Active mode-locking may involve using a modulator placed in the laser cavity and driven by an external signal to induce modulation of the optical longitudinal modes in the cavity. The modulating signal frequency must match the frequency spacing between modes (fixed by the laser cavity length) or a multiple of it to achieve stable operation [7]. Due to this modulation, each longitudinal mode will present sidebands that will coincide with adjacent longitudinal modes. These generated sidebands seed the neighbouring modes and act as optical injection locking signals which leads to mutual synchronisation and phase correlation [11], [12]. Passive mode-locking does not require an external modulating signal.

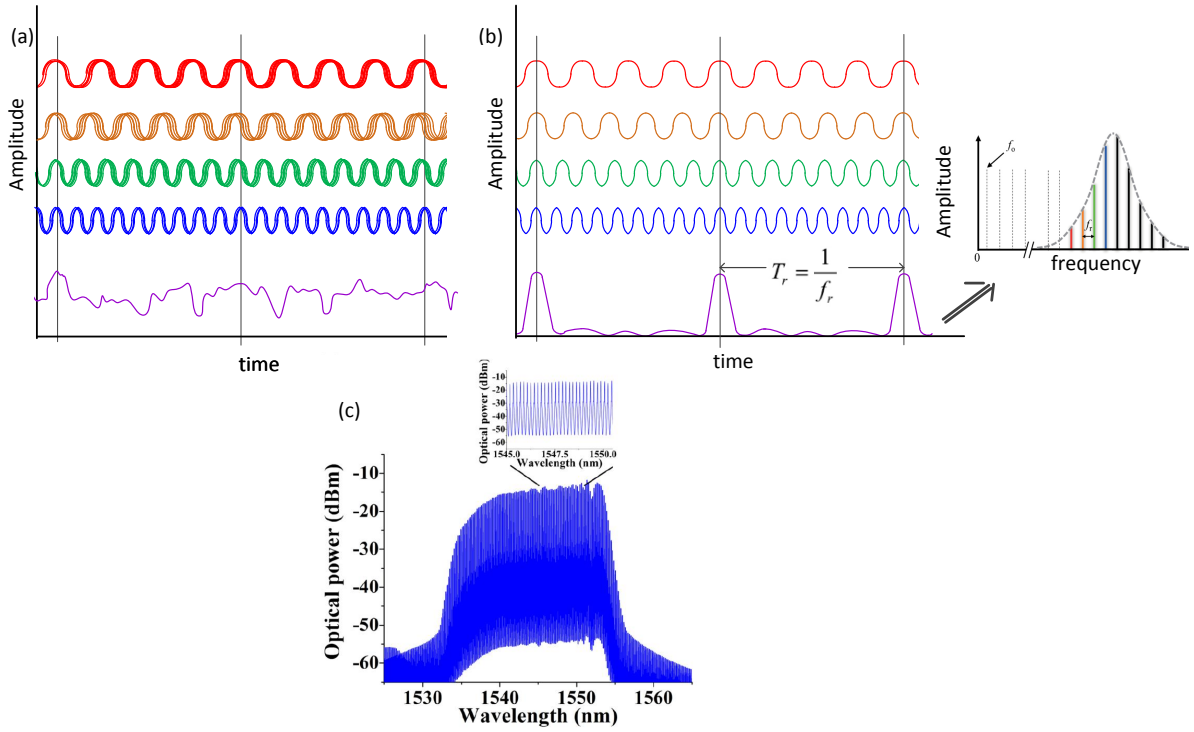

Figure 2.1: Illustration of MLL principle of operation. (a) Oscillating modes without phase correlation (b) Oscillating modes that are mode-locked (i.e. there is a fixed phase correlation) (c) Optical spectrum of a MLL.

It relies on non-linear optical effects in the device by employing unbiased saturable absorbers in the cavity [7] or specific quantum structure designs of the active region that increase non-linear coupling and beatings between longitudinal modes to provoke phase correlation [13], [14]. Saturable absorbers are optical intensity dependent components, whose absorption profile decreases with increasing incident light until a certain value, where it saturates and becomes completely transparent, transmitting the high intensity incident light. When placed in a laser cavity, a saturable absorber will selectively pass light with sufficient energy to saturate the absorber, which then reduces the losses (absorption) for a small period of time, allowing a pulse peak to travel through. As the light in the cavity oscillates, this process repeats, leading to the selective amplification of the high-intensity spikes, and the absorption of the low-intensity light. After many round trips, this leads to a train of short pulses and mode-locking of the laser. Hybrid-mode locking occurs when active and passive mode-locking are present simultaneously in the same laser.

MLL OFCS characteristics

A typical MLL spectrum is presented in Figure 2.1 (c). As observed, MLLs can generate broadband comb generation spanning over tens of nanometres with good spectral flatness from a single device. Their compactness and low power consumption resulting from monolithic integration is outstanding. However, the primary handicaps of MLLs for network deployment are the fixed frequency spacing, their noise properties and stability.

The frequency spacing is inherently determined by the cleaved cavity length and, thereby, the FSR cannot be flexibly tuned to adjust to different network systems, baud rates or traffic conditions, hindering its versatility and use in Flexible Networks. Furthermore, the individual comb tones have typically relatively large optical linewidth ($\sim$ 10 MHz) [15] which is prohibitive for advanced modulation formats that encode information in the carrier phase. Low linewidth MLLs and coherent system transmissions have been demonstrated by employing complicated phase noise reduction techniques based on external optical injection [16], [17], in contrast, the advantageous MLL broadband spectrum notably reduces. Additionally, the individual comb tones present an acceptable averaged RIN (below -120 dB/Hz) [18], [19] but exhibit increased RIN at low frequencies of the RIN power spectral density, which is detrimental for direct detected systems [20]. This elevated RIN is caused by mode partition noise in the laser, which is related to fluctuations of the power distribution amongst the modes that constitute the overall MLL spectrum competing for a common injected-carrier population [21]. Finally, from a practical perspective, MLLs may have control difficulties in starting and maintaining mode locking which directly affects the stability of the resultant OFCS [22].

2.3 Microresonator based Kerr OFCS

Kerr OFCS in compact integrated microresonators have recently gained attention due to the possibility of generating ultra-broadband coherent combs while conserving a low linewidth [23]- [25]. The underlying generation process is the non-linear Kerr effect in the microresonator [26] that takes place when a high-power optical signal (known as pump) is launched, as illustrated in Figure 2.2 (a). The optical Kerr effect consists of a variation in the refractive index of the resonator material proportional to the confined pump intensity [27] and enables the formation of new frequency components. As a result, the pump signal can generate two side-modes through Four-Wave Mixing (FWM), a non-linear process which is a consequence of the Kerr effect [27], [28] where two pump

photons are converted into a pair of photons that are up- and downshifted in frequency [23]. When optimal conditions are met (i.e. the optimization of pump polarization, pump power and wavelength into resonance), these newly generated modes coincide with the microresonator cavity modes and this non-linear process gets enhanced, leading to efficient cascaded FWM where the initially generated side modes interact with the original pump light and among themselves, producing new optical comb tones as depicted in Figure 2.2 (b).

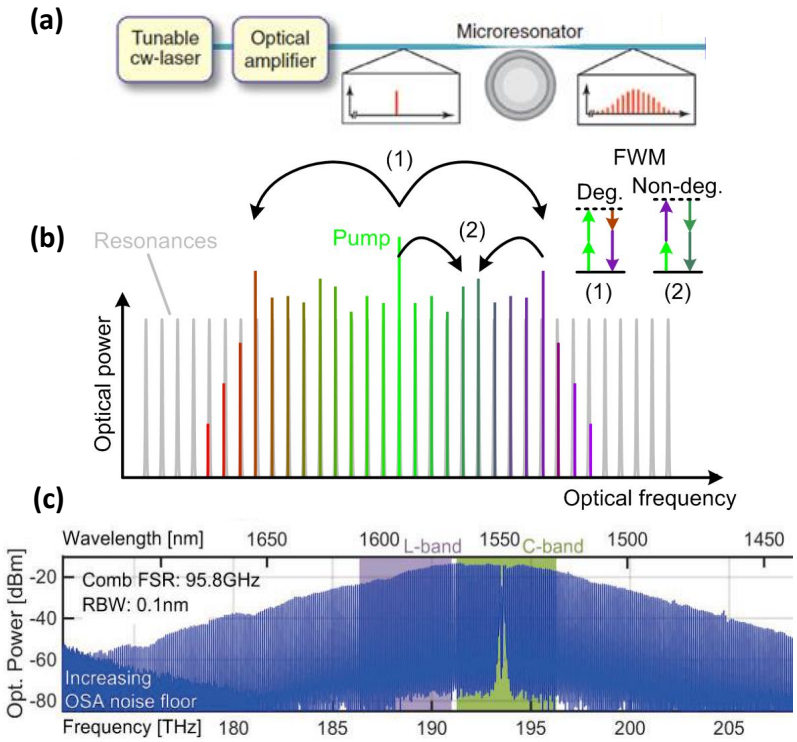

Figure 2.2: (a) Experimental set up for Microresonator based Kerr comb generation, (b) Representation of cascaded FWM processes in microresonator. Deg: degenerated FWM, Non-deg: Non-degenerated FWM. (c) Optical spectrum of a Microresonator based Kerr comb. Adapted from: [23], [25], [28]

Microresonator based Kerr OFCS characteristics

The optical spectrum of a microresonator based Kerr OFCS, illustrated in Figure 2.2 (c), expands over hundreds of nanometres, covering multiple telecommunication bands (such as the C and L) [29]. Kerr combs exhibit good OCNR, phase correlation [30] and low phase noise that matches the pump laser phase noise [31] which have enabled experimental coherent transmissions of up to 1.44 Tb/s [23]. Nevertheless, the obtained comb spectrum and phase noise depend precisely on

the pump power, polarization and wavelength detuning with respect to the cavity resonance, which have to be carefully and finely adjusted [24] to obtain maximum frequency conversion efficiency and optimum phase correlation. Moreover, stable long-term operation requires feedback control loops that locks the wavelength of the pump laser and maintain the microresonator power coupling efficiency stabilized [23].

Although microresonator based Kerr combs are very compact integrated devices, the strong optical pump power (>30 dBm [23]- [25], [29]) hamper the co-integration of the pump laser and microresonator on a single chip. Therefore, due to the intricate tuning process, difficulties for stable operation and integration, and fixed FSR determined by the resonator cavity, Kerr combs are currently far from commercial network deployment.

2.4 Parametric OFCS

A versatile OFCS intended for optical networks requires FSR and central wavelength adjustment, especially in future Flexible Networks, features not presented in MLLs and Kerr combs where the FSR is fixed by the cavity length.

Parametric OFCS generation is obtained from efficient cascaded FWM processes, also known as parametric mixing, in Highly Non-Linear Fibre (HNLF). In the simplest configuration, two free-running Continuous Wave (CW) pumps are used to seed a multi-stage parametric mixer formed by spans of HNLF and Standard Single Mode Fibre (SSMF) [32]. This cavity-less OFCS technique offers intrinsic FSR flexibility defined by the frequency spacing between the pump lasers. Numerous research studies have proposed various configurations for parametric OFCS generation [33]- [37] with focus on broad bandwidth [33], reduced pumping power [34], enhanced flatness [35], flexibility [36], and phase noise and correlation [32], [37]. The technique considered as the most suitable and that accomplishes the majority of desired requirements for optical networks is presented in Figure 2.3 (a).

A low linewidth CW master laser is phase modulated to obtain phase-correlated sidebands. Two slave lasers, that will act as the two CW comb seeds, are then each locked to a master sideband inheriting the master laser phase and thus, guaranteeing a high degree of phase correlation. In contrast to using free-running pumps, this approach with phase-correlated seeds ensures that the linewidth will be preserved and avoids linewidth broadening through phase-matched FWM processes [32]. In addition, locking of these slave lasers also provides improved OCNR, higher output power and

reduced RIN [32], [38] dictated by the slave lasers. Subsequently, the slave signals are further amplified, coupled and launched into the parametric mixer, consisting of multiple stages, with three HNLF and two SSMF. The obtained optical comb spectrum is shown in Figure 2.3 (b).

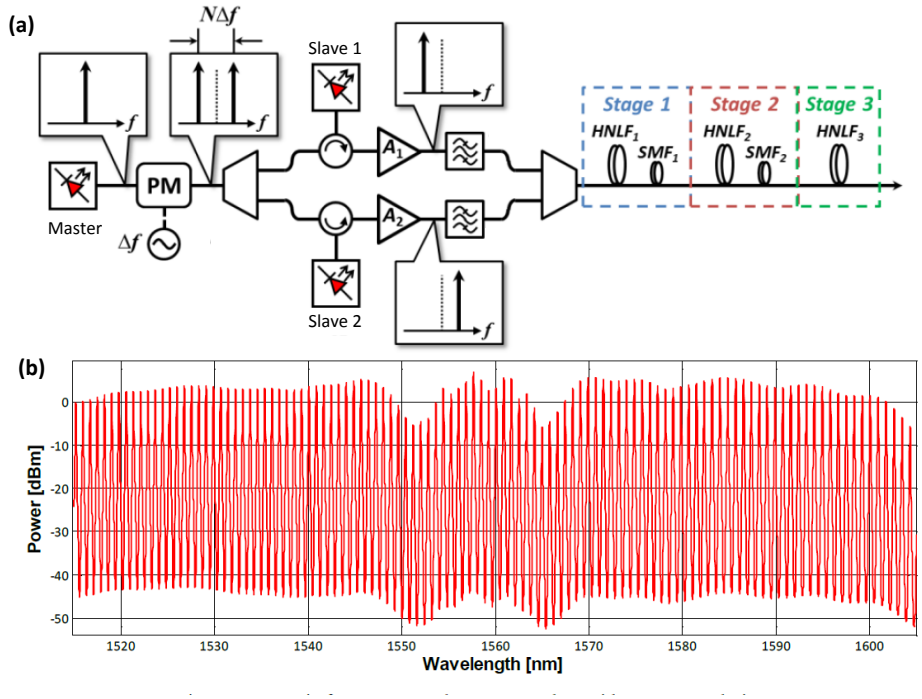

Figure 2.3: (a) Experimental set up for parametric comb generation. PM: phase modulator, A1, A2: amplifiers. (b) Optical spectrum of a parametric comb. After: [37]

Parametric OFCS characteristics

Parametric OFCS are capable of spanning hundreds of nanometres while offering tuneable FSR, overcoming the main limitation of MLLs and Kerr combs. Furthermore, the comb tones also present high power per line, good OCNR ($>$ 40 dB), low RIN and low phase noise transferred from the seeding laser. Due to these advantages, a commercial bench-top parametric OFCS has been recently developed by the company *RAM Photonics*.

However, this technology is costly and presents some associated implementation challenges, such as high component count, complexity, precise dispersion engineered fibres, and the inability for full chip scale integration which may prevent their adoption in communication systems, particularly in the future datacentre sector.

2.5 Electro-optic Modulator based OFCS

Electro-optic modulator based OFCS configurations comprise a laser in CW operation passed through one or multiple electro-optic modulators non-linearly driven by large amplitude sinusoidal RF signals. This large signal modulation (multiples of V_π), which requires the use of high-power RF amplifiers, introduces higher-order modulation harmonics of the driving RF signal around the optical frequency defined by the input laser. Hence, the resultant OFCS properties are dictated by the tunability and noise characteristics of the laser used, RF sinusoidal signal, modulators, and RF amplifiers.

However, electro-optic modulator based comb generation does not typically present broad bandwidth and good flatness, as the generated harmonics present irregular amplitude distribution conforming to Bessel functions. This can be explained and demonstrated considering the case of a single phase modulator driven by a large sinusoidal signal where the output signal can be expressed as:

$$E_0(t) = A(t) \cdot e^{j(w_0 t + \phi(t) + \beta \sin \Omega t)} \tag{2.1}$$

where $A(t) \cdot e^{j(w_0 t + \phi(t))}$ is the electric field of the input laser with A, w_0 and ϕ being the amplitude, angular frequency and phase, respectively. β and Ω are the amplitude and angular frequency of the large phase modulating sinusoidal signal.

Using the following Jacobi-Anger expansion [39]:

$$\mathrm{e}^{jz \sin \theta} = \sum_{n=-\infty}^{\infty} J_n(z) \mathrm{e}^{jn\theta} \tag{2.2}$$

where J_n is the n_{th} order first kind Bessel function:

$$E_0(t) = \sum_{n=-\infty}^{\infty} A(t) J_n(\beta) \mathrm{e}^{j(w_0 t + n\Omega t + \phi(t))} \tag{2.3}$$

As observed, the output signal demonstrates that multiple harmonics (comb tones) appear centred around the optical carrier with amplitudes dictated by Bessel functions.

Numerous electro-optic modulators configurations have been reported in the literature for comb flattening and expansion [40]- [45], as shown in Figure 2.4.

Better OFCS spectral flatness can be obtained by employing a single phase modulator driven with combined RF signals with different amplitudes and frequencies [40], as shown in Figure 2.4 (a) or by cascading several phase modulators, as in Figure 2.4 (b) [39], [41]. Dual drive MZM allows the optical non-flat spectra obtained from each phase modulator in the interferometric arms to become complementary by adjustment of amplitudes, frequencies and phases of the modulating signal ap-

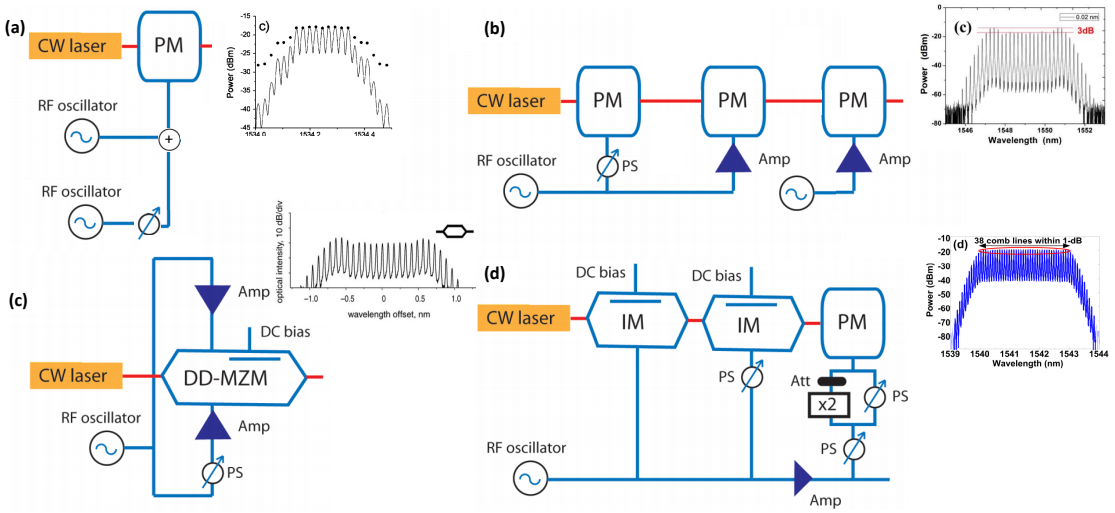

Figure 2.4: Electro-optic modulator based comb generation configurations and spectra: (a) Using a single phase modulator with combined RF signals [40], (b) cascaded phase modulators [39], (c) dual-drive Mach-Zehnder Modulator (MZM) [43] and (d) combination of cascaded intensity and phase modulators [45]. PM: phase modulator, Amp: RF amplifier, PS:phase shifter, IM: intensity modulator, Att: attenuator. Adapted from: [46]

plied, resulting in a combined flat optical comb spectrum illustrated in Figure 2.4 (c) [42], [43]. Cascading several MZMs presents similar performance to the case of phase modulators in tandem. Among all the different proposed configurations, a combination of intensity modulators and phase modulators probably is the most balanced configuration in terms of complexity, flatness, and tuning flexibility [44], [45] as illustrated in Figure 2.4 (d).

Electro-optic Modulator based OFCS characteristics

These OFCSs, although significantly bandwidth limited compared to previous presented techniques, are particularly flexible, present good noise properties and proved potential for integration which are all key features for network deployment. The central wavelength tunability, and RIN and phase noise of the resultant comb are determined exclusively by the external seeding CW laser. The FSR is also adjustable via the modulation frequency, and only limited by the maximum bandwidth of modulators and RF amplifiers used.

Nevertheless, a number of cascaded modulators are required to obtain a spectrally broad and flat comb, which translates into increased overall power consumption, elevated insertion losses that degrade the comb tones OCNR and poor stability. Feedback control loops can be created to com-

pensate for stability issues, such as bias drifts [47], but the extra complexity and power consumption may hinder their implementation in real systems. Recent research efforts on the photonic integration of electro-optic modulators have proved that Indium Phosphide (InP) [48] and Silicon-Organic Hybrid (SOH) based modulators can be used for comb generation [49]. A single SOH modulator driven with two large RF signals (23 dBm and 28 dBm) has shown 7 comb lines in a 3 dB spectral flatness with 40 GHz frequency spacing [50]. The large 21 dB insertion loss of the device is a major practical impediment, resulting in limited OCNR and low output powers between -27 dBm and -17 dBm per comb line.

2.6 Gain Switched OFCS

Gain switching is a technique that produces optical pulses, and consequently optical frequency combs, by directly modulating a semiconductor laser with a large amplitude RF signal [51]- [53]. This technique emerged in 1980 with the observation of the relaxation oscillation phenomenon [54], which is a dynamic process occurring in a semiconductor laser when biased abruptly. As a result, carrier and photon densities present a transient response with damped oscillations before reaching a steady state with continuous emission of light, as depicted in Figure 2.5 (a). Gain switching consists of forcing the laser to work in this non-linear regime continuously, switching it quickly from below to above threshold. The large RF signal is deliberately truncated before the second oscillation spike of the photon density appears, and only enabling the first spike of the relaxation oscillation to be excited. By repeating this process periodically, an optical pulse train is generated at the rate of the RF signal, as illustrated in Figure 2.5 (b). As observed, the injection current initially builds up the carrier density. The photon density does not start to grow until the carrier density reaches its threshold value, where lasing occurs. Then, the photon population rapidly increases through recombination, and thus, the carrier density starts to deplete which consequently reduces the photon density and leads to an optical pulse emission. The delay before the photon density builds up is known as *turn-on delay*, (t_d), which favourably impacts pulse generation, as the obtained optical pulse is considerably shorter than the half-period of the RF electrical signal applied.

Gain switching initially stirred a substantial attention for pulse generation. Due to the extensive increase of Internet data traffic and the relevance of multicarrier transmitters for better spectral efficiency, gain switching has been recently proposed as a comb generation scheme with first notable demonstrations reported in 2009 [55], [56]. Figure 2.6 (a) illustrates the experimental set up for

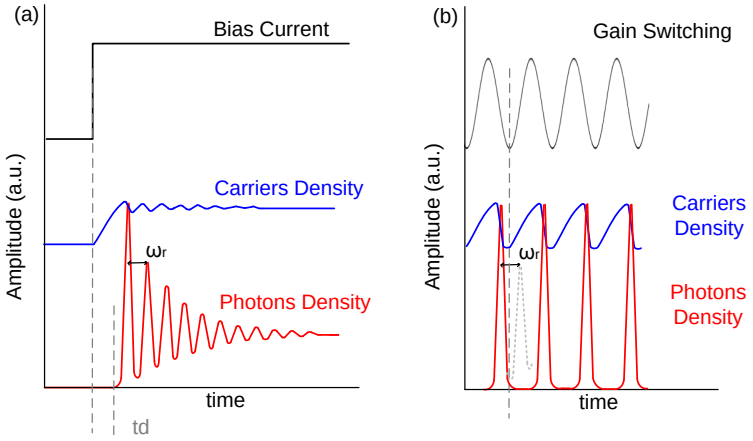

Figure 2.5: (a) Illustration of relaxation oscillation phenomenon in semiconductor lasers, (b) Gain switching principle of operation. t_d is the turn-on delay, w_r is the relaxation oscillation frequency.

Gain Switched Optical Frequency Comb Source (GS-OFCS) generation where a single mode semiconductor laser is driven by an amplified RF sinewave in conjunction with a dc bias current. The obtained OFCS is observed in Figure 2.6 (b) and presents eight comb tones in a 3 dB spectral ripple flatness where the FSR is determined by the frequency of the RF sinewave.

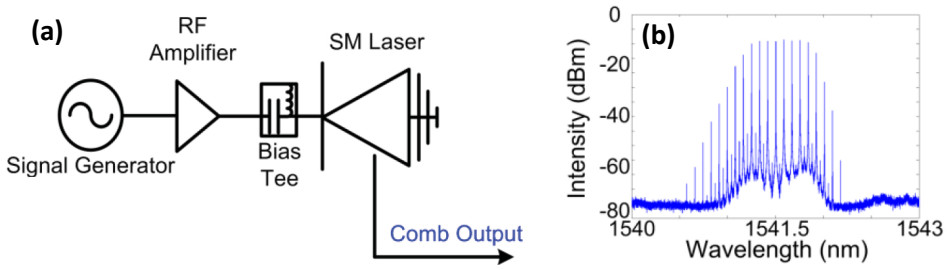

Figure 2.6: (a) Experimental set up for gain switched comb generation, (b) Optical spectrum of a gain-switched OFCS. SM: single mode. After: [61]

2.6.1 Principle of operation

Gain switching is the chosen technology for comb generation in this thesis. This section presents a basic theoretical analysis of the transient response of semiconductor lasers which serves as a basis for understanding the principle of operation of gain switching.

The dynamic behaviour of a semiconductor laser is given by a set of non-linear rate equations, which define the relationship between carrier and photon densities inside a laser cavity. The basic rate equations for a single mode laser can be written as [57]:

$$\frac{\partial N}{\partial t} = \frac{I(t)}{eV} - \frac{N}{\tau_e} - g(N - N_0)S \tag{2.4}$$

$$\frac{\partial S}{\partial t} = \Big[g(N - N_0) - \frac{1}{\tau_p}\Big]S + \beta\frac{N}{\tau_e} \tag{2.5}$$

where N is the carrier density, $I(t)$ is the time dependent injected bias current which consists of $I(t) = I_{bias} + I_{RF}\sin(2\pi f_{RF}t)$ to account for the gain switching signal, e is the electron charge, V is the volume of the laser active region, τ_e, denotes the carrier lifetime, g is the gain constant, N_0 is the carrier density at transparency, S is the photon density, τ_p is the photon lifetime and β is the spontaneous emission coupling factor.

The physical meaning of these rate equations are intuitively explained:

- Equation 2.4 describes the carrier density evolution with time. The first term refers to the contribution of carriers by the injected bias current applied to the laser, the second term defines the losses in the carrier density (as it is a negative term) due to spontaneous emission and the last term denotes the decay of carriers by recombination due to stimulated emission.
- Equation 2.5 describes the photon density evolution with time. The first term corresponds to the number of photons created by stimulated emission depending directly on the carrier density that induce them and the decay of photons from losses in the cavity. The last term refers to the spontaneously emitted photons that are coupled to the laser output.

The dynamics involved during the turn-on of a semiconductor laser diode are now considered, where a step current $I(t)$ is applied and, consequently, the carrier and photon densities can be considered to be disturbed around their steady state value [5], [58], which is mathematically described as:

$$N = \bar{N} + \delta N \tag{2.6}$$

$$S = \bar{S} + \delta S \tag{2.7}$$

where $\bar{N}$ and $\bar{S}$ are the steady state values, and δN and δS are the transient perturbations around the steady states for the carrier and photon densities, respectively. A detailed mathematical derivation of these equations is presented in Appendix B.

Substituting these expressions in the rate equations 2.4 and 2.5, neglecting second order terms (ie. $\delta N\delta S$) and assuming that the spontaneous emission is negligible:

$$\frac{\partial(\delta N)}{\partial t} = -\delta N(g\bar{S} + \frac{1}{\tau_e}) - \frac{\delta S}{\tau_p} \tag{2.8}$$

$$\frac{\partial(\delta S)}{\partial t} = \delta N g\bar{S} \tag{2.9}$$

The transient response of the photon density can be obtained by differentiating 2.9 with respect to time, and substituting $\frac{\partial(\delta N)}{\partial t}$ with the expression in 2.8 and δN with $\delta N = \frac{\partial(\delta S)}{\partial t}\frac{1}{g\bar{S}}$ from 2.9.

$$\frac{\partial^2 \delta S}{\partial t^2} + \frac{\partial \delta S}{\partial t}(g\bar{S} + \frac{1}{\tau_e}) + \frac{\delta S}{\tau_p} g\bar{S} = 0 \tag{2.10}$$

Equation 2.10 corresponds to a second order homogeneous differential equation that resembles the equation of the transient response of a second order system:

$$\frac{\partial^2(\delta S)}{\partial t^2} + 2\xi w_r \frac{\partial(\delta S)}{\partial t} + {w_r}^2 \delta S = 0 \tag{2.11}$$

where w_r is the undamped natural frequency, or relaxation oscillation frequency, and ξ is the damping ratio. An analogous expression can be obtained for the carrier density. The solution for the differential equation 2.11 can be expressed as [59]:

$$\delta S(t) = Ce^{-\xi w_r t} \sin([w_r \sqrt{1-\xi^2}]t) \tag{2.12}$$

where C is a constant that can be chosen to satisfy the initial conditions. Therefore, the photon density exhibits oscillations during the laser turn-on that decay accordingly until the steady state is achieved, as it was represented in Figure 2.5.

Comparing equations 2.11 and 2.12, the relaxation oscillation frequency can be expressed as 2.13. Additionally, the relaxation oscillation directly depends on the steady state of the photon density $\bar{S}$ which is proportional to the bias current applied to the laser I_{bias} [5]. As such, higher relaxation oscillation frequencies and thereby, higher range of FSR can be obtained by maximizing the relative bias current to the threshold current I_{th} and by decreasing the photon lifetime which is viable by using short cavity length laser diodes [5], [60].

$$w_r = \sqrt{\frac{g\bar{S}}{\tau_p}} = \sqrt{\frac{g(I_{bias} - I_{th})}{eV}} \tag{2.13}$$

GS-OFCS characteristics

Compared to previous comb schemes discussed in this chapter, the most significant advantages of GS-OFCS are the outstanding simplicity, cost efficiency, and stability while keeping FSR tunability [61]. The obtained number of comb tones from a GS-OFCS is comparable to cascaded electro-optic modulator based combs while the possible power per comb tone is still high (>0 dBm) as the gain switched laser power gets distributed between the comb tones without requiring additional lossy components. The frequency spacing is set by the RF signal frequency and therefore, precise and flexible FSR is easily achieved, but limited by the modulation frequency response of the gain

switched laser which dictates the maximum FSR range. The central wavelength of the comb is defined by the fixed laser emission wavelength, although restricted wavelength tunability ($\sim$ 2 nm) can be obtained through temperature or bias current tuning.

However, the major shortcomings with this proposed direct modulation technique are the large pulse temporal jitter and large phase noise of the comb lines, in excess of that of the CW laser [62], as a result of bringing the laser below threshold on every cycle of the gain switching process. These flaws limit its employability in systems employing advanced modulation formats but have been solved by employing optical external injection, which further improves the feasibility and quality of this comb generation technique by decreasing noise properties and enhancing flexibility with substantial potential for integrability and network deployment.

2.6.2 Optical external injection

Optical external injection [63]- [65] consists in coupling light from an optically isolated external laser source, usually named as master laser, into the cavity of a laser known as slave to improve its performance, typically in terms of modulation response enhancement [66]- [69], mode selectivity [70], and noise and frequency chirp reduction [71]- [73]. Thus, optical external injection disturbs the operating characteristics of the slave by introducing the master oscillating field into its cavity where these two fields may couple, producing a variety of interactions from non-linear processes that include beatings and FWM to an injection locking state. Under injection locking, the master lasing mode dominates and forces the slave to oscillate at the master laser frequency and phase, inheriting its noise properties. It is then said that the slave is *injection locked* to the master laser.

These non-linear interactions are determined by the used optical detuning Δw, defined as the frequency difference between master and slave lasing fields, and by the injected power ratio R which is the ratio of master (injected) and CW slave lasing powers. As such, if a low injected power or an excessive detuning is used, both lasers may interact and various parametric processes may appear, resulting in an un-locking state. Under a certain range of detuning and injected power ratio, known as the injection locking range, the stable injection locking state is achieved where a synchronization of both lasers is reached and master noise properties are transferred to the slave laser, which is of interest in this work.

Externally injected GS-OFCS can be mathematically described by the following modified rate equations that include the injection terms and where $I(t) = I_{bias} + I_{RF}\sin(2\pi f_{RF}t)$ to account for the

gain switching signal [64], [65], [74].

$$\frac{\partial N}{\partial t} = \frac{I(t)}{eV} - \frac{N}{\tau_e} - g(N - N_0)S \tag{2.14}$$

$$\frac{\partial S}{\partial t} = \Big[g(N - N_0) - \frac{1}{\tau_p}\Big]S + \beta\frac{N}{\tau_e} + 2k_c\sqrt{S_{inj}S}\cos(\phi - \phi_{inj}) \tag{2.15}$$

$$\frac{\partial \phi}{\partial t} = \frac{1}{2}\alpha g(N - N_0) - k_c\sqrt{\frac{S_{inj}}{S}}\sin[\phi - \phi_{inj}] - \Delta w \tag{2.16}$$

where the new terms are: k_c is the injection coupling coefficient, S_{inj} denotes the injected photon density, α is the linewidth enhancement factor, the detuning Δw is the frequency difference between the CW master and CW slave lasers, and ϕ and ϕ_{inj} are the phase of the slave and master injected optical fields, respectively. Clearly, by simply setting the injection terms to zero the equations revert back to 2.4 and 2.5.

Optical external injection is an extensive area of study with complex non-linear processes, widely investigated theoretically and experimentally over the last three decades [63]- [73]. A detailed analysis of this phenomenon is out of scope of this research. In this work, optical external injection is solely used empirically to enhance gain switched comb generation parameters, as illustrated in the experimental set up in Figure 2.7 (a) where a master tunable laser with low RIN and linewidth is externally injected into a gain switched slave laser, specifically a short cavity multimode Fabry-Pérot (FP) laser diode. Then, the comb tones inherit the low noise properties from the master laser.

In gain switching without optical injection, each pulse builds up from random spontaneous emission [62] and thereby, there is an arbitrary delay between pulses which is observed as a large amount of temporal jitter. In addition, due to the laser being driven below threshold on each cycle, and the pulses building up from spontaneous emission, the optical comb lines generated have excess phase noise. However, during optical external injection, a continuous rate of photons much larger than the spontaneously emitted photons are injected into the slave cavity and then, each pulse builds up from the injected photons through stimulated emission. Therefore, the successive pulses have a constant delay and are phase-locked to the master laser, ensuring pulse-to-pulse coherence [62].

If the FP slave laser is externally injected at an appropriate wavelength that matches one of the longitudinal modes, the mode subjected to the injection dominates over the others longitudinal modes which get suppressed [70]. Therefore, the FP laser is in a single mode operation at the same frequency of the injected signal. Simultaneous gain switching results in comb generation around

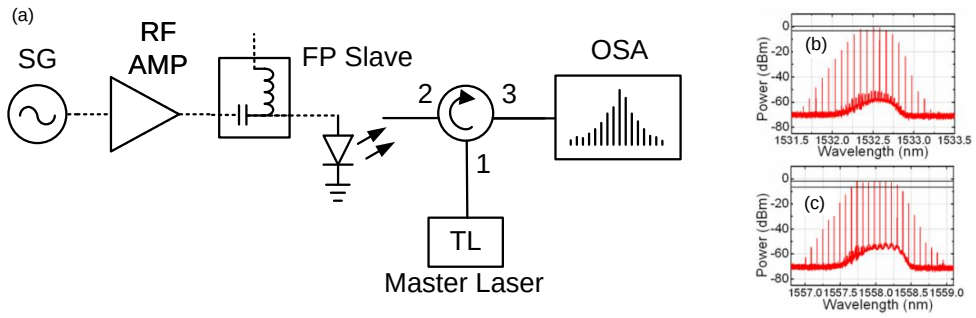

Figure 2.7: (a) Experimental set up for externally injected GS-OFCS with wavelength tunability, by using a FP laser a slave. (b) and (c) Optical spectra of externally injected GS-OFCS at central wavelengths of 1532.5 nm and 1558 nm. After: [75]

the injection locked single longitudinal mode. As a result, central wavelength tunability can be obtained by tuning the injection into different FP longitudinal modes [75], as illustrated in Figures 2.7 (b) and (c). Nevertheless, this achievable wavelength tunability would be discrete and localized at those wavelengths were the FP laser exhibits a longitudinal mode limiting the flexibility.

Finally, optical injection has been proven to provide an enhancement of the relaxation oscillation frequency [66]- [69] by up to three times. As previously presented, the relaxation oscillation frequency originates from the laser dynamic intrinsic interplay between carrier and photon densities. Strong optical injection can push the relaxation oscillation frequency towards high values way beyond the intrinsic capability of the slave laser. Therefore, externally injected gain switched combs exhibit highly increased FSR tunability range, demonstrated up to 33 GHz [76], overcoming the slave modulation response limitation.

2.6.3 Externally injected GS-OFCS characteristics

Externally injected GS-OFCSs offer flexible FSR (up to 33 GHz [76]) determined by the frequency of the sinusoidal modulation, discrete central wavelength tunability [75], and low RIN and phase noise transferred from the external injection [77]. The comb tones present excellent phase correlation and high OCNR >35 dB with an optical power per comb tone >0 dBm. This simple technique requires low component count and no sophisticated devices or fabrication process. It relies on the direct modulation and external injection of any commercially available laser diode, employing mature and well-established technologies. Furthermore, this master-slave configuration lends itself to monolithic integration which would further reduce the device footprint and increase the comb source cost-efficiency. As such, externally injected GS-OFCSs significantly meet the majority of

appealing requirements for future multicarrier sources, and could be deployed throughout the network in high capacity and also in flexible communication systems due to their versatility.

However, remaining constraints of this comb generation technique are: localized wavelength tunability, non-reconfigurability and performance inconsistency due to required manual optimizations that ensure injection locking and synchronization between the two lasers involved, and substantially reduced number of comb tones (optical bandwidth). All these issues are the focus of this thesis, in conjunction with an investigation of the de-multiplexing of the comb lines for modulation, resultant features and noise properties after photonic integration and performance in transmission system implementations. These objectives will be experimentally addressed in the following chapters to further enhance the usefulness and potential of these comb sources for imminent network deployment.

2.7 Conclusions

This chapter has reviewed several comb generation techniques and identified their main features for their use in high capacity, spectrally efficient and flexible optical networks.

Each technique offers its own desirable qualities and constraints. MLLs, microresonator based Kerr combs and parametric combs successfully generate large optical bandwidths, composed of hundreds of comb tones. However, MLLs typically suffer from fixed FSR, and large phase noise and RIN at low frequencies. Kerr combs that also present fixed FSR, and parametric combs overcome these significant noise limitations, but on the contrary, they exhibit current implementation challenges such as complexity, elevated pumping powers, difficulties for stable operation and inability of full chip integration. Electro-optic based combs and externally injected gain-switched combs, although unable to generate comparable number of carriers, provide remarkable flexibility, noise properties and potential for photonic integration, with the latter technique showing superior simplicity and stability. This makes comb generation based on gain switching an attractive and competitive technology for communication systems.

References

[1] T. Shao, H. Shams, P. M. Anandarajah, M. J. Fice, C. C. Renaud, F. van Dijk, A. J. Seeds, and L. P. Barry, "Phase Noise Investigation of Multicarrier Sub-THz Wireless Transmission System Based on an Injection-Locked Gain-Switched Laser," *IEEE Transactions on Terahertz Science and Technology*, vol. 5, no. 4, pp. 590–597, July 2015.

[2] B. Jerez, P. Martín-Mateos, E. Prior, C. de Dios, and P. Acedo, "Dual optical frequency comb architecture with capabilities from visible to mid-infrared," *Optics Express*, no. 24, pp. 14986–14994, 2016.

[3] V. Vujicic, C. Calo, R. Watts, F. Lelarge, C. Browning, K. Merghem, A. Martinez, A. Ramdane and L. P. Barry, "Quantum Dash Mode-Locked Lasers for Data Centre Applications," *IEEE Journal of Selected Topics in Quantum Electronics*, vol. 21, no. 6, pp. 53–60, Dec. 2015.

[4] P. Zhu, J. Li, L. Niu, Y. Xu, Y. Chen, X. Xie, X. Chen, B. Guo, Z. Chen, and Y. He, "Optical Comb-enabled Cost-effective ROADM Scheme for Elastic Optical Networks," in *Proceedings of Optical Fiber Communication Conference*, San Francisco, CA, paper W3B.5, 2014.

[5] G. P. Agrawal, "Fiber-Optic Communication Systems," 3rd ed.: Wiley, 2002.

[6] W. E. Lamb, "Theory of an optical maser," *Physical Review Letters*, vol. 134, no. 6A, pp. A1429, Jan. 1964.

[7] H. A. Haus, "Mode-Locking of Lasers," *Journal on Selected Topics in Quantum Electronics*, vol. 6, no. 6, pp. 1173–1185, Nov. 2000.

[8] L. A. Gomes, L. Orsila, T. Jouhti and O. G. Okhotnikov, "Picosecond SESAM-based ytterbium mode-locked fiber lasers," *IEEE Journal of Selected Topics in Quantum Electronics*, vol. 10, no. 1, pp. 129–136, Jan. 2004.

[9] L. Hargrove, R. Fork, and M. Pollack, "Locking of he:ne laser modes induced by synchronous

intracavity modulation," *Applied Physics Letters*, vol. 5, no. 1, pp. 4–5, July 1964.

[10] R. Koumans, R. van Roijen, "Theory for passive mode-locking in semiconductor laser structures including the effects of self-phase modulation, dispersion, and pulse collisions," *Journal of Quantum Electronics*, vol. 32, no. 3, pp. 478–492, March 1996.

[11] J. Renaudier, G.-H. Duan, P. Landais, P. Gallion, "Phase Correlation and Linewidth Reduction of 40 GHz Self-Pulsation in Distributed Bragg Reflector Semiconductor Lasers," *IEEE Journal of Quantum Electronics*, vol. 43, no. 2, pp. 147–156, Feb. 2007.

[12] Massachusetts Institute of Technology Open Courseware, Electrical Engineering and Computer Science, Ultrafast Optics Course, Chapter 5: Active Mode-locking, 2005. Available: https://ocw.mit.edu/courses/electrical-engineering-and-computer-science/6-977-ultrafast-optics-spring-2005/lecture-notes/chapter5.pdf

[13] F. Lelarge, B. Dagens, J. Renaudier, R. Brenot, A. Accard, F. van Dijk, D. Make, O. Le Gouezigou, J.-G. Provost, F. Poingt, J. Landreau, O. Drisse, E. Derouin, B. Rousseau, F. Pommereau, and G.-H. Duan, "Recent advances on InAs/InP Quantum Dash based semiconductor lasers and optical amplifiers operating at 1.55 μm," *IEEE Journal of Selected Topics in Quantum Electronics*, vol. 13, no. 1, pp. 111–124, Feb. 2007.

[14] M. G. Thompson, A. R. Rae, M. Xia, R. V. Penty and I. H. White, "InGaAs Quantum-Dot Mode-Locked Laser Diodes," *IEEE Journal of Selected Topics in Quantum Electronics*, vol. 15, no. 3, pp. 661–672, May 2009.

[15] T. Habruseva, S. O'Donoghue, N. Rebrova, F. Kéfélian, S. P. Hegarty, and G. Huyet, "Optical linewidth of a passively mode-locked semiconductor laser," *Optics Letters*, vol. 34, pp. 3307–3309, 2009.

[16] R. T. Watts, S. G. Murdoch and L. P. Barry, "Spectral linewidth reduction of single-mode and mode-locked lasers using a feed-forward heterodyne detection scheme," in *Proceedings of Conference on Lasers and Electro-Optics (CLEO)*, San Jose, CA, paper STh3O.8, 2014.

[17] E. Sooudi, S. Sygletos, A. D. Ellis, G. Huyet, J. G. McInerney, F. Lelarge, K. Merghem, R. Rosales, A. Martinez, A. Ramdane, and S. Hegarty, "Optical frequency comb generation using dual-mode injection-locking of quantum-dash mode-locked lasers: Properties and applications," IEEE J. Quantum Electron. 48, 1327–1338(2012).

[18] V. Panapakkam, A. P. Anthur, V. Vujicic, R. Zhou, Q. Gaimard, K. Merghem, G. Aubin, F.

Lelarge, E. A. Viktorov, L. P. Barry, and A. Ramdane, "Amplitude and Phase Noise of Frequency Combs Generated by Single-Section InAs/InP Quantum-Dash-Based Passively and Actively Mode-Locked Lasers," *IEEE Journal of Quantum Electronics*, vol. 52, no. 11, pp. 1–7, Nov. 2016.

[19] Cosimo Calò, Vidak Vujicic, Regan Watts, Colm Browning, Kamel Merghem, Vivek Panapakkam, Francois Lelarge, Anthony Martinez, Badr-Eddine Benkelfat, Abderrahim Ramdane, and Liam P. Barry, "Single-section quantum well mode-locked laser for 400 Gb/s SSB-OFDM transmission," *Optics Express*, vol. 23, pp. 26442-26449, 2015.

[20] Vidak Vujicic, Aravind P. Anthur, Arsalan Saljoghei, Vivek Panapakkam, Rui Zhou, Quentin Gaimard, Kamel Merghem, Francois Lelarge, Abderrahim Ramdane, and Liam P. Barry, "Mitigation of relative intensity noise of quantum dash mode-locked lasers for PAM4 based optical interconnects using encoding techniques," *Optics Express*, vol. 25, pp. 20–29, Jan. 2017.

[21] G. P. Agrawal, "Mode-partition noise and intensity correlation in a two-mode semiconductor laser," *Physical Review A*, vol. 37, no. 7, 2488, April 1988.

[22] N. Rebrova, T. Habruseva, G. Huyet, and S. P. Hegarty, "Stabilization of a passively mode-locked laser by continuous wave optical injection," *Applied Physics Letters*, vol. 97, 101105, 2010.

[23] J. Pfeifle, V. Brasch, M. Lauermann, Y. Yu, D. Wegner, T. Herr, K. Hartinger, P. Schindler, J. Li, D. Hillerkuss, R. Schmogrow, C. Weimann, R. Holzwarth, W. Freude, J. Leuthold, T. J. Kippenberg, and C. Koos, "Coherent terabit communications with microresonator Kerr frequency combs," *Nature Photonics*, vol. 8, pp. 375–380, April 2014.

[24] J. Pfeifle, M. Lauermann, D. Wegner, J. Li, K. Hartinger, V. Brasch, T. Herr, D. Hillerkuss, R. M. Schmogrow, T. Schimmel, R. Holzwarth, T. J. Kippenberg, J. Leuthold, W. Freude, and C. Koos, "Microresonator-Based Frequency Comb Generator as Optical Source for Coherent WDM Transmission," in *Proceedings of Optical Fiber Communication Conference/National Fiber Optic Engineers Conference*, Anaheim, CA, paper OW3C.2, 2013.

[25] J. Pfeifle, A. Kordts, P. Marin, M. Karpov, M. Pfeiffer, V. Brasch, R. Rosenberger, J. Kemal, S. Wolf, W. Freude, t. kippenberg, and C. Koos, "Full C and L-Band Transmission at 20 Tbit/s Using Cavity-Soliton Kerr Frequency Combs," in *Proceedings of Conference on Lasers and Electro-Optics*, San Jose, CA, Postdeadline Paper, paper JTh5C.8, 2015.

[26] P. Del'Haye, A. Schliesser, O. Arcizet, T. Wilken, R. Holzwarth, and T. J. Kippenberg, "Op-

tical frequency comb generation from a monolithic microresonator," *Nature*, vol. 450, pp. 1214, Dec. 2007.

[27] A.M. Scott, "Four wave mixing due to the optical kerr effect and Rayleigh-wing scattering," *Optics Communications*, vol. 45, no. 3, pp. 207–210, 1983.

[28] T. J. Kippenberg, R. Holzwarth, and S. A. Diddams, "Microresonator-Based Optical Frequency Combs," *Science*, vol. 332, pp. 555–559, Apr. 2011.

[29] P. Marin, J. Pfeifle, M. Karpov, P. Trocha, R. Rosenberger, K. Vijayan, S. Wolf, J. N. Kemal, A. Kordts, M. Pfeiffer, V. Brasch, W. Freude, T. Kippenberg, and C. Koos, "50 Tbit/s Massively Parallel WDM Transmission in C and L Band Using Interleaved Cavity-Soliton Kerr Combs," in *Proceedings of Conference on Lasers and Electro-Optics*, San Jose, CA, paper STu1G.1, 2016.

[30] J. Li, H. Lee, T. Chen, and K. J. Vahala, "Low-Pump-Power, Low-Phase-Noise, and Microwave to Millimeter-Wave Repetition Rate Operation in Microcombs," *Physical Review Letters*, vol. 109, no. 23, 233901, Dec. 2012.

[31] P. Liao, C. Bao, A. Kordts, M. Karpov, M. H. P. Pfeiffer, L. Zhang, A. Mohajerin-Ariaei, Y. Cao, A. Almaiman, M. Ziyadi, S. R. Wilkinson, M. Tur, T. J. Kippenberg, and A. E. Willner, "Dependence of a microresonator Kerr frequency comb on the pump linewidth," *Optics Letters*, vol. 42, pp. 779–782, Feb. 2017.

[32] Z. Tong, A. O. J. Wiberg, E. Myslivets, B. P. P. Kuo, N. Alic, and S. Radic, "Spectral linewidth preservation in parametric frequency combs seeded by dual pumps," *Optics Express*, vol. 20, pp. 17610–17619, 2012.

[33] J. M. Chavez Boggio, S. Moro, N. Alic, M. Karlsson, J. Bland-Hawthorn and S. Radic, "Nearly octave-spanning cascaded four-wave-mixing generation in low dispersion highly nonlinear fiber," in *Proceedings of European Conference on Optical Communications*, Vienna, pp. 1-2, 2009.

[34] E. Myslivets, B. P.P. Kuo, N. Alic, and S. Radic, "Generation of wideband frequency combs by continuous-wave seeding of multistage mixers with synthesized dispersion," *Optics Express*, vol. 20, pp. 3331–3344, 2012.

[35] V. Ataie, B. P. P. Kuo, E. Myslivets and S. Radic, "Generation of 1500-tone, 120nm-wide ultraflat frequency comb by single CW source," in *Proceedings of Optical Fiber Communication Conference and Exposition and the National Fiber Optic Engineers Conference*, Anaheim, CA,

Postdeadline paper, paper PDP5C.1, 2013.

[36] V. Ataie, E. Temprana, L. Liu, Y. Myslivets, P. P. Kuo, N. Alic, and S. Radic, "Flex-grid Compatible Ultra Wide Frequency Comb Source for 31.8 Tb/s Coherent Transmission of 1520 UDWDM Channels," in *Proceedings of Optical Fiber Communication Conference*, San Francisco, CA, Postdeadline Papers, paper Th5B.7, 2014.

[37] E. Temprana, V. Ataie, B. P. P. Kuo, E. Myslivets, N. Alic, and S. Radic, "Low-noise parametric frequency comb for continuous C-plus-L-band 16-QAM channels generation," *Optics Express*, vol. 22, pp. 6822–6828, March 2014.

[38] B. P. P. Kuo, E. Myslivets, V. Ataie, E. G. Temprana, N. Alic and S. Radic, "Wideband Parametric Frequency Comb as Coherent Optical Carrier," *Journal of Lightwave Technology*, vol. 31, no. 21, pp. 3414–3419, Nov. 2013.

[39] J. Zhang, N. Chi, J. Yu, Y. Shao, J. Zhu, B. Huang, and L. Tao, "Generation of coherent and frequency-lock multi-carriers using cascaded phase modulators and recirculating frequency shifter for Tb/s optical communication," *Optics Express*, vol. 19, no. 11, pp. 12891–12902, 2011.

[40] S. Ozharar, F. Quinlan, I. Ozdur, S. Gee, and P. J. Delfyett, "Ultraflat optical comb generation by phase-only modulation of continuous-wave light," *IEEE Photonics Technology Letters* vol. 20, no. 36, pp. 36–38, Jan. 2008.

[41] J. Zhang, J. Yu, N. Chi, Z. Dong, X. Li, Y. Shao, J. Yu, and L. Tao, "Flattened comb generation using only phase modulators driven by fundamental frequency sinusoidal sources with small frequency offset," *Optics Letters*, vol. 38, pp. 552–554, 2013.

[42] T. Sakamoto, T. Kawanishi, and M. Izutsu, "Asymptotic formalism for ultraflat optical frequency comb generation using a Mach-Zehnder modulator," *Optics Letters* vol. 32, no. 11, 1515–1517, Jun. 2007.

[43] T. Sakamoto, T. Kawanishi, and M. Izutsu, "Widely wavelength-tunable ultra-flat frequency comb generation using conventional dual-drive Mach-Zehnder modulator," *Electronic Letters*, vol. 43, no. 19, Sep. 2007.

[44] A. J. Metcalf, V. Torres-Company, D. E. Leaird and A. M. Weiner, "High-Power Broadly Tunable Electrooptic Frequency Comb Generator," *IEEE Journal of Selected Topics in Quantum Electronics*, vol. 19, no. 6, pp. 231–236, Nov. 2013.

[45] R. Wu, V. R. Supradeepa, C. M. Long, D. E. Leaird and A. M. Weiner, "Highly flat and

stable optical frequency comb generation using intensity and phase modulators employing quasi-quadratic phase modulation," in *IEEE International Topical Meeting on Microwave Photonics*, Montreal, QC, pp. 212–215, 2010.

[46] V. Torres-Company and A. M. Weiner, "Optical Frequency Comb Technology for Ultra-Broadband Radio-Frequency Photonics," *Laser and Photonics Reviews*, vol. 8, no. 3, pp. 368–393, 2013.

[47] T. Healy, F. C. G. Gunning, A. D. Ellis, "Multi-wavelength source using low drive-voltage amplitude modulators for optical communications," *Optics Express*, vol. 15, no. 6, pp. 2981–2986, Mar. 2007.

[48] N. Dupuis, C. R. Doerr, L. Zhang, L. Chen, N. J. Sauer, P. Dong, L. L. Buhl, and D. Ahn, "InP-Based Comb Generator for Optical OFDM," *Journal of Lightwave Technology*, vol. 30, no. 4, pp. 466–472, Feb. 2012.

[49] L. Alloatti, R. Palmer, S. Diebold, K. P. Pahl, B. Chen, R. Dinu, M. Fournier, J-M. Fedeli, T. Zwick, W. Freude, C. Koos, J. Leuthold, "100 GHz silicon–organic hybrid modulator," *Nature Photonics*, vol. 3, e173, May 2014.

[50] C. Weimann, P. C. Schindler, R. Palmer, S. Wolf, D. Bekele, D. Korn, J. Pfeifle, S. Koeber, R. Schmogrow, L. Alloatti, D. L. Elder, H. Yu, W. Bogaerts, L. R. Dalton, W. Freude, J. Leuthold, C. Koos, "Silicon-organic hybrid (SOH) frequency comb sources for terabit/s data transmission," *Optics Express*, vol. 22, no. 3, pp. 3629–3637, Feb. 2014.

[51] H. Ito, H. Yokoyama, S. Murata, H. Inaba, "Picosecond optical pulse generation from an R.F. modulated AlGaAs D.H. diode laser," *Electronic Letters*, vol. 15, no. 23, pp. 738–740, 1979.

[52] S. Tarucha and K. Otsuka, "Response of semiconductor laser to deep sinusoidal injection current modulation," *Journal of Quantum Electronics*, vol. 17, no. 5, pp. 810–816, May 1981.

[53] K. Y. Lau, "Gain switching of semiconductor injection lasers," *Applied Physics Letters*, vol. 52, no.4, pp.257, 1988.

[54] P. Torphammar and S. T. Eng, "Picosecond pulse generation in semiconductor lasers using resonance oscillation," *Electronic Letters*, vol. 16, no. 15, pp. 587–589, July 1980.

[55] P. M. Anandarajah, K. Shi, J. O'Carroll, A. Kaszubowska, R. Phelan, L. P. Barry, A. D. Ellis, P. Perry, D. Reid, B. Kelly, and J. O'Gorman, "Phase shift keyed systems based on a gain switched laser transmitter," *Optics Express*, vol. 17, no. 15, pp. 12668–12677, July 2009.

[56] P. M. Anandarajah, R. Maher, Y. Q. Xu, S. Latkowski, J. O'Carroll, S. G. Murdoch, R. Phelan, J. O'Gorman, L. P. Barry, "Generation of Coherent Multicarrier Signals by Gain Switching of Discrete Mode Lasers," *IEEE Photonics Journal*, vol. 3, no. 1, pp. 112–122, Feb. 2011.

[57] P. Paulus, R. Langenhorst and D. Jager, "Generation and optimum control of picosecond optical pulses from gain-switched semiconductor lasers," *IEEE Journal of Quantum Electronics*, vol. 24, no. 8, pp. 1519–1523, Aug. 1988.

[58] A. E. Siegman, "Lasers, University Science Books," Mill Valley, CA, 1986.

[59] P. Blanchard, R. Devaney, and G. R. Hall, "Differential equations," Thomson Brooks/Cole, 2006.

[60] Robert G. Hunsperger, "Integrated Optics: Theory and Technology," Springer Science & Business Media, April 2009.

[61] R. Maher, P. M. Anandarajah, S. K. Ibrahim, L. P. Barry, A. D. Ellis, P. Perry, R. Phelan, B. Kelly, and J. O'Gorman, "Low cost comb source in a coherent wavelength division multiplexed system," in *Proceedings of European Conference and Exhibition on Optical Communications*, Torino, pp. 1-3, 2010.

[62] S. P. Ó Dúill, R. Zhou, P. M. Anandarajah and L. P. Barry, "Analytical Approach to Assess the Impact of Pulse-to-Pulse Phase Coherence of Optical Frequency Combs," *IEEE Journal of Quantum Electronics*, vol. 51, no. 11, pp. 1-8, Nov. 2015.

[63] E. K. Lau, L. J. Wong and M. C. Wu, "Enhanced Modulation Characteristics of Optical Injection-Locked Lasers: A Tutorial," *IEEE Journal of Selected Topics in Quantum Electronics*, vol. 15, no. 3, pp. 618–633, May 2009.

[64] R. Lang, "Injection locking properties of a semiconductor laser," *IEEE Journal of Quantum Electronics*, vol. 18, no. 6, pp. 976–983, June 1982.

[65] F. Mogensen, H. Olesen and G. Jacobsen, "Locking conditions and stability properties for a semiconductor laser with external light injection," *IEEE Journal of Quantum Electronics*, vol. 21, no. 7, pp. 784–793, July 1985.

[66] T. B. Simpson, J. M. Liu, and A. Gavrielides, "Bandwidth enhancement and broadband noise reduction in injection-locked semiconductor lasers," *IEEE Photonics Technology Letters*, vol. 7, no. 7, pp. 709–711, Jul. 1995.

[67] J. Wang, M. K. Haldar, L. Li and F. V. C. Mendis, "Enhancement of modulation bandwidth of

laser diodes by injection locking," *IEEE Photonics Technology Letters*, vol. 8, no. 1, pp. 34–36, Jan. 1996.

[68] X. Jun Meng, T. Chau, and M. C. Wu, "Experimental demonstration of modulation bandwidth enhancement in distributed feedback lasers with external light injection," *Electronics Letters*, vol. 34, no. 21, pp. 2031–2032, Oct. 1998.

[69] H. K. Sung, E. K. Lau and M. C. Wu, "Optical Properties and Modulation Characteristics of Ultra-Strong Injection-Locked Distributed Feedback Lasers," *IEEE Journal of Selected Topics in Quantum Electronics*, vol. 13, no. 5, pp. 1215–1221, Sept. 2007.

[70] K. Iwashita and K. Nakagawa, "Suppression of mode partition noise by laser diode light injection," *IEEE Journal of Selected Topics in Quantum Electronics*, vol. 18, no. 10, pp. 1669–1674, Oct. 1982.

[71] N. Schunk and K. Petermann, "Noise analysis of injection-locked semiconductor injection lasers," *IEEE Journal of Selected Topics in Quantum Electronics*, vol. QE-22, no. 5, pp. 642–650, May 1986.

[72] P. Spano, S. Piazzolla and M. Tamburrini, "Frequency and intensity noise in injection-locked semiconductor lasers: Theory and experiments" *IEEE Journal of Selected Topics in Quantum Electronics*, vol. 22, no. 3, pp. 427–435, March 1986.

[73] F. Mogensen, H. Olesen and G. Jacobsen, "FM noise suppression and linewidth reduction in an injection-locked semiconductor laser," *Electronics Letters*, vol. 21, pp. 696–697, Aug. 1985.

[74] S. P. Ó Dúill, R. Zhou, P. M. Anandarajah and L. P. Barry, "Numerical investigation into the dynamics of externally-injected, gain-switched lasers for optical comb generation," in *Proceedings of European Conference on Optical Communications*, Cannes, pp. 1-3, 2014.

[75] R. Zhou, S. Latkowski, J. O'Carroll, R. Phelan, L. P. Barry, and P. Anandarajah, "40nm wavelength tunable gain-switched optical comb source," *Optics Express*, vol. 19, B415–B420, 2011.

[76] P. M. Anandarajah, R. Zhou, R. Maher, M. D. Gutierrez Pascual, F. Smyth, V. Vujicic, and L. P. Barry, "Flexible optical comb source for super channel systems," in *Optical Fiber Communication Conference*, Anaheim, CA, pp. OTh3I.8, 2013.

[77] R. Zhou, T. N. Huynh, V. Vujicic, P. M. Anandarajah, and L. P. Barry, "Phase noise analysis of injected gain switched comb source for coherent communications," *Optics Express*, vol. 22, 8120-8125, 2014.

Chapter 3

Software Reconfigurable Gain Switched Optical Frequency Comb Source

Further to the discussions in the previous chapter, where several types of optical comb generation techniques have been presented and analysed, externally injected gain switched optical frequency combs have been selected as the focus of this thesis.

Depending on the network topology and application, diverse requirements and specifications (such as transmission lengths, modulation formats and complexity) are stipulated. Furthermore, flexible optical networks are attracting significant attention due to their potential to dynamically reconfigure transmission parameters (as baud rate, modulation format and bandwidth occupancy) according to traffic conditions and network resources, providing optimized spectral efficiency and transmission performance. These network applications pose stringent requirements on a prospective versatile multicarrier transmitter, in terms of flexibility, automation, and intensity and phase noise. As such, a Gain Switched Optical Frequency Comb Source (GS-OFCS) would substantially benefit from extended flexibility and reconfigurability, while ensuring low intensity and phase noise that allow the employment of numerous advanced modulation formats.

Hence, this chapter presents experimental work entailing the design, generation and detailed characterisation of a stand-alone software reconfigurable GS-OFCS. This can be viewed as one of the novel contributions of this thesis. The developed GS-OFCS, based on the external injection of a temperature tuned Fabry-Pérot (FP) laser diode, enables automatic setting of the parameters to obtain an optimum comb (in terms of flatness and noise properties) targeting various flexible network applications. The source is demonstrated to avail from wide Free Spectral Range (FSR) and

continuous wavelength tunability across the telecommunications C-band, with consistent and excellent spectral quality, low noise properties and long term stability, highlighting its suitability for employment in next generation flexible optical transmission networks.

3.1 Introduction

Flexible optical networks, also referred to as elastic networks [1], are gaining a lot of attention thanks to their potential to provide enhanced spectral efficiency and improved flexibility to meet the incessant exponential growth of global data traffic [2]. Flexible networks enable an efficient usage of the available spectrum by dynamically allocating the bandwidth (elastic spectrum allocation) [3], [4] according to the traffic demands. Moreover, an optimized spectral efficiency and performance is offered by adjusting transmission parameters such as sub-channel bandwidths, information rates and modulation formats depending on the unoccupied bandwidth, required capacity and optical reach.

These networks require the spectral grid to evolve towards finer granularities or operate on a gridless architecture [5], [6] that allows the combination of an arbitrary number of small frequency slots to create bandwidth-fitted superchannels. This maximizes the use of the available spectrum and enables the transmission of high bit rate superchannels (400 Gb/s, 1 Tb/s, etc.) [7], [8] without increasing the order of the modulation format, which would impact the maximum transmission distance [1]. Thus, new standards such as the Flexible grid defined by the International Telecommunication Union (ITU) in the G.694.1 recommendation [9] are emerging to support their deployment. This Flexible grid defines channels with a granularity of 12.5 GHz, combined with the ability to define an aggregate superchannel spectral width of $N{\cdot}12.5$ GHz.

To support the aforementioned developments, flexible networks require innovative components such as spectrum selective switches (SSSs) and flexible transponders for switching, transmission and reception [10]. A key component in the transponders of these flexible optical systems may be an Optical Frequency Comb Source (OFCS) [11], [12], which enables the reduction or elimination of guard bands by ensuring constant frequency spacing between the carriers. Particularly, flexible networks would certainly benefit from an OFCS that offers reconfigurable and continuous FSR and wavelength tunability. These capabilities allow a single source to be easily adapted to suit the chosen symbol rate and to allocate a superchannel simultaneously to a specific wavelength band.

Externally injected GS-OFCS have been demonstrated to offer beneficial properties such as limited wavelength tunability [13], effective transference of the narrow linewidth of the master laser to the slave comb lines and improvement in the number of comb tones, making such comb sources particularly attractive for coherent superchannel applications [14]. However, these OFCSs lack reconfigurability and are far from network deployment as they require an accurate manual re-adjustment and optimization of the injection parameters (injected power and wavelength detuning) to successfully generate a flat comb with low noise when varying the FSR or operating wavelength [13], [15]. Moreover, the wavelength tunability demonstrated in [13] is discrete and localized at those wavelengths where the slave laser exhibits a longitudinal mode. Hence, these factors are potentially limiting the flexibility of the transmitter and its reconfiguration, thus, making it less attractive in the emerging flexible grid networks.

3.2 Reconfigurable Gain Switched Optical Frequency Comb Source Architecture

The reconfigurable GS-OFCS developed in this work is presented and schematically illustrated in Figure 3.1. The source comprises a commercially available FP laser which is encased in an optically un-isolated and temperature controlled high-speed butterfly package, with an internal bias tee and a Radio frequency (RF) connector to enable direct modulation. The package contains a thermistor with a nominal value of 10 kΩ around room temperature that senses the actual temperature of the laser and a Thermoelectric Cooler (TEC) that controls and stabilizes the temperature. The FP laser emits in the 1.55 μm window, and exhibited a threshold current (I_{th}) of 8 mA at room temperature and a small signal 3-dB modulation bandwidth of 11 GHz when biased at 45 mA ($\approx 5I_{th}$), as depicted in Figure 3.2.

A semiconductor based Tunable Laser (TL), acting as a master, externally injects light into the cavity of the FP laser via a polarization-maintaining circulator. Polarization-maintaining fibres are used throughout the source, avoiding the use of polarization controllers to align the polarization state of the injected light with the optical waveguide of the FP laser. This alignment is subjected to environmental variations such as temperature, mechanical vibrations, pressure, etc. which could cause instabilities and hinder an automated control of reconfigurable features.

The TL presents a low linewidth of 300 kHz, Relative Intensity Noise (RIN) of -130 dB/Hz and wavelength tunability of 30 nm with a minimum resolution of 1 pm. The wavelength and power

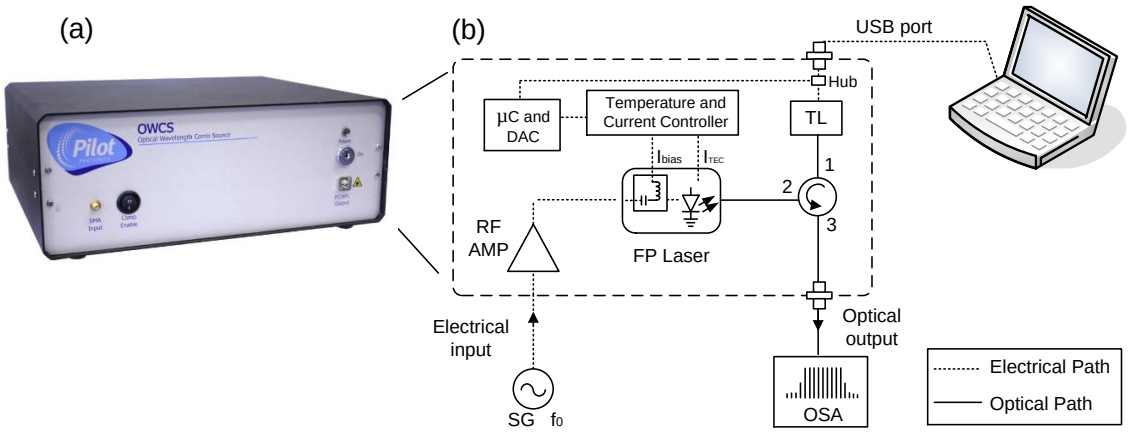

Figure 3.1: (a) Prototype and (b) Layout of the Reconfigurable Gain Switched Optical Frequency Comb

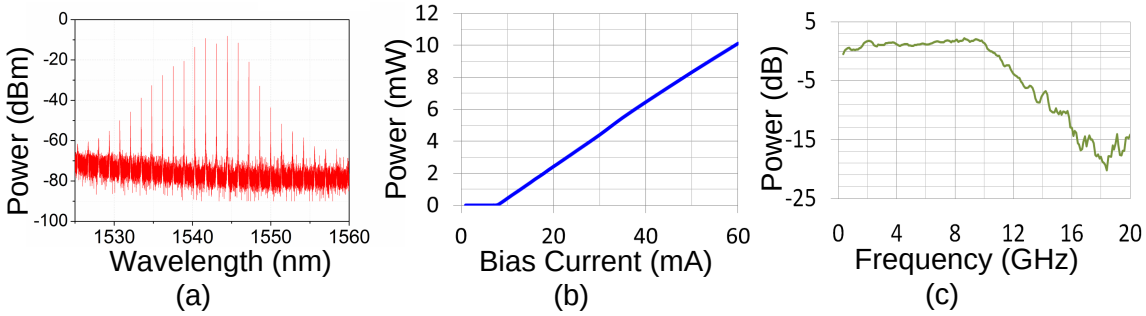

Figure 3.2: Slave FP laser basic characterisation: (a) Spectrum at 45 mA bias, (b) P-I curve, (c) Modulation Response at bias current of 45 mA

of the TL, which determine the detuning and injected power ratio respectively, are carefully chosen to ensure injection locking on a particular longitudinal mode of the FP laser. Then, the mode subjected to the injection dominates over the other longitudinal modes which get suppressed [17], and single mode operation at the selected wavelength is achieved. Consequently, gain switching of the externally injected FP laser results in an optical frequency comb generated around the injection locked single longitudinal mode. Gain switching is obtained by direct modulation with an amplified sinusoidal RF signal (∼24 dBm) from an external synthesizer, in conjunction with a fixed dc bias of 45 mA.

Precise injection locking into the different longitudinal modes of the FP laser, by modifying the wavelength of the TL appropriately, results in a GS-OFCS with central wavelength tunability over 20 individual operating points within the C-band (ranging from 1535nm-1565nm) [13]. However, this tunability is strictly limited by the wavelengths where the FP laser exhibits a longitudinal mode.

In order to achieve greater flexibility with continuous tunability and not only localized to a set of discrete wavelengths, the FP laser temperature could be also varied accordingly using the internal TEC in the butterfly module, to induce a wavelength shift in the longitudinal modes.

Accurate and fine tuning of the wavelength is required for network deployment and could prove complex, especially when synchronization between several parameters must be ensured, i.e. the temperature tuning and injection locking. This injection locking range is determined by the injected power ratio and wavelength detuning, as explained in Chapter 2. Furthermore, there are some trade-offs between the injection parameters and the number of comb tones, flatness and noise properties of the generated comb. Therefore, we automate this process with the aid of a microcontroller (μc) and a software program to control the parameters of the reconfigurable GS-OFCS without requiring manual calibration or optimization. The parameter setting algorithm calculates, according to the linear dependence of the wavelength with the temperature of $\Delta\lambda/\Delta T_{(^{\circ}C)}$ of 0.1 nm/°C (characterized from 0°C to 85°C) [18] and the Steinhart-Hart equations [19], the proper thermal tuning of the FP laser needed to obtain a longitudinal mode at the required wavelength. The temperature and current controller used provides two suitable analog inputs that can modify the set temperature and bias current of the laser by adding a dc component. Hence, the microcontroller controls a 12 bit Digital-to-Analog-Converter (DAC) that varies the FP set temperature by applying a determined analog voltage to the controller. Simultaneously, the software program communicates with the TL, through a USB port, to set a certain detuning and injected power that accomplishes the optimum injection locking on that specific longitudinal mode. Finally, in this experimental set up the software program also controls a synthesizer to set the GS-OFCS FSR. Obviously, an internal synthesizer could be also aggregated to the source. The resultant comb is then observed with a high resolution (0.16 pm) Optical Spectrum Analyser (OSA).

3.3 Experimental Characterisation

In this section, the aspects of GS-OFCS reconfigurability are analysed in detail starting with the flexible FSR and subsequently the widely and continuous tunable operating wavelength. The final aspect of the characterization includes RIN, phase noise and long term stability measurements on the reconfigurable GS-OFCS, as these parameters will determine the system performance that can be achieved when employing these comb sources in communication systems employing advanced modulation formats.

3.3.1 FSR Tunability

Figures 3.3 (a)-(h) illustrate the OFCS generated with repetition rates spanning a range of 6.25- 14 GHz. These results are achieved by externally injecting the FP laser with an injected power of -3 dBm to obtain single mode operation. Gain switching at these frequencies results in the generation of 4-14 clearly resolved and phase correlated optical comb tones within 3 dB of the spectral envelope peak, spaced by the drive frequency, with an Optical Carrier to Noise Ratio (OCNR) of 50 dB and a power per line of $\sim$2 dBm. It is important to notice that the flexible FSR is obtained by simply modifying the gain switching signal frequency.

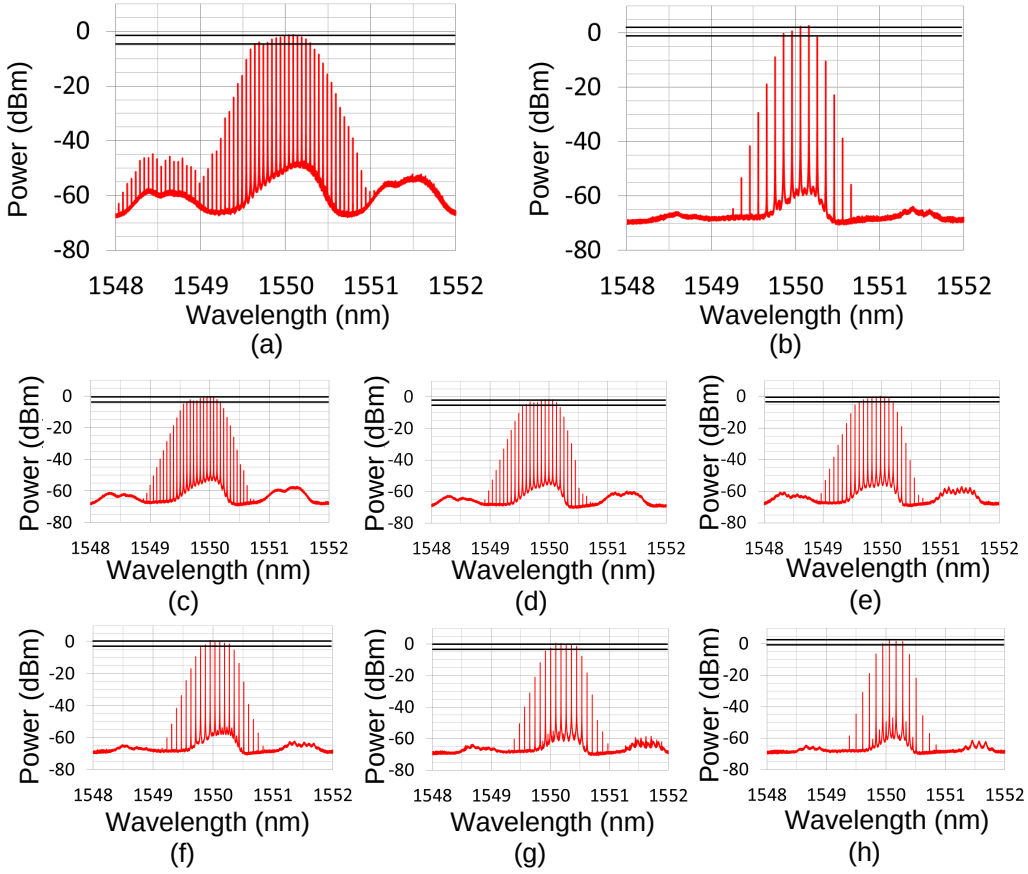

Figure 3.3: Optical spectra of the reconfigurable GS-OFCS generated with different FSRs: (a) 6.25 GHz; (b) 12.5 GHz; (c) 7 GHz; (d) 8 GHz; (e) 9 GHz; (f) 10 GHz; (g) 11 GHz; (h) 14 GHz. OSA resolution is 0.16 pm

The variation in the number of comb tones at different FSRs is a restraint dictated by the linewidth enhancement factor, α, the induced frequency chirp in the laser, and the inherent frequency response of the slave laser. The comb spectral envelop bandwidth is fixed and determined by the frequency

chirp produced in the pulse, the pulse shape and width, and the linewidth enhancement factor by the following relationship [20]:

$$\delta t \delta v = k\sqrt{1+\alpha^2} \tag{3.1}$$

where $\delta t \delta v$ is known as the *time-bandwidth product* of a pulse which is the product of its temporal duration δt and spectral width in frequency domain δv, and k is a constant which depends on the pulse shape ($\sim$ 0.44 for Gaussian-shaped pulses, $\sim$ 0.315 for sech^2-shaped pulses). From this equation, it can be observed that shorter pulses and higher linewidth enhancement factors result in broader gain switched combs. Additionally, the obtained spectral broadening δv is directly related to the frequency chirp that the pulse suffers due to the large variations in the carrier density during gain-switching, which affect the refractive index and thus, the instantaneous emission frequency. The frequency chirp is defined as:

$$\Delta v(t) = \frac{\alpha}{4\pi}[g(N-N_0) - \frac{1}{\tau_p}] \tag{3.2}$$

where $\Delta v(t)$ is the frequency chirp, α is the linewidth enhancement factor, g is the material gain, $N - N_0$ is the carrier density swing, and τ_p is the photon lifetime.

Hence, as the overall spectral width is fixed, lower FSR will yield a larger number of comb tones, as observed in Figure 3.3 where an FSR of 6.25 GHz presents 14 comb tones (corresponding to a total optical bandwidth of 87.5 GHz) and 9 GHz FSR exhibits 9 comb tones (optical bandwidth of 81 GHz). On the other hand, at higher FSRs (>12 GHz) the limitation comes from the slave frequency response bandwidth that, as explained in Chapter 2, depends directly on the relaxation oscillation frequency. Figure 3.2 (c) illustrates the frequency response of the laser, which is limited to 11 GHz. At higher FSRs the gain-switching signal effect will be degraded, causing a reduced swing of the carrier density and thus, an increased pulse width and reduced chirp [21]. As a result, the optical bandwidth reduces and fewer comb tones are observed, as low as 4 comb tones at 14 GHz, corresponding to a total bandwidth of 56 GHz.

It should be noted that the source presented here could also avail from expansion techniques that will be studied and presented in Chapter 4, to further enhance the practicality and potential for network deployment.

The 6.25 GHz and 12.5 GHz FSRs, with 14 and 6 comb lines within a 3 dB flatness window

respectively, are highlighted here due to their direct compatibility with the proposed ITU-T flexible grid recommendation in G.694.1 [9]. Furthermore, the high degree of flexibility will allow the use of this comb source in future flexible networks where the frequency slot might be further reduced [5], [6]. Even though these results focus on a narrow band of FSR tunability, limited by the slave laser in use, the technique offers itself for continuous broadband FSR tunability ranging from 5 to 40 GHz [11].

3.3.2 Central Wavelength Tunability

The developed reconfigurable comb source also presents full and continuous central wavelength tunability in the telecommunications C-band. Figure 3.4 presents the spectra of the FP slave laser, free-running and injection locked at 1539.623, 1549.343 and 1557.025 nm. Injection locking at specific longitudinal modes enhances the optical gain in that mode and significantly suppresses other modes. The performance of the single mode operation is often characterized by the Side-Mode-Suppression Ratio (SMSR) that should exceed 30 dB [22], defined as the difference $P_{mm}(dB) - P_{sm}(dB)$ where $P_{mm}(dB)$ is the power of the main mode and $P_{sm}(dB)$ is the power of the most dominant side mode in dB. The SMSR of the obtained injection locked FP is higher than 45 dB.

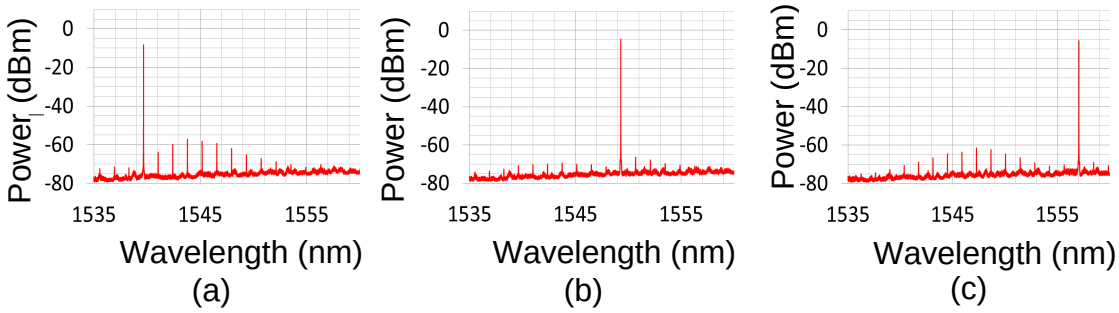

Figure 3.4: Optical spectra of the injection locked FP laser showing single mode operation at different wavelengths across the C-band: (a) 1539.623 nm, (b) 1549.343 nm and (c) 1557.025 nm.

In the same manner, the wavelength tunability of the comb source over the C-band is demonstrated, when the slave laser is also gain switched. The TL is tuned in wavelength to a detuning, $\Delta\lambda$, of -0.16 nm to inject -3 dBm into different longitudinal modes of the FP laser. This precise injection results, as presented before, in a single mode operation of the FP which is subsequently gain switched with an amplified 10 GHz sinewave to generate an optical frequency comb.

Figures 3.5 (a)-(c) present the resultant reconfigurable GS-OFCS at three representative central wavelengths, at the edges and middle of the C-band: 1535 nm, 1550 nm and 1565 nm, respectively. The generated combs exhibit ∼7 clearly resolved comb lines within a 3 dB of the spectral flatness, OCNR larger than 50 dB and more than 60 dB of SMSR.

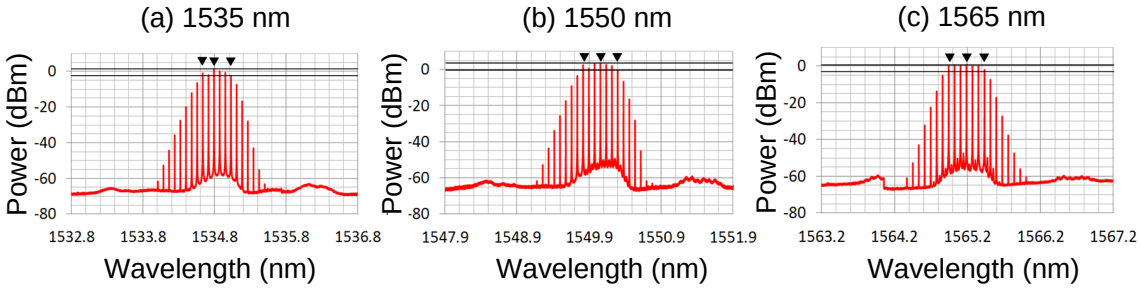

Figure 3.5: Optical spectra of the 10 GHz spaced, reconfigurable GS-OFCS generated at three different operating wavelengths over the C-band: (a) 1535 nm (b) 1550 nm and (c) 1565 nm.

Precise wavelength tunability between the discrete longitudinal modes can be achieved by a fine thermal tuning of the FP slave laser which produces a shift of its gain curve. The wavelength shift of the longitudinal modes due to temperature variation is dictated by a linear relation $\Delta\lambda/\Delta T_{(^\circ C)}$ of 0.1nm/°C [18], [23]. In this reconfigurable GS-OFCS the temperature is controlled by interrogating a thermistor inside the FP package, which serves as an inexpensive and accurate temperature monitor [23]. The values of a thermistor resistance (in Ohms) are related to the actual temperature through a non-linear characteristic that can be modelled to a high degree of accuracy using the empirical Steinhart-Hart equation. The equation is named after John S. Steinhart and Stanley R. Hart who first published the relationship in 1968 [19]:

$$\frac{1}{T_{(K)}} = A + B\ln(R) + C(\ln(R))^3 \tag{3.3}$$

where $T_{(K)}$ is the temperature of the laser (in Kelvins), R is the correspondent resistance of the thermistor (in Ohms) at a temperature $T_{(K)}$, and A, B and C are the Steinhart-Hart coefficients which vary depending on the type and nominal resistance of the thermistor. In our experiment, the nominal resistance of the thermistor was 10 kΩ at 25°C and therefore, the Steinhart-Hart coefficients are [23]:

$$\begin{aligned} A &= 1.125308 \times 10^{-3} \\ B &= 2.347118 \times 10^{-4} \\ C &= 8.566351 \times 10^{-8} \end{aligned} \tag{3.4}$$

Given the temperature tuning needed to produce a specific wavelength shift of the longitudinal

modes (calculated through $\Delta\lambda/\Delta T_{(^\circ C)}$ =0.1nm/°C), the new tuned slave laser temperature, $T'_{(^\circ C)}$, will be:

$$T'_{(^\circ C)} = T_{initial(^\circ C)} + \Delta T_{(^\circ C)} \tag{3.5}$$

with $T_{initial(^\circ C)}$ being the initial and default slave laser temperature in Celsius degrees.

As such, the required thermistor resistance for that specific temperature, $T'_{(^\circ C)}$, that produces the desired wavelength shift, is obtained using the inverse of the Steinhart-Hart equation:

$$R = e^{(\sqrt[3]{y-\frac{x}{2}} - \sqrt[3]{y+\frac{x}{2}})} \tag{3.6}$$

where:

$$x = \frac{1}{C}\Big(A - \frac{1}{T'_{(K)}}\Big) \tag{3.7}$$

$$y = \sqrt{\Big(\frac{B}{3C}\Big)^3 + \Big(\frac{x}{2}\Big)^2} \tag{3.8}$$

and $T'_{(K)}$ is the laser temperature in Kelvin degrees that can be calculated as:

$$T'_{(K)} = T'_{(^\circ C)} + 273.15 = T_{initial(^\circ C)} + \Delta T_{(^\circ C)} + 273.15 \tag{3.9}$$

Once the required temperature resistance, R, is calculated using 3.6, the microcontroller applies the corresponding voltage, through a 12-bit DAC, to the temperature controller which varies the temperature by 16 kΩ per voltage applied and produces the fine thermal tuning. Then, the wavelength of the TL is detuned accordingly to ensure injection locking and single mode operation on the specific longitudinal mode. In Figure 3.6, the central wavelength of a 10 GHz spaced comb is being tuned by 0.48 nm at a time, which corresponds to variations of 4.8 °C in the FP laser temperature, covering a full 5 nm span as a proof-of-concept demonstration. The illustrated spectra consistently exhibit 7 clearly resolved comb tones in a 3 dB spectral flatness and OCNR of 55 dB. This wavelength tunability is continuous and covers the span between FP longitudinal modes (1.37 nm) with a minimum wavelength step of 1 pm (∼125 MHz), limited by the wavelength setting resolution of the TL being used. The fine thermal tuning resolution is, in this case, 0.34 pm (∼ 42.5 MHz) dictated by the FP longitudinal mode spacing and the DAC resolution (12-bit).

The coarse central wavelength tuning time (between any longitudinal modes) across the C-band would be determined by the fast switching speed of the TL used, which could typically be in the nanoseconds range. On the other hand, the continuous wavelength tuning time depends on thermal

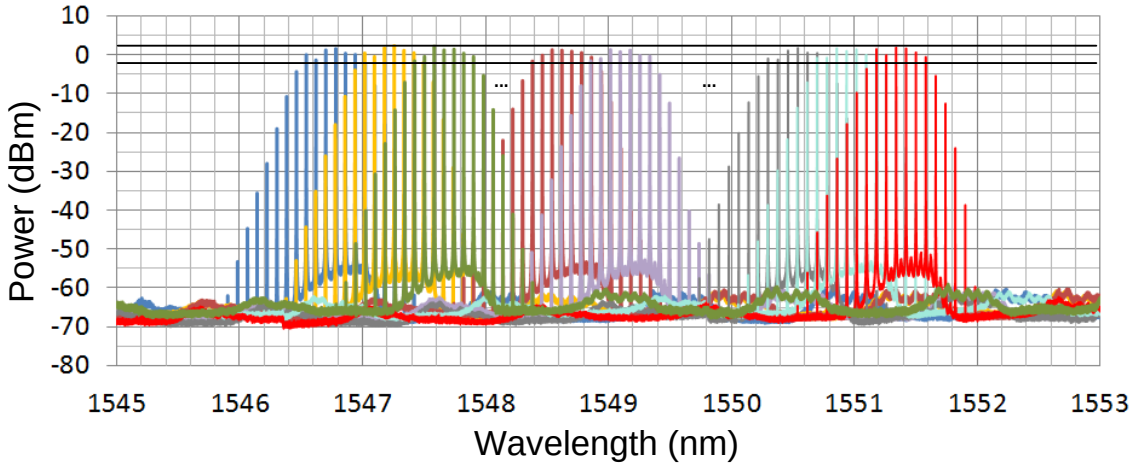

Figure 3.6: Continuous central wavelength tunability of the 10 GHz spaced reconfigurable GS-OFCS demonstrated around 1550 nm.

tuning, a slower process determined by the settling time of the slave laser to a new temperature, which is in the milliseconds range. Consequently, the thermal tuning would be used for fine wavelength tuning and could be employed for applications in flexible networks where millisecond-level reconfiguration times are suitable, such as the allocation of new connections to the network, re-allocation of the spectrum for a more efficient usage and to avoid fragmentation, and management and restoration schemes [1], [24]. Thus, the wavelength tuning time here presented is not expected to reduce the practicability of the source in many flexible network applications.

3.3.3 RIN

The RIN is an important parameter to characterize as it is an indicator of the noise properties of the transmitter [25], specifically when using modulation formats that convey information in the intensity. Future optical transmission systems will potentially adopt the IEEE 802.3 GBase standard which defines minimum RIN requirements specified for Gigabit Ethernet, according to the data rate employed. As such, this standard tolerates RINs of -128 dB/Hz for 40 Gbit/s transmissions (40GBase-ER4 interface), while slightly more stringent RIN requirements below -130 dB/Hz are expected for commercial 100 Gbit/s systems (100GBase-ER4 interface) [26].

The optical power of a laser can be considered to be power fluctuations, $\delta P(t)$, caused by spontaneous emission with an average value, P_0:

$$P(t) = P_0 + \delta P(t) \tag{3.10}$$

Then, the RIN describes the relative intensity noise (optical power fluctuations), normalized to the average power level. The RIN is mathematically defined as the ratio of the mean-squared power fluctuations to the squared average optical power P_0 [27]:

$$RIN = \frac{< \delta P(t)^2 >}{{P_0}^2} \tag{3.11}$$

It can be observed that the RIN is, in fact, proportional to the ratio of the corresponding photodetected electrical powers (i.e. the square of the optical power) when employing a fast photodetector. Then, the photocurrent, I, is proportional to the responsitivity of the photodetector, R, and the optical power by: $I(t) = RP(t)$. And thus, the RIN can be ideally expressed as [28]:

$$RIN = \frac{< R^2 \delta I(t)^2 >}{R^2 I_0^2} = \frac{< \delta I(t)^2 >}{I_0^2} = \frac{< \delta P_{EI}(t) >}{P_{0EI}} \tag{3.12}$$

where $\delta P_{EI}(t)$ and P_{0EI} are the associated power fluctuations of the photocurrent (ac component), and the average power (dc component) of the photocurrent.

RIN is usually presented in the frequency domain as a power spectral density (through a Fourier transform) over a certain noise frequency range. As a result, RIN is typically obtained by analysing the spectrum of the photodetected ac signal using an Electrical Spectrum Analyzer (ESA). This RIN power spectral density is commonly represented in a logarithm scale, with units of dB/Hz.

The RIN measurements are carried out using the experimental set up illustrated in Figure 3.7. The optical output of the device is passed through an isolator (ISO) which suppresses any unsought feedback reflections. The optical output is then filtered using a narrow Optical Band Pass Filter (OBPF) to select specific comb tones, amplified with an Erbium Doped Fibre Amplifier (EDFA) to compensate for the loss and detected using a 50-GHz Photodetector (PD) from U2T. The output of the PD is passed through a bias tee that separates the dc and ac component of the photocurrent.

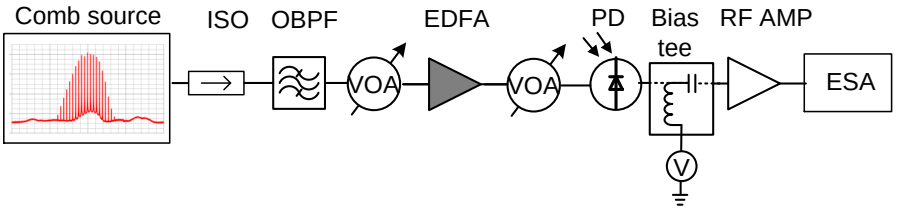

Figure 3.7: Experimental set up for RIN measurements. ISO: isolator, OBPF: optical band pass filter, VOA: variable optical attenuator, EDFA: erbium doped fibre amplifier, PD: photodiode, RF AMP: RF amplifier, ESA: electrical spectrum analyser.

The ac signal is amplified and characterized with the aid of an ESA while the dc component is acquired with a multimeter [28]. The Amplified Spontaneous Emission (ASE) noise generated by the EDFA varies depending on the input power launched into it which influences the RIN measured. Therefore, a Variable Optical Attenuator (VOA) is placed in line between the filter and EDFA to ensure constant power at its input, and thereby similar ASE for all measurements, allowing an objective relative comparison of the RIN results. A VOA is also used to keep the power launched to the PD constant, at 1 dBm.

For clarity of demonstration, the RIN was measured at three selected operating wavelengths (1535, 1550 and 1565 nm) across the C-band. For each operating wavelength the RIN of the overall unfiltered comb and the RIN of three individually filtered comb lines are analysed. The three filtered comb lines are indicated by arrows in Figures 3.5 (a)-(c) at the left edge, central and right edge of the 3-dB spectral flatness window. These RIN measurements are then compared to the RIN of the TL master laser in Continuous Wave (CW) operation. The achieved results are shown in Figure 3.8. The noise floor is the minimum perceivable noise level of the equipment used in these measurements and is presented as a reference (-140 dB/Hz). The averaged RIN (from dc to 10 GHz) is -130 dB/Hz for all the measurements, which is the same as the RIN of the master TL. The low RIN of the comb tones (transferred from the TL) is a beneficial outcome of the external injection which reduces the spontaneous emission in the slave laser and thus, the RIN associated with each of the comb tones [29]. Moreover, these results demonstrate that, even though the source relies on a multimode FP laser, the reconfigurable OFCS is not affected by mode partition noise unlike mode-locked laser based comb sources [30], due to proper injection locking.

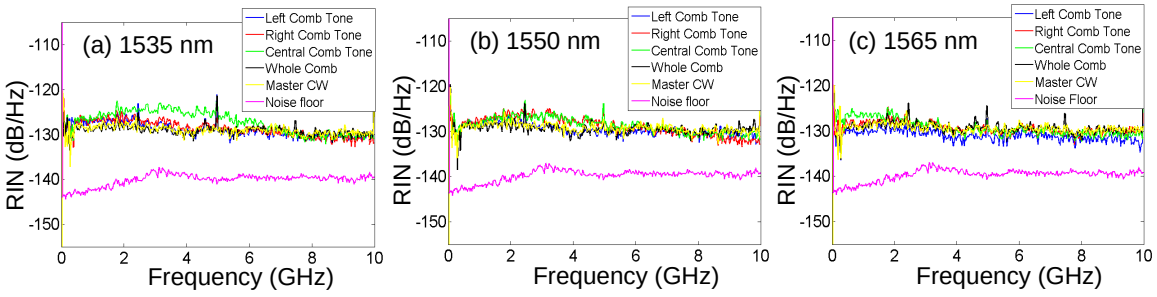

Figure 3.8: Measured RIN power spectral density at different operating central wavelengths across the C-band: (a) 1535 nm; (b) 1550 nm; (c) 1565 nm. Measurements were carried out for three comb tones at each wavelength (left comb tone in blue, right comb tone in red and central comb tone in green), for the overall unfiltered comb in black and for the Master CW in yellow.

It is important to note that the measured RIN is also consistent for the three different operating wave-

lengths, hence, similar system performance should be expected across the whole C-band.

3.3.4 Phase Noise

The phase noise of an optical transmitter is a crucial parameter when advanced modulation formats are employed for coherent superchannel applications [14]. The phase noise requirements for system transmissions depends on the modulation format and baud rate employed, as well as the phase recovery algorithms implemented at the receiver. For example, the linewidth requirements according to [31] for 10 Gbaud are 10 MHz for QPSK and 500 kHz for 16-QAM using a decision-directed phase-locked loop. In [32], the linewidth requirements for 10 Gbaud QPSK and 16-QAM are 4.1 MHz and 1.4 MHz, respectively, employing a digital feedforward carrier recovery algorithm.

The optical linewidth value is considered an important criterion indicating the phase noise. However, previous studies have pointed out that the observed optical linewidth can appear significantly broadened using conventional measurements techniques as the Delayed Self-Heterodyne (DSH) [33]- [35], due to excess low frequency noise which masks the intrinsic linewidth caused by spontaneous emission in the laser. The low frequency noise is commonly referred to as *1/f* noise as it presents a power spectral density inversely proportional to the noise frequency, and thus has a slope of *1/f*. In this reconfigurable GS-OFCS, the observed optical linewidth could potentially be affected by excess low frequency noise from the electronics used (switchable power supply, ordinary laser bias current sources, microcontroller, etc.) that transfers to the lasers through fluctuations in their carrier density. Therefore, the phase noise of the comb source is here characterized by carrying out a detailed analysis of the Frequency Modulated (FM)-noise spectrum, which fully describes the noise processes contributing to the overall phase noise as well as their origin [16], [33]. The FM-noise spectrum is a power spectral density of the instantaneous frequency fluctuations originated from the phase noise [16], [33]- [35].

The experimental characterisation of the FM-noise spectrum is performed via a phase noise measurement method previously developed [33], whose set up is observed in Figure 3.9. The reconfigurable comb is followed by an EDFA before being passed to a narrow OBPF that selects the individual comb lines for phase characterisation. The phase noise measurement technique consists of a modified DSH method [33]. The signal is split into two arms by a coupler, where one arm is delayed by a 12 km of Standard Single Mode Fibre (SSMF) to de-correlate the signal respectively to the other arm. The signal in the second arm is phase modulated, with a phase modulator driven

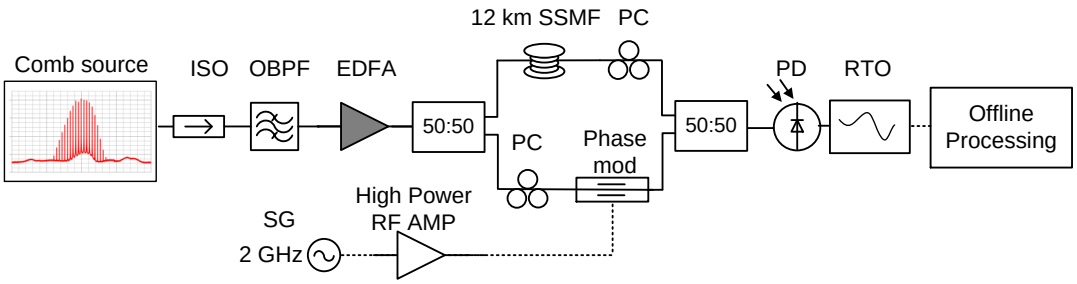

Figure 3.9: Experimental set up for phase noise measurements using the modified delay self-heterodyne detection method. ISO: isolator, OBPF: optical band pass filter, EDFA: erbium doped fibre amplifier, SSMF: standard single mode fibre; PC: polarization controller; SG: signal generator; RF AMP: RF amplifier; Phase mod: phase modulator; PD: photodiode, RTO: real time oscilloscope.

by a high power 2 GHz signal to achieve second order harmonics. The light from the delayed and phase modulated arms are recombined via a second coupler and photodetected. The detected heterodyne signal will present copies of the doubled-linewidth at 2 GHz harmonics, which are captured with a real time oscilloscope and sent for offline digital processing to recover the differential phase error [33].

The phase noise measurements were carried out on the same comb lines and wavelengths previously mentioned in the RIN measurement, marked in Figures 3.5 (a)-(c). These measurements are then compared with the phase noise characteristic of the TL (master) at those specific wavelengths over a frequency range up to 1 GHz. As illustrated in Figures 3.10 (a)-(c), the FM-noise spectrum of the master is dominated by a flat white FM-noise component, S_0 = 1.75x10^5 Hz^2/Hz, which corresponds to an intrinsic linewidth, δf, of 300 kHz ($\delta f = S_0 \cdot \frac{\pi}{2} \approx 300$ kHz [34], where the factor 2 is due to the nature of the self-heterodyne method, where these measurements are twice the actual values). As observed, the master FM-noise does not present a low frequency, *1/f*, noise component at the frequencies measured using our set up (which measures down to 2 MHz), thus, the observed optical linewidth would not be affected.

The filtered comb lines at each wavelength have identical FM-noise spectrum as the master at lower frequencies (below 200 MHz). Therefore, the optical linewidth of the comb tones follows that of the master, 300 kHz [13], [16]. At high frequencies the phase noise of the filtered comb lines presents an acceptable deviation from the master. This deviation was studied in [16] and is a consequence of residual phase noise from the slave laser, which depends on the injection parameters used (injected power and wavelength detuning). A trade-off was clearly identified where the deviation could be reduced if the flatness of the obtained comb is sacrificed.

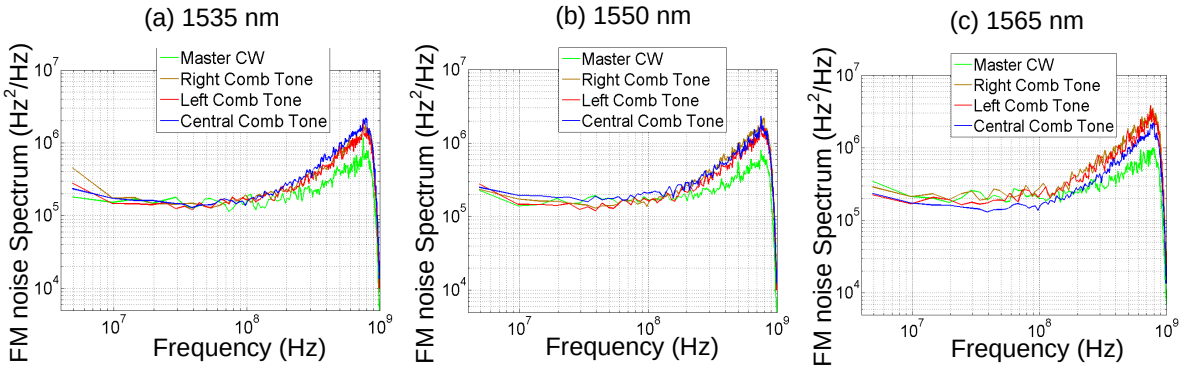

Figure 3.10: Measured FM-noise spectrum at different operating central wavelengths across the C-band: (a) 1535 nm; (b) 1550 nm; and (c) 1565 nm. Measurements were carried out for three comb tones at each wavelength (right comb tone in brown, right comb tone in red and central comb tone in blue), and for the Master CW at each wavelength in green.

From the results presented in Figures 3.10 (a)-(c), the deviation in the FM-noise spectrum is acceptable hence suggesting optimum injection parameters for the reconfigurable GS-OFCS. These results indicate that the comb tones would impose zero or minimum penalties (compared to the master) when being employed in a coherent communication system [16]. Finally, we point out that the three operating wavelengths present a similar FM-noise spectrum. It could be expected that as we inject into the extreme longitudinal modes in the gain curve of the FP laser (1535 nm and 1565 nm), the injection locking could be more challenging to achieve than in the centre of the FP gain curve (1552 nm), where the longitudinal modes have more power concentrated. These results highlight that proper chosen injection parameters (injected power and detuning) can guarantee consistent performance and phase noise properties across the C-band.

3.3.5 Long Term Stability

Other FSR and wavelength flexible OFCS configurations with potential for network deployment include the use of strongly driven electro-optic modulators, which suffer from bias drifts over long periods of time [12] and may require a feedback based dc bias control to maintain stable operation [37]. In comparison, externally injected gain switched OFCSs have been presented as a more stable alternative. However, this superior stability has never been fully characterized in the literature.

The two main parameters governing the overall stability of an OFCS are the optical power and wavelength variations of individual comb tones over time. Hence, these two parameters are mea-

sured in this reconfigurable GS-OFCS by monitoring the optical spectrum of the comb source at ambient temperature with a high resolution OSA (0.16 pm). Traces were captured every 30 seconds over a total period of 24 hours. The comb monitored was generated with an FSR of 12.5 GHz and at a central wavelength of 1550.5 nm. For that, the temperature of the FP laser was tuned to 25°C (thermistor value of 10 kΩ) while being injection locked by the TL into that particular longitudinal mode of the FP laser. Figure 3.11 illustrates the power fluctuations over time of the 6 clearly resolved comb lines within a spectral ripple of 3 dB, depicted in Figure 3.11 (b). The maximum fluctuation in optical power over 24 hours was found to be 0.5 dB for the worst case, and limited by a power repeatability of 0.2 dB of the OSA in use [36]. It can be observed that not all the comb tones present the same level of power variation. The smallest deviation is only 0.2 dB for the strongest comb tone in power. In comparison to electro-optic modulators based comb generation techniques that have shown up to 1.9 dB power fluctuations in a three-hour measurement after implementing an auto-bias control circuit [37], this small deviation proves that comb generation by gain switching an externally injected laser is a simple and robust technique that offers excellent stability suitable for network deployment without any additional stabilization circuity.

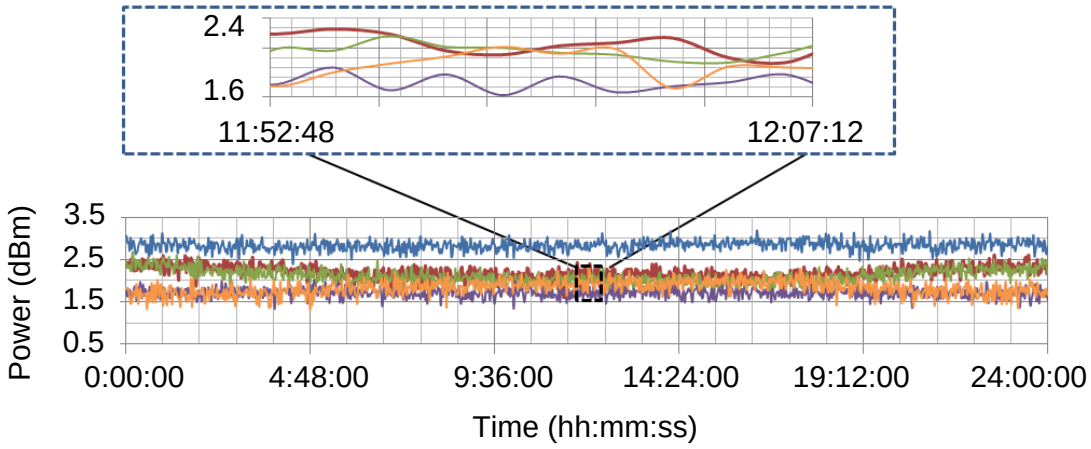

Figure 3.11: Power stability measurement of the individual comb tones of the 12.5 GHz reconfigurable GS-OFCS over a period of 24 hours.

Figure 3.12 shows a simultaneous measurement carried out where the wavelengths of the same individual comb tones were monitored. In this case, the wavelength deviation of any comb line is no more than 5 pm. It has to be mentioned that the wavelength deviation for each comb tone is the same at any time, as the comb tones are phase locked and the frequency spacing between the comb tones is fixed. Thus, all comb tones experience the same wavelength variation and drift together,

avoiding inter-channel interferences when using high spectrally efficient multi-carrier modulation techniques as Nyquist-Wavelength Division Multiplexing (WDM) and all-optical Orthogonal Frequency Division Multiplexing (OFDM).

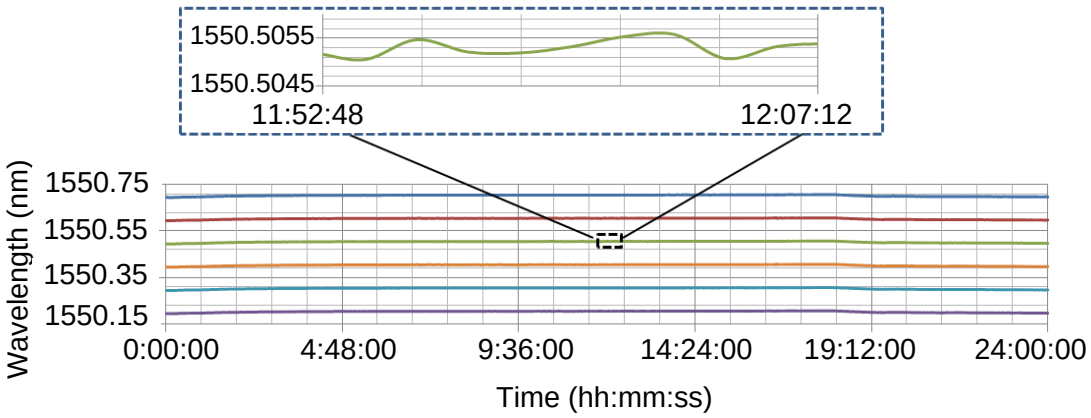

Figure 3.12: Wavelength stability measurement of the individual comb tones of the 12.5 GHz reconfigurable GS-OFCS over a period of 24 hours.

As such, these stability measurements highlight the robustness of the proposed reconfigurable GS-OFCS which offers long-term operational stability without requiring automated feedback control or manual adjustments.

3.4 Conclusions

Flexible networks have recently stirred a lot of attention due to their capabilities to maximize spectral efficiency by adapting to the actual conditions of the network and data rates for variable traffic demands. These networks, however, pose challenges on the multicarrier transmitters that are required to provide a new degree of flexibility, automation and control of their characteristics.

This chapter has presented a highly flexible software reconfigurable gain switched optical comb source and provided detailed characterization of all of the major parameters of interest for the flexible optical networks. The software which allows the reconfigurability and selection of the comb parameters could be applied to an elastic optical network for dynamic spectrum allocation and adjustment of transmission parameters. The source offers wide FSR and central wavelength tunability over the C-band, generated by seeding a thermally tuned gain switched FP laser with a tunable laser. These flexible features, in conjunction with a demonstrated exceptional long term stability

and consistent low RIN and low phase noise performance for any operating wavelength, prove the suitability of this source for next generation flexible optical transmission networks. Moreover, the externally injected gain switched scheme intrinsically offers key parameters for network deployment such as simplicity, cost-efficiency and potential for monolithic integration that would further reduce the footprint of the source.

The practicability of gain switched comb sources is further enhanced in the next chapter, where several techniques for comb expansion are studied, while maintaining flexibility and low noise properties.

References

[1] O. Gerstel, M. Jinno, A. Lord, and S. J. B. Yoo, "Elastic optical networking: a new dawn for the optical layer?," *IEEE Commununications Magazine*, vol. 50, no. 2, pp. 12–20, 2012.

[2] Cisco V. N. I. Forecast, "Cisco visual networking index: forecast and methodology 2015-2020," Available: http://www.cisco.com/c/en/us/solutions/collateral/service-provider/visual-networking-index-vni/complete-white-paper-c11-481360.html

[3] K. Christodoulopoulos, I. Tomkos, and E. A. I. Varvarigos, "Elastic bandwidth allocation in flexible OFDM based optical networks," *Journal of Lightwave Technology*, vol. 29, no. 9, pp. 1354–1366, 2011.

[4] D. Rafique, T. Rahman, A. Napoli, M. Kuschnerov, G. Lehmann, and B. Spinnler, "Flex-grid optical networks: spectrum allocation and nonlinear dynamics of super-channels," *Optics Express*, vol. 21, no. 26, pp. 32184–32191, 2013.

[5] G. Shen and Q. Yang, "From coarse grid to mini-grid to gridless: how much can gridless help contentionless?" in *Proceedings of Optical Fiber Communication Conference and Exposition*, paper OTuI3, Los Angeles, CA, March 2011.

[6] M. Tornatore, C. Rottondi, A. Morea, and G. Rizzelli, "Complexity and flexible grid networks," in *Proceedings of Optical Fiber Communication Conference and Exposition*, paper W3A.1, San Francisco, CA, March 2014.

[7] S. Gringeri, E. B. Basch, and T. J. Xia, "Technical considerations for supporting data rates beyond 100 Gb/s," *IEEE Commununications Magazine*, vol. 50, no. 2, pp. 21–30, 2012.

[8] S. Zhang, M. Tornatore, G. Shen, J. Zhang, and B. Mukherjee, "Evolving traffic grooming in multi-layer flexible grid optical networks with software-defined elasticity," *Journal of Lightwave Technology*, vol. 32, no. 16, pp. 2905–2914, 2014.

[9] ITU-T Recommendations, "Spectral grids for WDM applications: DWDM frequency grid," G.694.1, 2012. Available: https://www.itu.int/rec/T-REC-G.694.1/en

[10] N. Sambo, G. Meloni, F. Paolucci, F. Cugini, M. Secondini, F. Fresi, L. Potì, and P. Castoldi, "Programmable transponder, code and differentiated filter configuration in elastic optical networks," *Journal of Lightwave Technology*, vol. 32, no. 11, pp. 2079–2086, 2014.

[11] P. Anandarajah, R. Zhou, R. Maher, M. D. Gutierrez Pascual, F. Smyth, V. Vujicic, and L. Barry, "Flexible optical comb source for super channel systems," in *Proceedings of Optical Fiber Communication Conference and Exposition and the National Fiber Optic Engineers Conference*, paper OTh3I.8, Anaheim, CA, 2013.

[12] A. J. Metcalf, V. Torres-Company, D. E. Leaird, and A. M. Weiner, "High-power broadly tunable electro-optic frequency comb generator," *IEEE Journal of Selected Topics in Quantum Electronics*, vol. 19, no. 6, pp. 231–236, 2013.

[13] R. Zhou, S. Latkowski, J. O'Carroll, R. Phelan, L. P. Barry, and P. Anandarajah, "40 nm wavelength tunable gain-switched optical comb source," *Optics Express*, vol. 19, no. 26, pp. B415–B420, 2011.

[14] V. Vujicic, J. Pfeifle, R. Watts, P. C. Schindler, C. Weimann, R. Zhou, W. Freude, C. G. Koos, and L. Barry, "Flexible terabit/s Nyquist-WDM superchannels with net SE $>$ 7bit/s/Hz using a gain-switched comb source," in *Proceedings of Conference on Lasers and Electro-Optics (CLEO) - Laser Science to Photonic Applications*, paper SW1J.3, San Jose, CA, 2014.

[15] R. Zhou, P. M. Anandarajah, D. Gutierrez Pascual, J. O'Carroll, R. Phelan, B. Kelly, and L. P. Barry, "Monolithically integrated 2-section lasers for injection locked gain switched comb generation," in *Proceedings of Optical Fiber Communication Conference and Exposition* paper Th3A.3, San Francisco, CA, 2014.

[16] R. Zhou, T. N. Huynh, V. Vujicic, P. M. Anandarajah, and L. P. Barry, "Phase noise analysis of injected gain switched comb source for coherent communications," *Optics Express*, vol. 22, no. 7, pp. 8120–8125, 2014.

[17] K. Iwashita and K. Nakagawa, "Suppression of mode partition noise by laser diode light injection," *IEEE Journal of Selected Topics in Quantum Electronics*, vol. 18, pp. 1669–1674, 1982.

[18] J. O'Carroll, R. Phelan, B. Kelly, D. Byrne, L. P. Barry, and J. O'Gorman, "Wide temperature range $0 < T < 85$ °C narrow linewidth discrete mode laser diodes for coherent communications

applications," *Optics Express*, vol. 19, no. 26, pp. B90–B95, 2011.

[19] J. S. Steinhart and S. R. Hart, "Calibration curves for thermistors," *Deep Sea Research and Oceanographic Abstracts*, vol. 15, no. 4, pp. 497–503, Aug. 1968.

[20] P. P. Vasil'ev, I. H. White, and J. Gowar, "Fast phenomena in semiconductor lasers," *Reports on Progress in Physics*, vol. 63, no. 12, pp. 1997-2042, 2000.

[21] P. M. Anandarajah, S. P. Ó'Dúill, R. Zhou and L. P. Barry, "Enhanced Optical Comb Generation by Gain-Switching a Single-Mode Semiconductor Laser Close to Its Relaxation Oscillation Frequency," *IEEE Journal of Selected Topics in Quantum Electronics*, vol. 21, no. 6, pp. 592-600, Dec. 2015.

[22] G. P. Agrawal, "Fiber-Optic Communication Systems," 3rd ed.: Wiley, 2002.

[23] Newport Corporation application note, "Thermistor calibration and the Steinhart-Hart equation," Available: http://assets.newport.com/webDocuments-EN/images/AN04_Thermistor_Calibration_IX.PDF

[24] K. Wen, X. Cai, Y. Yin, D. J. Geisler, R. Proietti, R. P. Scott, N. K. Fontaine, and S. J. B. Yoo, "Adaptive spectrum control and management in elastic optical networks," *EEE Journal on Selected Areas in Communications*, vol. 31, no. 1, pp. 39–48, Jan. 2013.

[25] Z. Zan, M. Premaratne, and A. J. Lowery, "Laser RIN and linewidth requirements for direct detection optical OFDM," in *Proceedings of Conference on Lasers and Electro-Optics/Quantum Electronics and Laser Science Conference and Photonic Applications Systems Technologies*, paper CWN2, San Jose, CA, 2008.

[26] IEEE 802.3^{TM}-2015 – IEEE Standard for Ethernet, Available: http://standards.ieee.org/getieee802/download/802.3-2015.zip, 2015.

[27] L. A. Coldren, S. W. Corzine, M. L. Masanovic, "Diode Lasers and Photonic Integrated Circuits," 2nd Edition, John Wiley & Sons, 2012.

[28] Eagleyard-Photonics, "Relative Intensity Noise of Distributed Feedback Lasers," [Online]. Available: http://www.eagleyard.com/fileadmin/downloads/documents/eyP_App_Note_RIN__1-6.pdf

[29] X. Jin and S. L. Chuang, "Relative intensity noise characteristics of injection-locked semiconductor lasers," *Applied Physics Letters*, vol. 77, no. 9, pp. 1250–1252, 2000.

[30] A. Akrout, A. Shen, R. Brenot, F. Van Dijk, O. Legouezigou, F. Pommereau, F. Lelarge, A. Ramdane, and G.-H. Duan, "Separate error-free transmission of eight channels at 10 Gb/s using comb generation in a Quantum-Dash based Mode-Locked laser," *IEEE Photonics Technology Letters*, vol. 21, no. 23, pp. 1746–1748, 2009.

[31] K. Kikuchi, "Coherent optical transmission systems," *in Proceedings of OptoElectronics and Communications Conference (OECC)*, pp.120-121, Sapporo, Japan, 2010.

[32] T. Pfau, S. Hoffmann, and R. Noe, "Hardware-efficient coherent digital receiver concept with feedforward carrier recovery for M-QAM constellations," *Journal of Lightwave Technology*, vol. 27, no. 8, pp.989–999, 2009.

[33] T. N. Huynh, L. Nguyen, and L. Barry, "Phase noise characterization of SGDBR lasers using phase modulation detection method with delayed self-heterodyne measurements," *Journal Lightwave Technology*, vol. 31, no. 8, pp. 1300–1308, 2013.

[34] K. Kikuchi, "Characterization of semiconductor-laser phase noise and estimation of bit-error rate performance with low-speed offline digital coherent receivers," *Optics Express*, vol. 20, pp. 5291-5302, 2012.

[35] K. Kikuchi, "Impact of 1/f-type FM noise on coherent optical communications," *IEEE Electronics Letters*, vol. 23, no. 17, pp. 885–887, 1987.

[36] Apex Technologies, Optical Spectrum Analyser datasheet. Available: http://www.apex-t.com/pdf/optical-spectrum-analyzer.pdf

[37] T. Sakamoto, I. Morohashi, and T. Kawanishi, "Mach-Zehnder-modulator-based flat comb generator with auto bias control," in *Proceedings of International Topical Meeting on Microwave Photonics jointly held with the 2008 Asia-Pacific Microwave Photonics Conference*, Gold Coast, Qld, pp. 154-157, 2008.

[38] M. D. Gutierrez Pascual, R. Zhou, F. Smyth, P. M. Anandarajah, and L. P. Barry, "Software reconfigurable highly flexible gain switched optical frequency comb source," *Optics Express*, vol. 23, pp. 23225-23235, August 2015.

Chapter 4

Coherent Expansion Techniques for Reconfigurable Gain Switched Combs

A Gain Switched Optical Frequency Comb Source (GS-OFCS) offers substantial advantages for practical implementation in future optical networks that may be highly demanding in flexibility and throughput. The previous chapter presented and investigated a simple and cost-efficient reconfigurable GS-OFCS offering flexible Free Spectral Range (FSR) and central wavelength tunability, while ensuring low noise properties as Relative Intensity Noise (RIN) and phase noise [1].

However, a key issue still to be considered when compared to other comb generation techniques such as Mode-locked lasers (MLLs), Kerr based combs or parametric combs, is the restricted number of comb tones that can be achieved in reconfigurable GS-OFCSs. This is a major restraint that may reduce the practicability of GS-OFCSs in some communication applications.

As such, this chapter proposes two novel techniques for bandwidth coverage expansion of GS-OFCSs. The expansion methods are first experimentally demonstrated and the resultant expanded combs are subsequently characterised in detail. Both configurations offer flexible features with central wavelength tunability within the C-band, low optical linewidth, high phase correlation and good Optical Carrier to Noise Ratio (OCNR). Furthermore, these expansion techniques are simple and potentially integrable, yielding further footprint reduction and improved cost-efficiency.

4.1 Introduction

Numerous communication applications may benefit from OFCSs, which are generally expected to deliver diverse spectral properties. OFCSs that offer large number of carriers [2] with strong phase correlation [3], central wavelength and FSR flexibility [4], good OCNR and low optical linewidth are usually desired in flexible superchannel transmission systems [5] and millimetre wave generation/radio-over-fibre (RoF) applications [6]. Other qualities of an Optical Frequency Comb Source (OFCS) that would be favourable for multiple applications include configuration simplicity, potential for photonic integration, and stability.

Fulfilling all the aforementioned comb properties simultaneously has proven to be difficult. A conventional MLL based comb source provides a large number of comb tones yet suffers from relatively large optical linewidth (normally in MHz range) [7], which is not a favourable property for their use with high order modulation formats. Kerr combs may overcome this significant noise limitation but also present lack of tunability, with a fixed FSR, unsuitable for flexible networks. On the other hand, parametric combs and cascaded strongly-driven modulators offer tuning flexibilities and low noise properties, but both schemes exhibit complicated configuration arrangements and implementation challenges such as large component count, elevated power consumption (due to the use of high pumping powers or multiple high power amplifiers), and difficulties for stable operation [8].

GS-OFCSs provide excellent noise properties, flexibility and reconfigurability while keeping a remarkable simplicity and stability. However, gain switching is unable to generate a large number of carriers and, thus, several expansion techniques have been investigated.

Expansion of gain switched comb sources has been demonstrated by using electro-optic phase modulators [9]. The gain switched comb is launched into a phase modulator, driven by an amplified sinewave (several orders of V_π) drawn from the same signal generator used for gain switching. The phase modulation proves to be an effective way of improving the comb line number and flatness, while keeping the central wavelength tunability across the C-band. However, high insertion losses and instabilities in the modulators are still problematic and jeopardize the practicality of the expanded GS-OFCS.

Another gain switched comb expansion approach entails the use of dispersion compensating fibre followed by Highly Non-Linear Fibre (HNLF) [10] which is difficult to control and increases the complexity, footprint and power consumption (due to the need of elevated launched powers which

require Erbium Doped Fibre Amplifier (EDFA)). Moreover, the resultant wavelength tunability is limited, as the dispersion coefficient of the fibres are highly dependent on the wavelength and thus, limit the flexibility of the expanded GS-OFCS.

As such, expansion and broadband generation of gain switched combs with a simplified and cost-efficient set up, that could be integrated while low noise properties and extended flexibility are preserved, would be highly attractive and would enhance the viability and potential of GS-OFCSs for network deployment.

4.2 Gain Switched Comb Expansion by Cascading Fabry-Pérot (FP) Lasers

The first technique proposed for coherent expansion of reconfigurable GS-OFCSs is based on cascading multiple injected gain switched FP lasers with matched cavity lengths. The conceptual schematic illustrating the operating principle is shown in Figure 4.1.

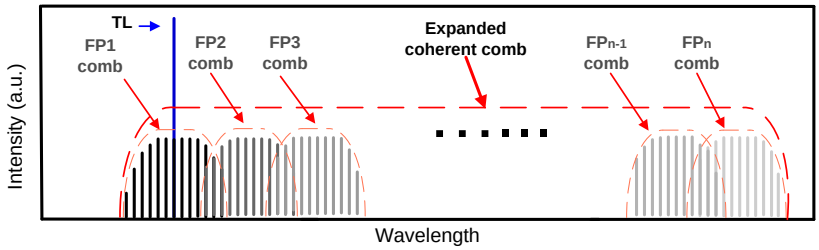

Figure 4.1: Schematic illustrating the principle of operation of the proposed technique for expanding an externally injected, gain switched comb source.

One of the longitudinal modes of the first FP laser (FP1) is injection locked with the aid of a low linewidth Tunable Laser (TL) thereby achieving single mode operation, as explained in Chapter 3. All FP lasers are then gain switched. The gain switching of FP1 results in a frequency comb generated around the injection locked single longitudinal mode, which can be tunable in FSR and central wavelength, as demonstrated in Chapter 3. Each of the FP lasers is then temperature tuned to ensure partial overlap of their gain switched comb spectra envelope with the adjacent FP. This ensures that the outer comb lines from FP1 externally inject the subsequent gain switched FP laser (FP2) and so on. This gain switched and now injection locked FP2 emits a frequency comb around its injected single longitudinal mode, merging into the previous FP1 comb thereby achieving coherent expansion. This configuration can be scaled by subsequently cascading more lasers and thereby

increasing the number of tones, hence providing a low loss and scalable technique for comb expansion. Moreover, this method lends itself to photonic integration [11], thereby enhancing its compactness, cost-efficiency and ease of manufacture.

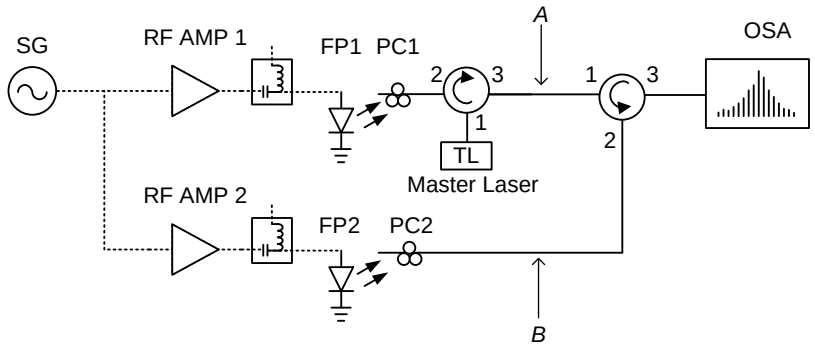

Figure 4.2: Experimental set up for the proposed expansion technique of GS-OFCS consisting of two cascaded gain switched FP lasers. SG: signal generator; RF AMP: RF amplifier; PC: polarization controller; TL: tunable laser; OSA: optical spectrum analyser.

The experimental setup for the expanded reconfigurable GS-OFCS generation is illustrated in Figure 4.2. The two FP lasers used (FP1 and FP2) are individually encased in a temperature controlled high-speed butterfly package and emit in the 1.5 μm window. Both FPs exhibited a threshold current (I_{th}) of 8 mA at room temperature and a small signal modulation bandwidth of 11 GHz when biased at 40 mA ($5I_{th}$). Gain switching of both lasers is achieved by applying an amplified 10 GHz sinusoidal Radio frequency (RF) signal (24 dBm) in conjunction with a dc bias of 45 mA and 40 mA, respectively, through bias tees. A semiconductor based TL with low linewidth ($\sim$80 kHz) is used as the master laser. The TL injects light into FP1 via a circulator. The wavelength of the TL is tuned to overlap one of the longitudinal modes of FP1 with an injected incident power of about 6 dBm to injection lock, thereby forcing it into single mode emission at the injected wavelength. The gain switched optical comb obtained from FP1 is subsequently injected into FP2 through another circulator. The polarization controllers (PC1 and PC2) are used to align the polarization state of the injected light with the optical waveguides of the two FP lasers. The expanded reconfigurable gain switched comb is then observed with a high resolution Optical Spectrum Analyser (OSA).

4.2.1 Experimental Results

Figure 4.3 presents the spectra at the output of each FP, at the points A and B marked in Figure 4.2. The spectrum in Figure 4.3 (a) corresponds to the resultant comb from the gain switched

FP1 externally injected by the TL, which is represented by a blue circle. As observed, the TL is injection locking the FP1 forcing it into single mode operation and the generated comb exhibits 6 comb tones within 3 dB of spectral flatness, spaced by 10 GHz. This gain switched comb from FP1 will subsequently inject into FP2. Figure 4.3 (b) shows the spectrum of the gain switched FP2, at point B, which results in the gain switching of all the FP longitudinal modes.

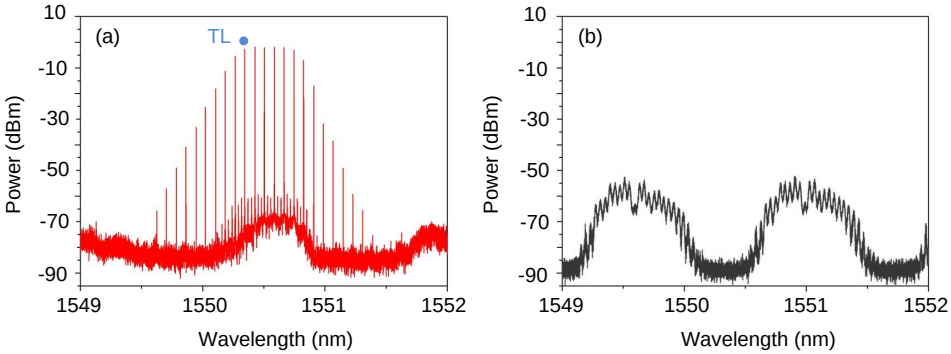

Figure 4.3: (a) Resultant externally injected and gain switched comb generated from FP1, at point *A* in Figure 4.2. TL is positioned at the comb tone marked with a blue dot. (b) Gain switched FP2, at point *B* in Figure 4.2, where all longitudinal modes are gain switched.

Figure 4.4 (a) illustrates the two previous independent spectra overlaid. As observed, the TL, indicated by the blue circle, will inject exclusively into FP1. Furthermore, it can be clearly seen that the initial gain switched comb from FP1 and one of the gain switched longitudinal modes of FP2 are partially overlapped. Therefore, the comb tones at the long wavelength edge are positioned such that they will injection lock FP2, leading to comb generation around the injection locked mode of FP2.

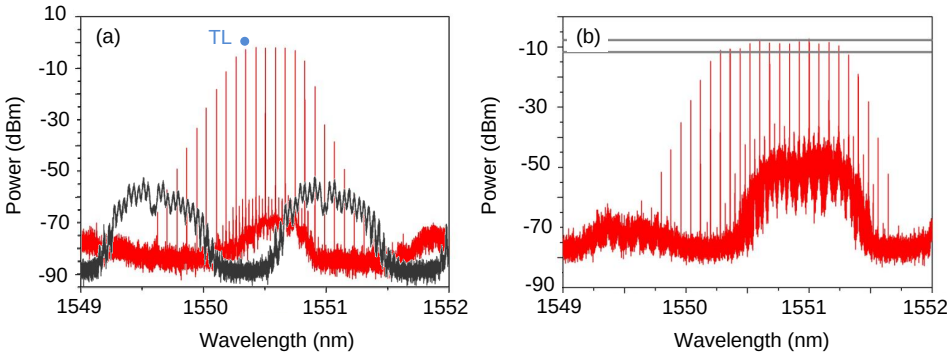

Figure 4.4: (a) Superimposition of gain switched comb from FP1 with TL injection, and FP2 gain switched with no injection. (b) Resultant expanded GS-OFCS presenting 13 comb tones in a 3 dB spectral flatness.

The optical spectrum of the resultant expanded comb, depicted in Figure 4.4 (b), comprises 13 clearly resolved comb tones within a spectral ripple of 3 dB at 10 GHz FSR, an optical power per comb tone of $\sim$ -5 dBm and an OCNR of 25 dB. As such, this proposed expansion technique has successfully almost doubled the bandwidth of the initial comb source (from FP1).

4.2.1.1 Central Wavelength Tunability

The experimentally demonstrated expansion technique permits wavelength tunability over the C-band. The TL is tuned in wavelength to inject into a different longitudinal mode of FP1. This precise injection results in a single mode operation at the injected wavelength of FP1, which is subsequently gain switched with an amplified 10 GHz sinewave to generate the comb. By subsequent injection of the spectrally adjacent longitudinal mode of FP2, the resultant expanded comb can be achieved at different wavelengths.

Figure 4.5 (b) and (c) present the expanded reconfigurable GS-OFCS at two representative central wavelengths 20 nm apart, at 1542 nm and 1563.5 nm respectively as a proof-of-concept of the wavelength tunability. Both generated combs offer similar characteristics, with 13 clearly resolved comb tones within a 3 dB spectral envelope, optical power per comb tone of $\sim$ -5 dBm and an OCNR of 25 dB. The Side-Mode-Suppression Ratio (SMSR) with respect to suppressed longitudinal modes is larger than 45 dB.

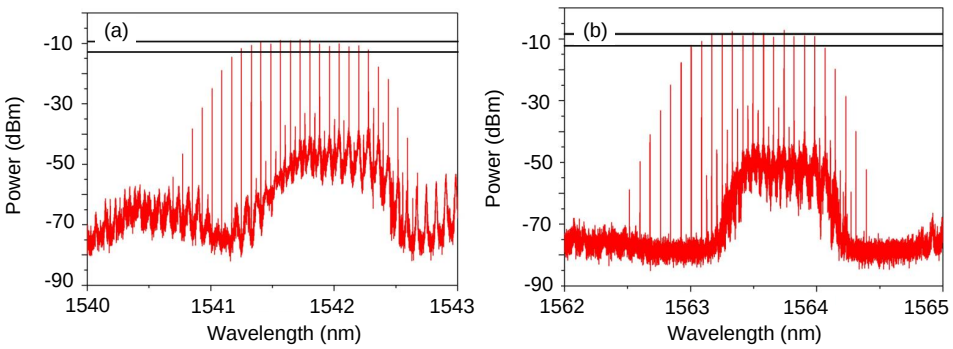

Figure 4.5: Central Wavelength Tunability: Resultant expanded comb at central wavelengths of (a) 1542 nm, and (b) 1563.8 nm.

Precise continuous wavelength tunability can be achieved by fine temperature tuning of both lasers accordingly, through the same procedure explained in Chapter 3. Furthermore, it is important to mention that this expansion technique offers tunable FSR by modifying the gain switching signal

frequency.

4.2.1.2 Phase Noise

The obtained phase noise is characterized by measuring the optical linewidth. External injection locking ensures an effective transfer of the narrow emission linewidth from the master to the slave comb tones. As such, the optical linewidth of the individual comb tones is measured to determine the level of phase noise and, additionally, to corroborate the locking of both FP lasers to the master TL laser.

The optical linewidth is characterized using the Delayed Self-Heterodyne (DSH) technique [12], illustrated in Figure 4.6. A tunable Optical Band Pass Filter (OBPF) is used to select out individual comb lines which are then amplified with an EDFA. The signal is then equally split with a coupler into two paths. In one arm, the signal is phase modulated at 2 GHz while in the second arm, the signal is delayed by a 12 km of Standard Single Mode Fibre (SSMF) to de-correlate both arms and thus, when both beams are mixed with a photodetector, they combine as if they are from two independent lasers. The linewidth is then retrieved from the observed beat signal at 2 GHz in an Electrical Spectrum Analyzer (ESA).

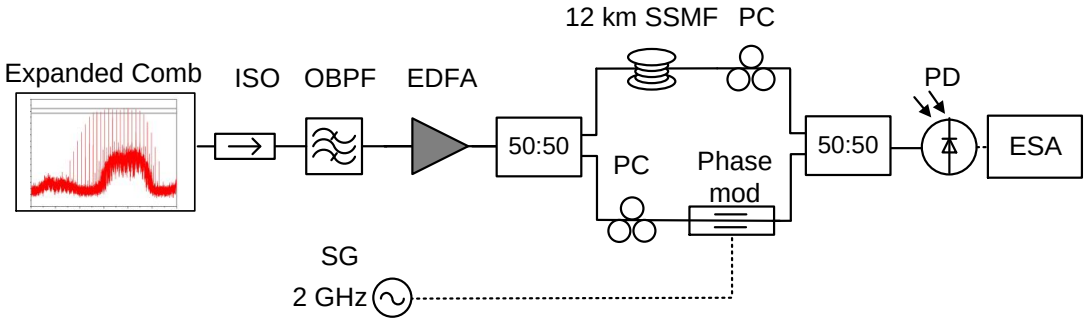

Figure 4.6: Delayed Self-Heterodyne experimental set up for optical linewidth measurement. ISO: isolator; OBPF: optical band pass filter; EDFA: Erbium doped fibre amplifier; SSMF: standard single mode fibre; PC: polarization controller; SG: signal generator; PD: photodetector; ESA: electrical spectrum analyser.

For the case of a Lorentzian lineshape, the occupied bandwidth measured at full width at -20 dB of the power spectrum of the superimposed beams is related to the original linewidth as, δf [13]:

$$\delta f = \frac{OccBW_{-20dB}}{2\sqrt{99}} \tag{4.1}$$

The optical linewidths of the FP longitudinal modes without external injection are around 3 MHz. However, due to external optical injection locking, the optical linewidth from the master effectively transfers to the comb lines. As such, the optical linewidths of three individually filtered comb lines, indicated in Figure 4.7 (a) at the left edge (-6), central (0) and right edge (6) of the 3 dB window, were measured and found to be approximately 80 kHz (based on full width at -20 dB measurement of 1.5 MHz) following that of the master laser as presented in Figure 4.7 (b).

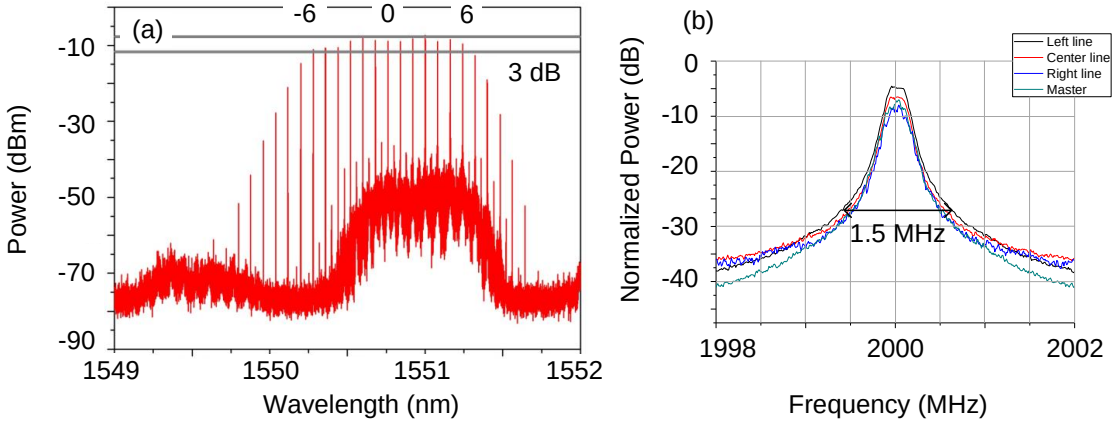

Figure 4.7: (a) Resultant expanded GS-OFCS with marked comb tones for optical linewidth measurement and phase correlation. (b) Measured optical linewidth for Left comb tone (-6) in black, Central comb tone (0) in red, Right comb tone (6) in blue and Master TL in green.

The required length of fibre that produces enough delay to de-correlate the signal in the DSH technique needs to be longer than the so-called *coherence length* of the laser, L_{coh}, which is defined as:

$$L_{coh} = \frac{c}{n\delta f} \tag{4.2}$$

where c is the speed of light, δf is the laser linewidth, and n refers to the refractive index of the fibre. According to this equation, the experimental measurement set up presented in Figure 4.6 allows linewidth measurements down to $\approx$ 17 kHz [12], [14].

4.2.1.3 Phase Correlation

In order to ensure that the expanded comb lines exhibit a high degree of phase correlation with each other, the RF beat tone linewidth is characterised. The spectral linewidth of the RF beat tone, which is generated at the frequency that corresponds to the spectral separation between the comb tones, is determined by the phase noise of the comb tones and the level of correlation between them. If

there is no correlation between the comb tones, the beat signal has a linewidth equal to the sum of the optical linewidths of the optical tones. If a strong phase correlation exists, these phase noises cancel each other out. Therefore, the spectral linewidth of the RF beat tone reduces as the phase correlation between the tones improves [16].

The RF beat tone linewidth is then characterised using the experimental set up illustrated in Figure 4.8 (a) [15]. The expanded gain switched comb is followed by an EDFA before being passed to a programmable Wavelength Selective Switch (WSS). The WSS selects pair of comb lines, in steps of 10 GHz, to be analysed. Subsequently, the filtered tones are detected with a 70 GHz Photodetector (PD) and the obtained RF beat tone linewidth is observed with a 40 GHz ESA. An external harmonic mixer is also employed when the frequency spacing of the filtered comb lines is in the range of 40 GHz to 60 GHz (outside the bandwidth of the ESA) for down conversion.

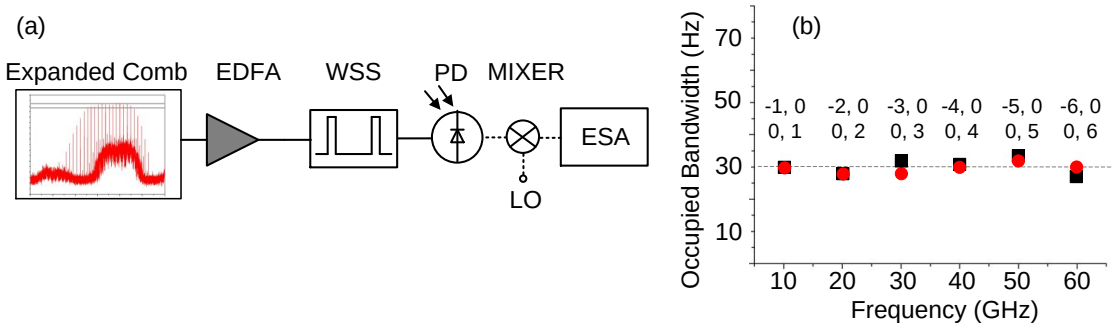

Figure 4.8: (a) Experimental set up for RF beat tone linewidth measurement for phase correlation. (b) RF beat tone linewidth measured between the comb tone 0 and the consecutive tones. WSS: wavelength selective switch; PD: photodetector; LO: local oscillator.

The results of the linewidth measurement of the RF beat tone of the expanded GS-OFCS lines are given in Figure 4.8 (b). The measurements when beating the comb tone 0 (as marked in Figure 4.7 (a)) and the consecutive tones to each side up to a separation of 60 GHz (tone -6 and 6) are illustrated with squares and circles representing the negative and positive sides respectively.

The 3 dB linewidth of the RF beat tone measured is found to be constant at around 30 Hz in all cases (limited by the resolution of the ESA), thus proving the excellent correlation between the comb lines of the expanded GS-OFCS.

4.3 Broadband Combs by Dual Mode Injection Locking of FPs

The second technique proposed for broadband and reconfigurable GS-OFCS generation comprises an externally injected and gain switched FP, where the optical injection takes place between two neighbouring FP longitudinal modes. As a result comb generation happens simultaneously at both gain switched FP modes and an expanded OFCS is achieved. The technique requires a small component count and provides low complexity and power consumption, while delivering high spectral purity, flexibility and broadband comb spectrum. Moreover, this simple technique is suitable for photonic integration, yielding further footprint and power consumption reduction.

The experimental set up for the proposed technique is illustrated in Figure 4.9 (a). The lasers employed in this experiment are the same used in Chapter 3. The FP laser is encased in an optically un-isolated and temperature controlled high-speed butterfly package, emits in the 1.5 µm window and exhibits a threshold current (I_{th}) of 8 mA and a small signal modulation bandwidth of 11 GHz when biased at 40 mA ($5I_{th}$). Gain switching of all the longitudinal modes is obtained by direct modulation with an amplified sinusoidal RF signal (24 dBm) in conjunction with a dc bias of 45 mA. A semiconductor based TL with a low linewidth of 300 kHz, acting as a master, was used in this configuration to inject light into the cavity of the FP laser (slave) via a polarization-maintaining circulator. All optical components in the experimental set up are pigtailed with polarization-maintaining fibres to maintain the state of polarization.

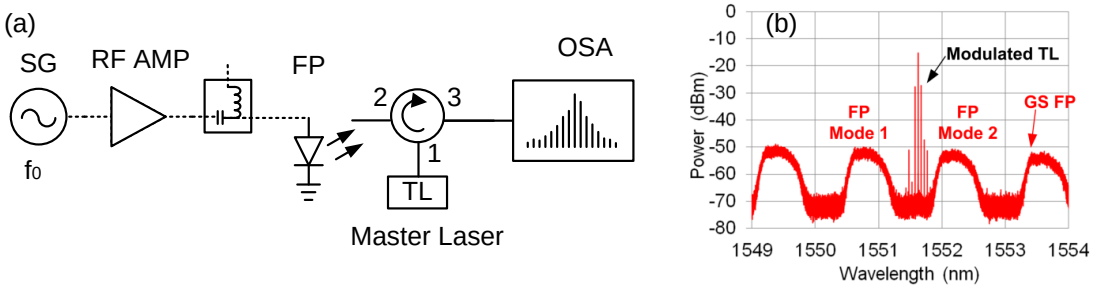

Figure 4.9: (a) Experimental set up for broadband gain switched comb generation; (b) Modulated TL through the gain switched FP cavity. SG: signal generator; RF AMP: RF amplifier

The light injected from the TL, on its pass through the FP cavity is also modulated by the large RF signal applied to the FP laser. This large modulation generates harmonic sidebands around the TL wavelength spaced exactly by the gain switching signal frequency, f_0, as observed in Figure 4.9 (b). The spectrum in this figure was observed by applying a substantially low RF power signal.

As a consequence, the FP longitudinal modes present some level of spectral broadening that is insufficient to overlap with the modulation sidebands around the external injection.

The optical injection power ratio ($P_{INJ}(dBm)$ – $P_{FP}(dBm)$ = 10 dB), with an injected power of 15 dBm, and the wavelength detuning ($\lambda_{SLAVE} - \lambda_{MASTER}$) are carefully chosen to ensure that these master sidebands overlap partially with two adjacent gain switched FP longitudinal modes, marked as *FP mode 1* and *FP mode 2* respectively in Figure 4.9 (b). As the RF power is increased, the spectral width of the FP modes broaden and more harmonic sidebands are generated around the TL.In this case, instead of ensuring single mode operation of the FP, high power is injected to produce sidebands with enough power to inject into two FP modes. Simultaneous injection locking of these two neighbouring modes is then achieved, thereby forcing the FP into dual mode emission at the selected longitudinal mode wavelengths. This results in a broadened gain switched comb generation around the wavelengths of the dual injection locked FP, observed with a high resolution (0.16 pm) OSA.

4.3.1 Experimental Results

The optical spectrum of the resultant broadband GS-OFCS, when gain switching the FP at 6.25 GHz, is depicted in Figure 4.10 (a). This FSR is chosen due to the direct compatibility with the proposed International Telecommunication Union (ITU) flexible grid recommendation in G.694.1 [17]. The generated broadband comb exhibits some comb tones dropping in power between the two FP modes. Nevertheless, the extreme comb tones within 3 dB of the spectral envelope peak are separated by 275 GHz and comprise 44 clearly resolved highly coherent comb tones at 6.25 GHz FSR with an OCNR of 35 dB. The overall 3 dB bandwidth achieved (275 GHz) and the remarkable simplicity of the technique clearly highlight its potential for millimetre and sub-THz wave generation.

To further enhance the practical viability of this configuration for coherent superchannel transmission where the spectral flatness is a crucial requirement, the broadband GS-OFCS is passed through a programmable gain flattening filter. The optical spectrum of the resultant flattened comb presents 52 clearly resolved comb tones (overall bandwidth of 325 GHz) within a 6 dB spectral ripple while still preserving a good OCNR of 30 dB, as illustrated in Figure 4.10 (b).

Figure 4.10 (c) shows the spectrum of the conventional gain switched FP laser, with low power external injection into a singular longitudinal mode. As observed, the comb exhibits 11 comb tones

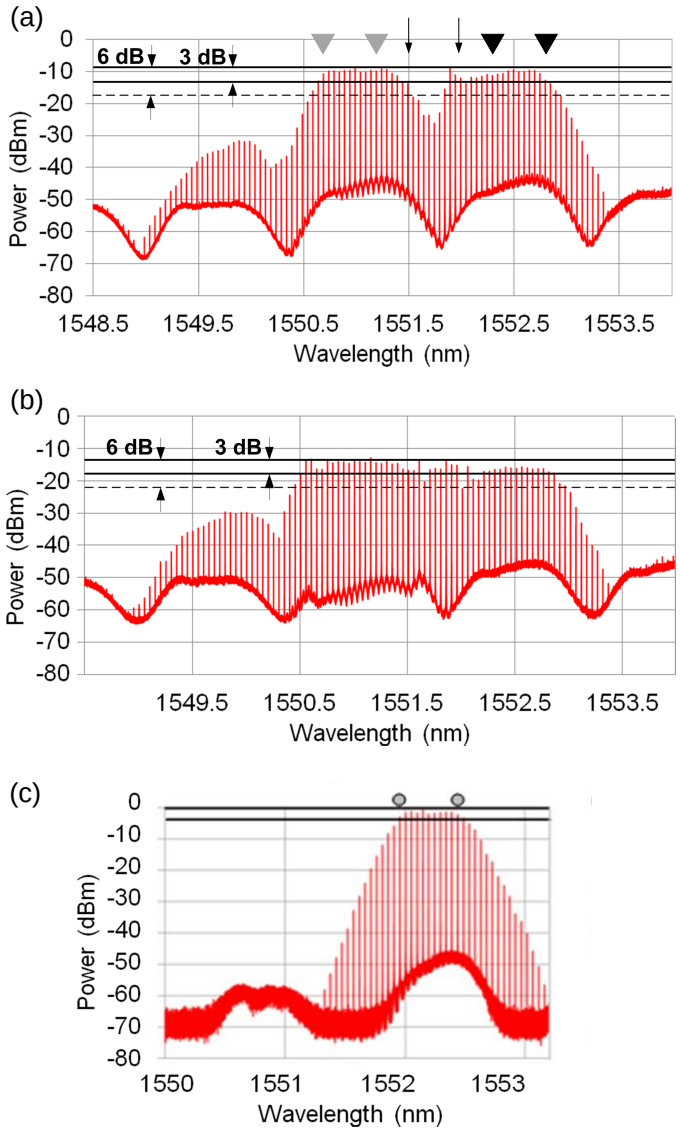

Figure 4.10: (a) Resultant broadband comb by dual mode injection locked of a gain switched FP laser (b) Flattened broadband comb after a programmable gain flattening filter. The spectrum was amplified to overcome the insertion losses of the filter and (c) Gain switched single mode injection locked FP laser.

in a 3 dB spectral flatness with an OCNR of 45 dB. Consequently, the proposed expansion technique based on the simultaneous injection locking of two FP modes, has successfully quadrupled the overall 3 dB bandwidth compared to the case where injection locking only takes place in a single longitudinal mode. However, the flatness and OCNR are compromised.

4.3.1.1 Central Wavelength Tunability

This scheme offers continuous wavelength tunability over 30 nm, as presented in Figure 4.11 (a) and (b) where the broadband gain switched comb is generated at central wavelengths of 1536.5 nm and at 1565.8 nm, respectively. These results are obtained by tuning the wavelength of the TL to inject into a different pair of longitudinal modes of the FP slave laser.

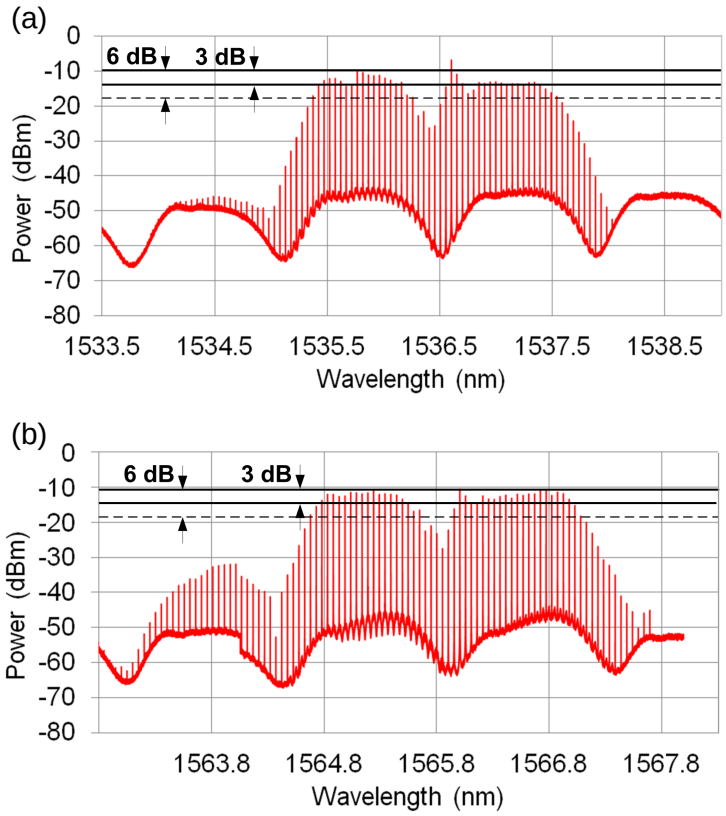

Figure 4.11: Central Wavelength Tunability: Broadband comb generation at central wavelengths of (a) 1536.5 nm, and (b) 1565.8 nm;

Therefore, broadband comb generation by dual mode injection locking is successfully obtained consistently within the C-band. The extreme comb tones within a 3 dB of spectral flatness are separated by 275 GHz, comprising 44 clearly resolved highly coherent comb tones with an OCNR of 45 dB.

4.3.1.2 Phase Noise

The optical linewidth of the comb lines was measured using the DSH technique, illustrated in Figure 4.6. The optical linewidth of the master TL used in this experimental set up exhibits a linewidth of 300 kHz which is effectively transferred to the comb tones as depicted in the measured optical linewidth of the comb lines in Figure 4.12, due to external injection locking. This linewidth was obtained by measuring a full width at -20 dB of 5.8 MHz, that corresponds to approximately 300 kHz using equation 4.1.

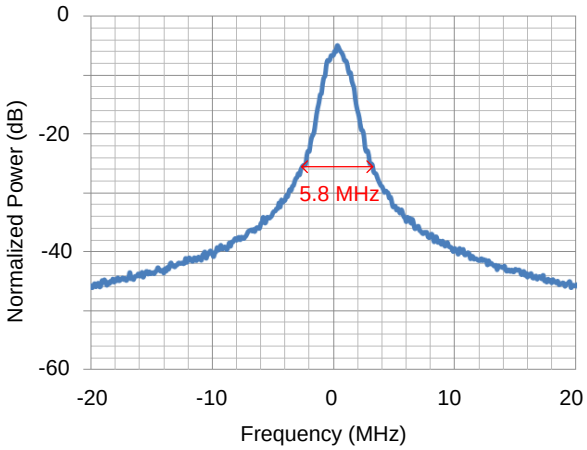

Figure 4.12: Measured optical linewidth

4.3.1.3 Phase Correlation

The high quality of phase correlation is confirmed by characterising the RF beat tone linewidth, using the experimental set up depicted in Figure 4.8. In these measurements, the WSS selects a pair of comb lines separated by 62.5 GHz and after detection, the beat signal is down converted using a mixer with a Local Oscillator (LO) at 63.5 GHz and observed with a 3 GHz bandwidth ESA.

The measurement when beating the comb tones across the two locked FP longitudinal modes, marked in Figure 4.10 (a) with arrows, is compared with beating tones along the individual FP modes to prove simultaneous injection locking. The comb tones to be analysed in the FP mode 1 and FP mode 2 are marked in Figure 4.10 (a) with grey and black triangles, respectively. Finally, the RF beat tone linewidth of a comb generated around a single injection locked longitudinal mode is also measured as a reference of the ideal phase correlation. The pair of comb tones selected, illustrated by grey circles in Figure 4.10 (c), are also separated by 62.5 GHz for adequate

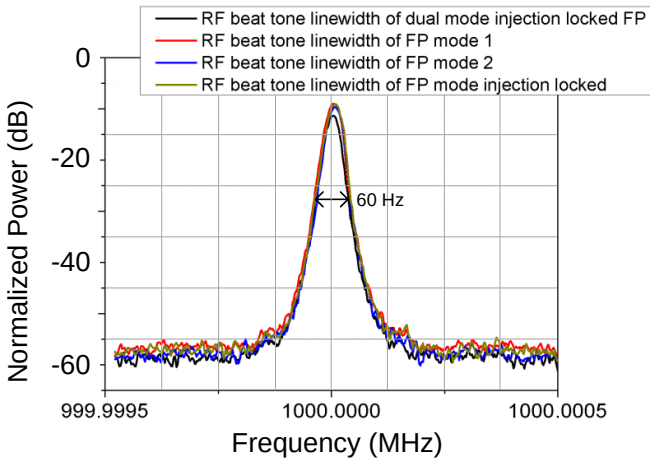

Figure 4.13: RF beat tone linewidth measured on different scenarios to prove phase correlation and simultaneous injection locking of two FP longitudinal modes.

comparison.

The RF beat tone linewidths are measured by observing the occupied bandwidth full width at -20 dB. The RF beat tone linewidth for all scenarios were found to be around 60 Hz, with a resolution bandwidth of 30 Hz from the ESA and limited by the noise of the RF source used to gain switch. These measurements prove an exceptional high phase correlation between the comb tones and thus, additionally confirming that the two longitudinal FP modes are simultaneously injection locked to the same master laser.

4.4 Conclusions

This chapter has proposed two novel techniques for bandwidth expansion of reconfigurable gain switched OFCS. Both configurations present low optical linewidth, excellent phase correlation and continuous central wavelength tunability within the C-band, targeting numerous applications in next generation optical transmission networks.

The first configuration consists of the expansion of GS-OFCS by seeding a gain switched FP laser with a comb from another gain switched, and injection locked, FP laser. The resultant expanded comb presents a doubling in bandwidth of the initial source and exhibits a remarkable spectral flatness. This technique can be escalated which is subject for further study and simulation work, and is potentially integrable but the component count is high and power consuming (due to the use of multiple high power amplifiers).

The second configuration comprises an externally injected and gain switched FP laser, where the optical injection takes place between two neighbouring FP longitudinal modes. As a result, comb generation happens simultaneously at both gain switched FP modes. This proposed method is exceptionally simple but effective for broadband comb generation (hundreds of GHz). It requires a small component count, is suitable for photonic integration and provides low complexity and power consumption. However, the flatness is degraded and equalisation techniques may be needed for coherent superchannel applications.

These features will make each of these expansion techniques more suitable for employment in a variety of communication applications, including next generation flexible superchannel transmission and millimetre wave generation.

References

[1] M. D. Gutierrez Pascual, R. Zhou, F. Smyth, P. M. Anandarajah, and L. P. Barry, "Software reconfigurable highly flexible gain switched optical frequency comb source," *Optics Express*, vol. 23, pp. 23225-23235, August 2015.

[2] P. Marin, J. Pfeifle, M. Karpov, P. Trocha, R. Rosenberger, K. Vijayan, S. Wolf, J. N. Kemal, A. Kordts, M. Pfeiffer, V. Brasch, W. Freude, T. Kippenberg, and C. Koos, "50 Tbit/s Massively Parallel WDM Transmission in C and L Band Using Interleaved Cavity-Soliton Kerr Combs," in *Proceedings of Conference on Lasers and Electro-Optics*, San Jose, CA, paper STu1G.1, 2016.

[3] E. Temprana, E. Myslivets, B.P.-P. Kuo, L. Liu, V. Ataie, N. Alic, and S. Radic, "Overcoming Kerr-induced capacity limit in optical fiber transmission," *Science*, vol. 348, no. 6242, pp. 1445–1448, Jun 2015.

[4] P. Zhu, J. Li, L. Niu, Y. Xu, Y. Chen, X. Xie, X. Chen, B. Guo, Z. Chen, and Y. He, "Optical Comb-enabled Cost-effective ROADM Scheme for Elastic Optical Networks," in *Proceedings of Optical Fiber Communication Conference*, San Francisco, CA, paper W3B.5, 2014.

[5] V. Vujicic, J. Pfeifle, R. Watts, P. C. Schindler, C. Weimann, R. Zhou, W. Freude, C. G. Koos, and L. Barry, "Flexible Terabit/s Nyquist-WDM Superchannels with net SE ¿7bit/s/Hz using a Gain-Switched Comb Source," in *Proceedings of Conference Conference on Lasers and Electro-Optics*, paper SW1J.3, San Jose, CA, 2014.

[6] T. Shao, H. Shams, P. M. Anandarajah, M. J. Fice, C. C. Renaud, F. van Dijk, A. J. Seeds, and L. P. Barry, "Phase Noise Investigation of Multicarrier Sub-THz Wireless Transmission System Based on an Injection-Locked Gain-Switched Laser," *IEEE Transactions on Terahertz Science and Technology*, vol. 5, no. 4, pp. 590-597, July 2015.

[7] T. Habruseva, S. O'Donoghue, N. Rebrova, F. Kéfélian, S. P. Hegarty, and G. Huyet, "Optical linewidth of a passively mode-locked semiconductor laser," *Optics Letters*, vol. 34, no. 21, pp.

3307-3309, 2009.

[8] R. Wu, V. R. Supradeepa, C. M. Long, D. E. Leaird and A. M. Weiner, "Highly flat and stable optical frequency comb generation using intensity and phase modulators employing quasi-quadratic phase modulation," in *IEEE International Topical Meeting on Microwave Photonics*, Montreal, QC, pp. 212–215, 2010.

[9] R. Zhou, S. Latkowski, J. O'Carroll, R. Phelan, L. P. Barry, and P. Anandarajah, "40 nm wavelength tunable gain-switched optical comb source," *Optics Express*, vol. 19, no. 26, pp. B415–B420, 2011.

[10] P. M. Anandarajah, R. Maher, Y. Q. Xu, S. Latkowski, J. O'Carroll, S. G. Murdoch, R. Phelan, J. O'Gorman, L. P. Barry, "Generation of Coherent Multicarrier Signals by Gain Switching of Discrete Mode Lasers," *IEEE Photonics Journal*, vol. 3, no. 1, pp. 112–122, Feb. 2011.

[11] R. Zhou, P. M. Anandarajah, D. Gutierrez Pascual, J. O'Carroll, R. Phelan, B. Kelly, and L. P. Barry, "Monolithically integrated 2-section lasers for injection locked gain switched comb generation," in *Proceedings of Optical Fiber Communication Conference and Exposition* paper Th3A.3, San Francisco, CA, 2014.

[12] T. Okoshi, K. Kikuchi, and A. Nakayama, "Novel method for high resolution measurement of laser output spectrum," *Electronics Letters*, vol. 16, no. 16, pp. 630-631, July 31 1980.

[13] Dennis Derickson, "Fiber optic test and measurement," Prentice Hall PTR, 1998.

[14] R. Zhou, "Optical frequency comb source for next generation access networks," PhD thesis, Dublin City University, 2014. Available: http://doras.dcu.ie/20213/1/Thesis_Final_Rui.pdf

[15] A. P. Anthur, R. T. Watts, R. Zhou, P. Anandarajah, D. Venkitesh, and Liam P. Barry, "Penalty-free wavelength conversion with variable channel separation using gain-switched comb source," *Optics Communications*, vol. 324, pp. 69-72, Aug. 2014.

[16] Kazuro Kikuchi, "Characterization of semiconductor-laser phase noise and estimation of bit-error rate performance with low-speed offline digital coherent receivers," *Opt. Express*, vol. 20, pp. 5291-5302, 2012.

[17] ITU-T Recommendations, "Spectral grids for WDM applications: DWDM frequency grid," G.694.1, 2012. Available: https://www.itu.int/rec/T-REC-G.694.1/en

[18] M. D. Gutierrez Pascual, P. M. Anandarajah, R. Zhou, F. Smyth, S. Latkowski, and L. P. Barry, "Cascaded Fabry-Pérot lasers for coherent expansion of wavelength tunable gain switched

comb," in *Proceedings of European Conference on Optical Communication*, paper Mo.3.4.4, Sept. 2014.

[19] M. D. Gutierrez Pascual, R. Zhou, F. Smyth, and L. P. Barry, "Coherent Expansion of Gain Switched Optical Frequency Comb by Cascading Fabry-Pérot Lasers," *in Proceedings of Photonics Ireland*, Cork (Ireland), Sept. 2015.

[20] M. D. Gutierrez Pascual, R. Zhou, F. Smyth, T. Shao, P. M. Anandarajah, and L. P. Barry, "Dual mode injection locking of a Fabry-Pérot laser for tunable broadband gain switched comb generation," in *Proceedings of European Conference on Optical Communication*, Sept. 2015.

Chapter 5

Photonic Integrated Gain Switched Comb and its De-multiplexing for Spectrally Efficient Optical Transmission Systems

Previous chapters have proposed experimental approaches to enhance the practicality of a Gain Switched Optical Frequency Comb Source (GS-OFCS) in terms of reconfigurability, and bandwidth coverage expansion. As such, externally injected GS-OFCSs are able to generate multiple equally spaced optical carriers that may span over large bandwidths (hundreds of GHz) with excellent phase correlation, low Relative Intensity Noise (RIN) and narrow optical linewidth transferred from the optical external injection, high Optical Carrier to Noise Ratio (OCNR) and flexible features that include central wavelength and Free Spectral Range (FSR) tunability, which are all desirable qualities for multi-carrier sources.

Nevertheless, commercial networks benefit from photonic integrated circuits where optical components can be combined in a single chip, reducing fabrication processes, footprint and associated costs in assembly, packaging and testing. Thus, the photonic integration of GS-OFCSs is of paramount interest to further enhance its usefulness and viability in optical networks. Additionally, an extended issue among multi-carrier sources is the necessity of de-multiplexing the carriers for independent modulation which typically requires the use of optical amplifiers which are costly and

enlarge the transmitter footprint.

This chapter presents a detailed experimental characterization of two novel Indium Phosphide (InP) integrated circuits for the generation of an externally injected GS-OFCS and comb de-multiplexing based on injection locking. Finally, this thesis investigates the performance of the integrated GS-OFCS in two different data transmission systems that employ advanced modulation formats to study the influence of the device noise properties and to validate the versatility of the GS-OFCS for diverse systems throughout the network.

The functionality, performance and compactness of these devices further improve the potential and quality of GS-OFCSs for future optical networks deployment.

5.1 Introduction

Data traffic has experienced incessant exponential growth over the last decade due to the appearance of new cloud services and web applications [1], [2]. In order to keep meeting the demand for bandwidth, optical networks must evolve towards higher performance and throughput, spectral efficiency, and reduced power consumption [3], [4]. This significant transformation is required throughout the network, from communications links within datacentres, in metro and into the backbone [5]- [7].

Depending on the network topology and application, diverse requirements and specifications (such as transmission lengths, modulation formats and complexity) are stipulated. Transmission links within datacentres are expected to be shorter than 3 km, and while several potential modulation formats have been considered [8]- [10], 4-level Pulse Amplitude Modulation (PAM) has gained remarkable attention [11], [12]. In metro and long-reach links, however, coherent communications are used due to the high receiver sensitivity, frequency selectivity and superiority of digital signal processing for compensation of transmission impairments with transmissions lengths over 50 km [13]- [15].

Optical frequency comb sources have proven to be key components in spectrally-efficient optical transmission systems [14]- [19], thanks to their low complexity, and precise and stable frequency spacing between the carriers enabling the reduction or elimination of guard bands in advanced multicarrier modulation techniques. Additionally, an Optical Frequency Comb Source (OFCS) may also offer FSR flexibility that allows a single source to be easily adapted to suit different modulation

formats and symbol rates [20].

Optical comb generation by gain switching of an externally injected semiconductor laser diode is a remarkably simple and flexible technique that relies on the direct modulation of the current injected to any commercial off-the-shelf laser [21]- [24]. It inherently offers FSR tunability and strong phase correlation between the optical carriers. Moreover, low RIN unaffected by mode partition noise [17], [19], and narrow emission linewidth from the external injected light can be effectively transferred to the comb lines [22], [25]. As such, the GS-OFCS presents desirable qualities and offers itself as a single versatile source with potential to meet the requirements of various optical networking scenarios from intra-datacentre, to long-haul optical transport.

Nevertheless, in order to yield further compactness, cost-efficiency and ease of fabrication, the photonic integration of injected GS-OFCSs and active comb de-multiplexers are crucial for viable network deployment.

5.1.1 Photonic Integration

Photonic integrated circuits are miniaturised circuits that operate at optical frequencies and consist on a number of individual inter-connected components fabricated in a common substrate. Photonic integration offers numerous advantages to next generation optical networks as compact footprint of devices, realization of complex systems in a single chip, energy efficiency, reliability, reduced costs and large scale manufacturing [26].

Photonic integrated circuits are being developed in parallel in two main substrate materials, InP and Silicon, each offering different merits according to its material properties [27]:

Indium Phosphide (InP): InP is a direct bandgap III-V compound semiconductor material that supports the integration of active components as efficient lasers, optical amplifiers and also manifest good electro-optical properties for sensitive photodetection and fast modulators [27], [28]. The InP technology beneficially allows the integration on a single platform of passive and active components, however, passive sections exhibit high losses and require current injection for transparent transmission.

Silicon (Si): Silicon is an indirect bandgap semiconductor material [27] and, consequently, is very inefficient in generating or detecting optical signals. Therefore, waveguides in this platform present very low optical losses, ideal for passive components. Additionally, silicon material is abundant on the Earth surface and compatible with CMOS technology. Thus, silicon photonic devices can

be made in standard CMOS processes, and allow the attractive potential for integrating photonic and electronic components on a single chip [28]. However, the indirect bandgap nature of the silicon platform prevents effective amplification and laser generation which have been the main impediments for this technology to succeed.

In monolithic integration, the different compound materials are fabricated on the same wafer substrate (InP or Si) allowing simpler manufacturing processes and, thus, cost effectiveness and ease of fabrication. However, the devices and their performance are limited to the substrate material used. Alternatively, a lot of research is focusing in hybrid integration, where different components are fabricated in separated wafer substrates with the most suitable material, which are then combined to obtain the final device.

5.2 Photonic Integrated Gain Switched Comb

The fabricated Photonic Integrated Circuit (PIC) for comb generation is schematically represented in Figure 5.1 (a). The overall length of the device is $\sim$1.5 mm, consisting of four electrically independent sections. The material structure of the device is standard 1550 nm laser material with five strained AlGaInAs quantum-wells in the active region, on an n-doped InP substrate. The comb generator comprises two integrated Discrete Mode Laser Diodes (DMLD) [29] in a master-slave configuration, where the light generated from the master is injected into the slave cavity.

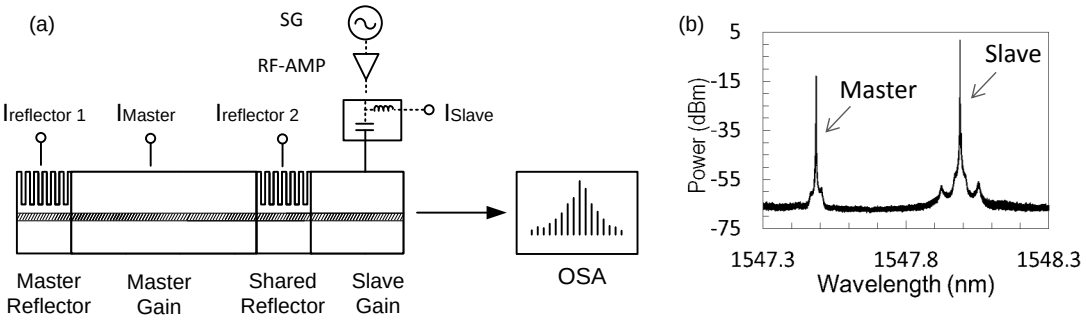

Figure 5.1: (a) Schematic of the photonic integrated device and experimental set up for the gain switched comb generation (b) Continuous Wave (CW) optical spectrum of the two integrated lasers, Master section biased at 40 mA, Slave section biased at 70 mA.

These lasers are regrowth free Fabry-Pérot (FP) lasers that include a mirror section consisting of a number of slots, with different grating periods, that have been etched close to the active region to

provide a regular refractive index perturbation and thus, optical feedback that ensures single mode operation. These slots are defined by standard electron-beam lithography allowing precise control of the slot width and slot periods with nm resolution.

The master laser is formed by a long gain section and two reflector sections at each side to provide enough reflection to create a lasing cavity and single mode emission, as depicted in Figure 5.1 (b). Both reflector sections are 215 µm long and consist of 22 slots etched 1.395 µm deep into the ridge waveguide. Because the lasing does not require a cleaved facet, this laser is suitable for monolithic integration with other photonic components in a single epitaxial growth. The reflector on the right end of the master gain section is shared by the slave cavity, effectively reducing the overall length of the PIC. Thus, the slave laser cavity is formed by a shorter gain section to allow high speed modulation, enclosed by the shared reflector section and the cleaved facet on the right end of the gain section. The master and slave sections are 711 µm and 355 µm long, respectively. As shown in Figure 5.1 (b), two independent single mode emissions can be achieved.

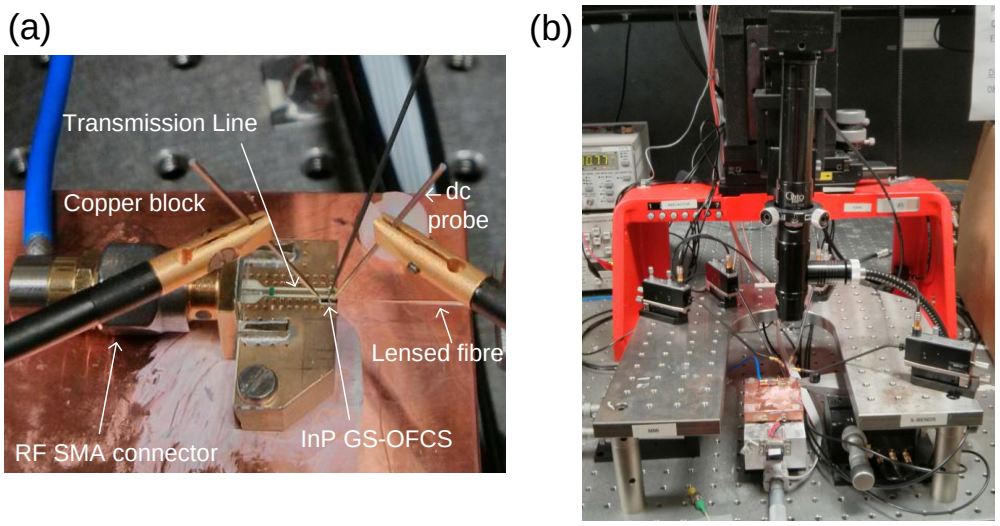

Figure 5.2: (a) Fabricated PIC for gain switched GS-OFCS, mounted on a high speed subcarrier that includes an Radio frequency (RF) connector and terminating resistor for gain switching and (b) Fabricated PIC under test in a probe station

Four independent metal contacts were deposited to allow independent bias of the sections. Gain switching is achieved by applying an amplified sinusoidal RF signal (24 dBm) to the slave section in conjunction with a dc bias through a bias tee. In order to enable gain switching with high speed signals, the PIC was subsequently mounted onto a subcarrier that includes an RF connector, a Conductor-Backed Coplanar Waveguide (CBCPW) transmission line, and a terminating 47 Ω

resistor ball bonded to the slave section for matching impedance, as shown in Figure 5.2 (a). The subcarrier was then placed on a temperature-controlled copper block for probe testing, as illustrated in Figure 5.2 (b). The device temperature was maintained at 20 °C using a Thermoelectric Cooler (TEC) module and coupling was achieved using lensed fibres on piezoelectric actuated stages. The resultant comb generated is then observed with a high resolution (0.16 pm) Optical Spectrum Analyser (OSA).

Before demonstrating the comb generation results and the enhancement on the obtained comb bandwidth due to the use of external optical injection, shown in Figures 5.3 (a) and (b) are the normalised frequency response of the device with the master section turned off (i.e. without external injection) and on (i.e. with external injection), characterised by performing small signal modulation analysis with the aid of a network analyser.

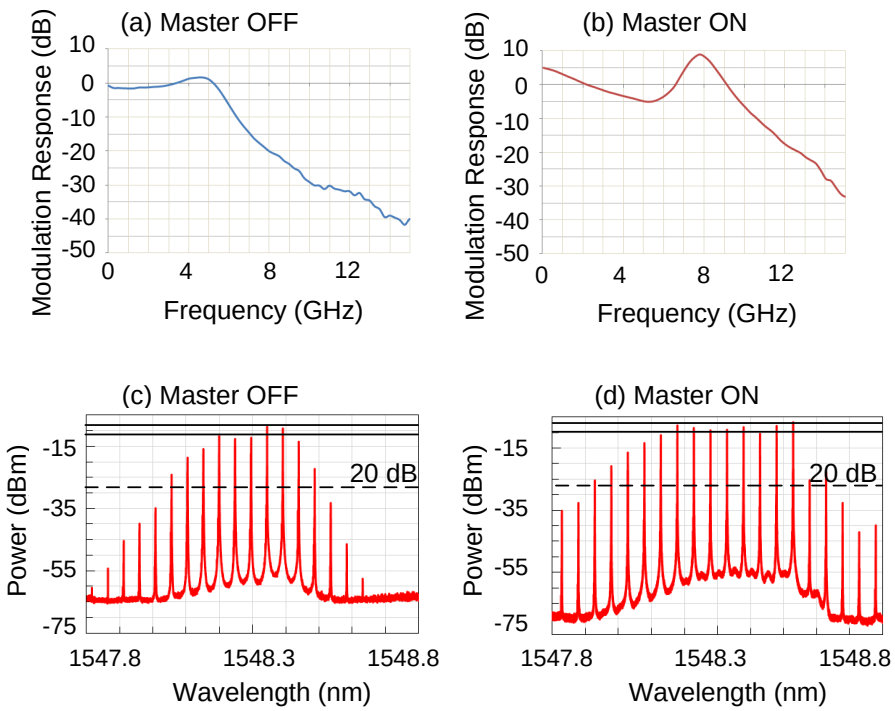

Figure 5.3: Modulation Response of device when (a) Master is OFF (without external injection) and (b) Master is ON, biased at 80 mA (with external injection). Resultant comb generated with an FSR of 6.25 GHz for: (a) No injection with Master section switched off and (b) External injection optimized with Master section biased to 80 mA.

A 3-dB modulation response bandwidth of approximately 5.5 GHz for the CW slave section is noticed. However, it can be also seen that the inherent bandwidth of this device could be improved up to around 9 GHz by properly biasing the master section (to 80 mA), therefore injecting into the

slave section.

The spectra illustrated in Figure 5.3 (c) and (d) demonstrate the obtained comb at the output of the device when the slave section is being gain switched at 6.25 GHz. In Figure 5.3 (c) the master section is turned off while the slave gain and the reflector sections are biased at 70 mA and 55 mA, respectively. As a result, 10 clearly resolved comb tones are observed within 20 dB of the spectral envelope peak, corresponding to a 20 dB bandwidth of 62.5 GHz. The comb tones present an OCNR of around 45 dB but the resultant flatness consists of only 2 comb tones within a 3 dB spectral window. In comparison, Figure 5.3 (d) illustrates the case when the master section current is turned on and the slave section current is kept to the same value. In this case, the master bias current is set to 80 mA for optimum modulation response enhancement and thereby, comb generation. It can be clearly seen that with optical injection from the master section, the resultant comb presents an improved flatness and bandwidth. The overall 20 dB bandwidth increases to 94 GHz, comprising 15 clearly resolved comb tones. These results agree with the improvement of the modulation bandwidth of the slave section due to external optical injection [24], [30]. Additionally, the flatness of the comb has been greatly enhanced with a total of 8 comb tones within a 3 dB spectral window with an OCNR in excess of 45 dB.

5.2.1 FSR Tunability

The FSR tunability of the comb is a key feature of gain switched OFCSs for numerous applications [25], [31]- [33], especially for future flexible optical transport solutions allowing the adjustment of the frequency spacing between the carriers to accommodate different modulation formats and baud rates. Figures 5.4 (a)-(d) illustrate the resultant GS-OFCS spectra generated with frequency spacings between the optical carriers spanning a range of 7-10 GHz.

Gain switching at these FSRs results in the generation of coherent frequency combs consisting of 4-8 clearly resolved comb tones within 3 dB of the spectral envelope peak, with a power per comb tone of $\sim$ -10 dBm and OCNR $>$ 35 dB. These results are achieved by changing the modulation frequency of the synthesizer used to gain switch. It is important to mention that the FSR can be continuously tuned and the minimum resolution is dictated by the electrical RF synthesizer although for simplicity, only four frequency spacings are shown. The restricted upper FSR and overall bandwidth can be attributed to the limited inherent bandwidth of the device, shown in Figure 5.3 (b). The frequency response could be improved in next iterations by decreasing the length of

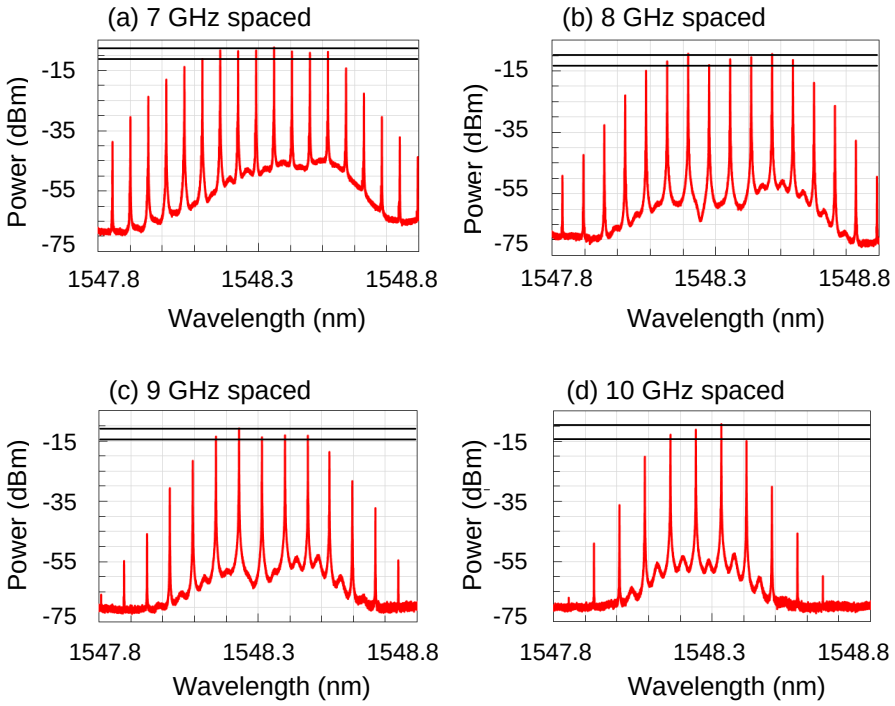

Figure 5.4: Resultant photonic integrated GS-OFCS at different FSRs: (a) 7 GHz with 8 comb tones in 3 dB window, (b) 8 GHz with 7 comb tones in 3 dB window, (c) 9 GHz with 5 comb tones in 3 dB window and (d) 10 GHz with 4 comb tones in 3 dB window.

the wire bond and size of the metal contact pads to reduce the device parasitics.

5.2.2 RIN

The RIN of the generated comb with an FSR of 6.25 GHz is then characterized, as an important indicator of the noise properties of the transmitter for data transmission. The RIN measurements were carried out using the experimental set up explained in Chapter 3 [35].

Due to the low power per comb tone after filtering ($\sim$ -24 dBm), an Erbium Doped Fibre Amplifier (EDFA) is required to measure the RIN [35]. Therefore, these measurements are influenced by Amplified Spontaneous Emission (ASE) and the actual RIN values for each comb tone are expected to be probably lower than presented here. The ASE generated by the EDFA varies depending on the input power launched into it which influences the RIN measured. Therefore, a Variable Optical Attenuator (VOA) is placed in line between the filter and EDFA to ensure constant power at its input, and thereby similar ASE for all measurements, allowing an objective relative comparison of the RIN results. Comb tone number 6 presents the lowest optical power after filtering (corresponding

to -24 dBm) and, therefore, dictates the optical power set at the input of the EDFA (through the VOA).

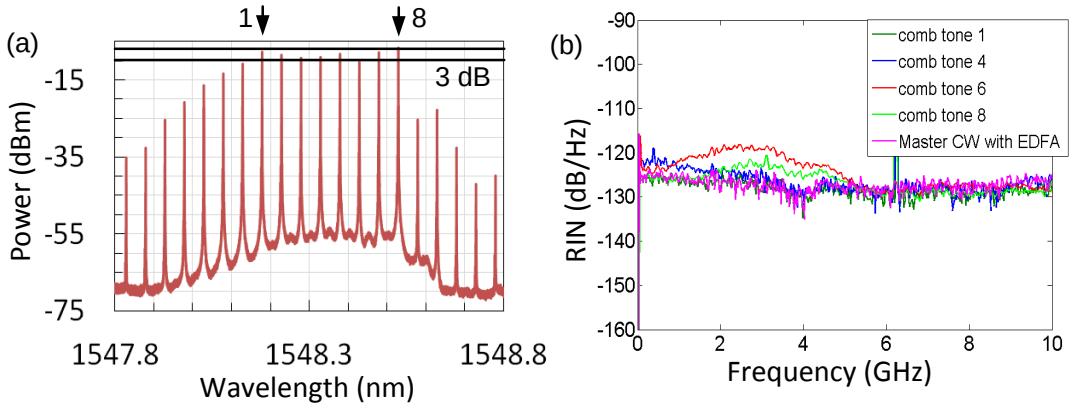

Figure 5.5: Relative intensity noise measurements: (a) Comb spectrum obtained with an FSR of 6.25 GHz, with comb tones marked with numbers, and (b) Measured relative intensity noise for 4 selected comb tones, and master CW over 10 GHz bandwidth.

The RIN of the master and the selected comb tones (marked with arrows and numbers in Figure 5.5 (a)) used for data transmission has been measured over a 10 GHz bandwidth, although only five measurements are shown in Figure 5.5 (b) for clarity of presentation. These measurements correspond to four representative comb tones and the master in CW operation.

The RIN of the master CW (dc to 6 GHz) is -129 dB/Hz. The obtained averaged RIN (dc-6 GHz) of the selected comb tones vary in the range of -122.5 to -129.3 dB/Hz with the highest averaged RIN (-122.5 dB/Hz) corresponding to comb tone 6 that also presents the lowest power and OCNR and thereby, is most influenced by ASE noise. This variation in RIN levels can also lead to a degradation of the system performance as it will be presented later in this Chapter.

Nevertheless, these results demonstrate that this type of integrated GS-OFCS presents satisfactory low RIN values suitable for advanced modulation formats with a relatively uniform distribution over the frequency span, and thereby, it is not affected by mode partition noise unlike some mode-locked lasers comb sources where high RIN is observed at low frequencies which may hinder their use in some optical systems [17], [19]. In order to provide a sufficient power per comb line after filtering/demultiplexing for practical systems, an integrated injection locked de-multiplexer is proposed in the Section 5.3, which provides simultaneous de-multiplexing and amplification of the comb tones while keeping their phase correlation.

5.2.3 OCNR

OCNR has also been recognized as a limiting parameter for the performance of advanced intensity modulated systems [36] and thus, it is subsequently characterized. Figure 5.6 presents the averaged RIN (from dc to 6 GHz, and marked in black circles) and the OCNR (in blue squares) for the 8 selected comb tones. The OCNR ranges from 46 to 51 dB and presents a trend of reduced OCNR when moving from lower wavelength comb tones towards higher ones in accordance with the shape of the optical spectrum envelope. Comb tone 6 exhibits the lowest OCNR caused by its reduced optical power that can be observed as a marked dip in the optical spectrum in Figure 5.3 (d). The system performance will significantly depend on the OCNR and RIN levels of the optical comb tones employed [17], [36] and consequently, it can be noted that comb tone 6 will reveal the worst performance as it possesses the lowest OCNR of 46 dB and highest RIN of –122.5 dB/Hz. On the contrary, comb tone 1 exhibits high OCNR levels of 51 dB and low RIN of -128.6 dB/Hz which can ensure very good performance of the system.

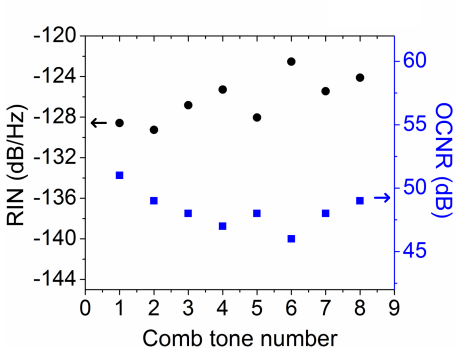

Figure 5.6: RIN (black circles) and OCNR (blue squares) of the comb tones.

5.2.4 Phase Noise and Phase Correlation

The phase noise was characterized by measuring the Frequency Modulated (FM)-noise spectrum using an optical quadrature receiver front end as in [37], [38]. The comb tones were filtered and coherently detected with the aid of a low linewidth local oscillator (linewidth $<$ 80 kHz). The two optical fields are superposed in a 2x4 90° hybrid whose output signals are detected by two balanced photodetectors for offline phase noise analysis. The receiver detects a beat between the signal under test (comb tone) and the local oscillator. Therefore, the obtained linewidth is the sum of the linewidth of the comb tone and the local oscillator, as both optical fields are de-correlated.

The FM-noise spectrum was analysed for the 8 selected comb tones within the 3 dB of spectral ripple, although only four representative measurements are shown in Figure 5.7 (a). These results are compared to the phase noise of the CW master laser (when the slave section is biased at transparency current, which allows the master signal to pass through without giving enough gain to the slave laser to emit).

The FM-noise spectra demonstrate similar levels of phase noise, presenting a *1/f* noise component at low frequencies (below 20 MHz), a clearly dominant white FM noise, and a small high-frequency component region above 1 GHz related to the relaxation oscillation of the injection-locked slave laser. The intrinsic optical linewidth of each comb tone can be obtained from the white FM-noise component, which corresponds to 1.5 MHz [37] ($\delta f = S_0 \cdot \pi \approx 5\text{x}10^5 \cdot \pi \approx 1.5$ MHz). Since the phase noise of the comb tones are much larger (1.5 MHz) than that of the local oscillator used (80 kHz), the phase noise of the beat can be consider almost identical with that of the comb tones. As illustrated, the FM-noise spectra of each comb tone demonstrate similar levels of phase noise, thereby, following the optical linewidth of the master [25], [39], due to the external injection locking.

The excess *1/f* noise and relatively high intrinsic optical linewidth will potentially impact the performance in optical coherent communication systems that will be further investigated in this Chapter.

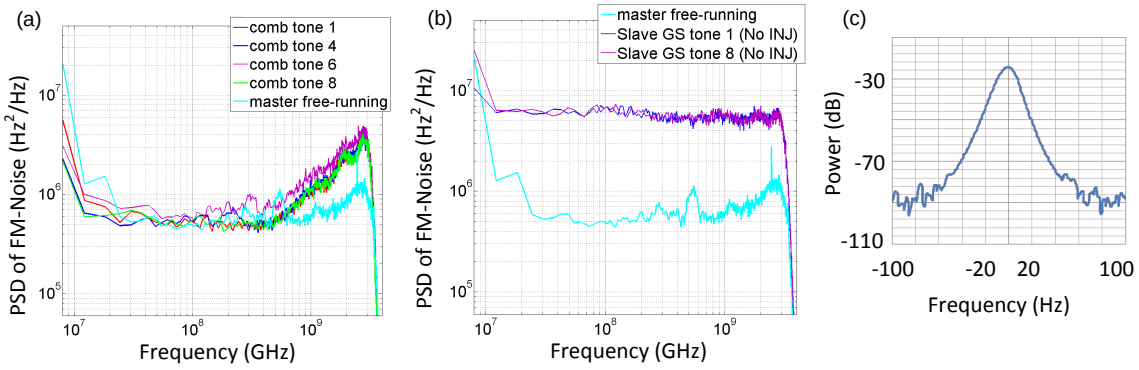

Figure 5.7: Phase noise properties: (a) FM-noise spectra for four representative comb tones and free-running master laser. (b) FM-noise spectra of Gain Switched Slave section without external injection (Master section switched off) for two representative comb tones. (c) RF beat tone linewidth measured.

In comparison, Figure 5.7 (b) presents the FM-noise spectrum of the comb tones obtained from the gain switched slave section when the master is turned off. As observed, the obtained linewidth is

approximately 19 MHz ($S_0 \approx$ 6x10^6, 12 times the linewidth of the externally injected GS-OFCS), as a result of the excess random spontaneous emission from bringing the laser below threshold on every cycle of the gain switching process.

In order to ensure that the comb tones exhibit a high degree of phase correlation with each other, the RF beat tone linewidth at 6.25 GHz (which corresponds to the FSR) is finally evaluated by detecting the whole GS-OFCS with a high speed photodiode. In Figure 5.7 (c), the observed 6.25 GHz RF beat tone measured at -20 dB from the peak is 40 Hz, with a 10 Hz resolution bandwidth of the Electrical Spectrum Analyzer (ESA), confirming the high quality of phase correlation of the comb tones limited by the noise of the RF source used to gain switch.

5.3 Photonic Integrated Comb De-multiplexer Based on Injection Locking

A critical problem relating to the usefulness of optical combs in network equipment is the necessity of separation (de-multiplexing) of the individual comb tones for independent data modulation before being coupled back together for transmission. Conventional approaches comprise an Arrayed Waveguide Grating (AWG), or passive optical filtering with narrow band optical band pass filters or wavelength selective switches. However, with these techniques it can be difficult to achieve the required suppression of adjacent wavelengths with narrow sub-channel spacing. Furthermore, they usually present substantial insertion losses, and thus, require the use of an EDFA which adds noise, tends to be costly and bulky, reducing the suitability of comb sources for practical implementation in transceivers.

De-multiplexing based on optical injection locking [40]- [42] has been proposed as an active comb tone selection method that retains the phase correlation of the comb lines, does not require optical amplification and causes less OCNR degradation when compared with conventional passive optical filtering [43]. In de-multiplexers based on injection locking, whose schematic is presented in Figure 5.8, the optical frequency comb at the input is passively split between *N* number of lanes. On the output side of the de-multiplexer there is an array of *N* single mode lasers. Each of these lasers is tuned by current to modify its emission wavelength to enable locking to a specific comb tone. Thus, each de-multiplexer laser is injection-locked to one particular comb tone which gets selected at the corresponding de-multiplexer output. As a result, the output from the de-multiplexer consists of *N* separated optical carriers (at each of the selected comb wavelengths), which are still frequency

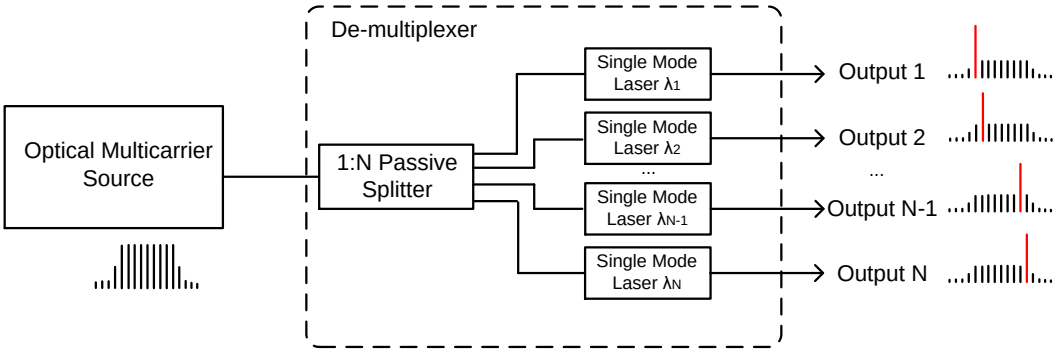

Figure 5.8: Schematic of the optical comb de-multiplexer based on injection locking

locked and have excellent phase correlation (transferred from the input comb) [44]. Furthermore, the high output power of each de-multiplexer laser is sufficiently large for driving the modulators in high spectrally efficient transceivers to encode high-order modulation formats.

A potential solution to achieve the benefits of OFCS within network equipment would see the monolithic photonic integration of the demultiplexer with the OFCS to further enhance the compactness, cost-efficiency, ease of manufacture and viability of the transceiver. As such, a four-output monolithically integrated de-multiplexer using optical injection locked semiconductor lasers for coherent comb tone separation is experimentally characterized in this thesis.

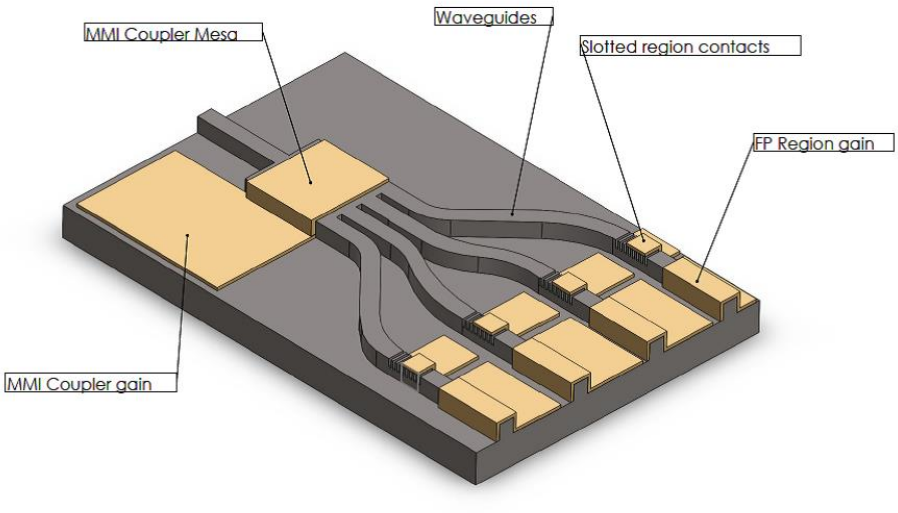

Figure 5.9: Illustration of the photonic integrated 1x4 comb de-multiplexer based on injection-locked lasers. It comprises a Multi-Mode Interference (MMI) section for passive splitting of the input comb into four copies, and four slave DMLDs that select a specific comb tone for de-multiplexing.

The device, schematically illustrated in Figure 5.9, comprises a 1x4 MMI coupler based on the self-imaging phenomenon, which is the replication of the input signal in multiple copies at periodic intervals along the waveguide, as illustrated in Figure 5.10. As such, the length of the MMI is designed for optimal splitting into four identical copies of an input comb. The four outputs of the MMI are followed by output linear tapers and curvature s-bends that couple the light into four individual single facet DMLDs [29]. These lasers, as previously explained, comprise a gain section and a mirror section consisting of a number of slots that have been etched close to the active region to provide a regular refractive index perturbation and create a single mode emission. These lasers, acting as slave lasers, are then tuned in wavelength such that they will each be injection locked to different comb lines (which may not necessarily be adjacent or equally spaced [42]). This results in the selective de-multiplexing of those comb lines, in what is effectively an active optical filter.

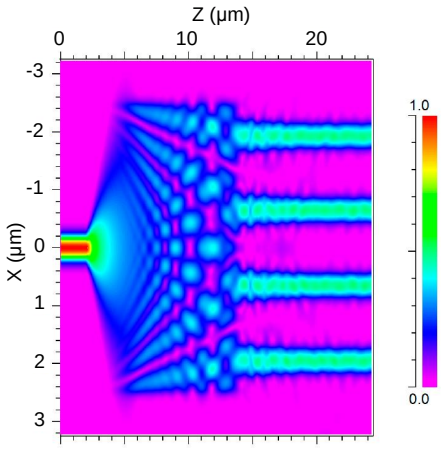

Figure 5.10: Example of the 2D propagation profile from a 1x4 multimode interference coupler. After: [45]

In order to demonstrate the de-multiplexer performance, an externally injected and 10 GHz gain-switched FP laser is used as an input OFCS for the de-multiplexer, as illustrated in Figure 5.11. The GS-OFCS spectrum, depicted in the inset of Figure 5.11, presents four comb tones within a 3 dB spectral ripple with an OCNR of 55 dB, optical power per comb tone of -2 dBm and optical linewidth of 300 kHz.

Figure 5.12 (a) shows the de-multiplexer PIC under test, which is approximately 3.2 mm long and 2 mm wide. The material structure is standard 1550 nm laser material on an InP substrate with five strained AlGaInAs quantum-wells in the active region. Individual metal contacts were deposited

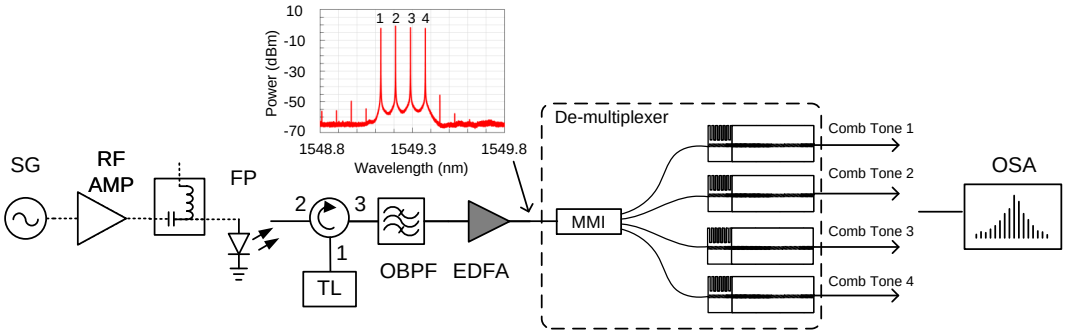

Figure 5.11: Experimental set up for comb de-multiplexing based on injection-locked lasers. Inset illustrates the GS-OFCS spectrum launched at the input of the 1x4 comb de-multiplexer. SG: Signal Generator; RF AMP: RF amplifier; FP: Fabry-Perot laser; TL: Tunable Laser; EDFA: Erbium Doped Fibre Amplifier; OBPF: Optical Band Pass Filter; MMI: Multimode interference coupler; OSA: Optical Spectrum Analyser.

for independent current injection to each section, which allows the MMI and s-bends sections to be biased to transparency and output wavelength and power tuning of each slave laser. The device was placed on a temperature-controlled copper block for probe testing, as illustrated in Figure 5.12 (b). The device temperature was maintained at 20 °C using a TEC module and coupling at input and output were achieved using lensed fibres on piezoelectric actuated stages. A high resolution (0.16 pm) OSA is used to observed the resultant spectra.

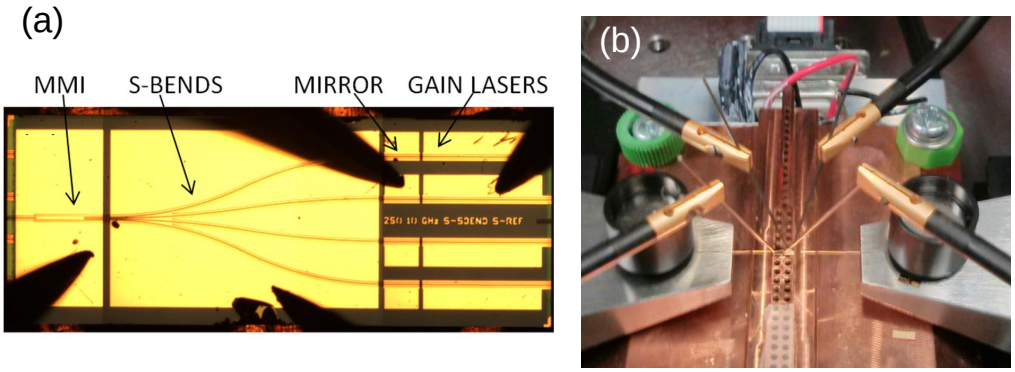

Figure 5.12: (a) Top view of the fabricated PIC for comb de-multiplexing based on injection locking observed with a microscope. (b) 1x4 comb de-multiplexer PIC under test in a probe station.

The individual selected comb tones at each output of the de-multiplexer are presented in Figures 5.13 (a)-(d). The mirror section of each de-multiplexer slave laser is biased in current accordingly to produce a wavelength tuning that ensures locking to a specific comb tone, while the gain section of each de-multiplexer laser is set to obtain a similar optical power in all the de-multiplexed comb

tones (3 dBm).

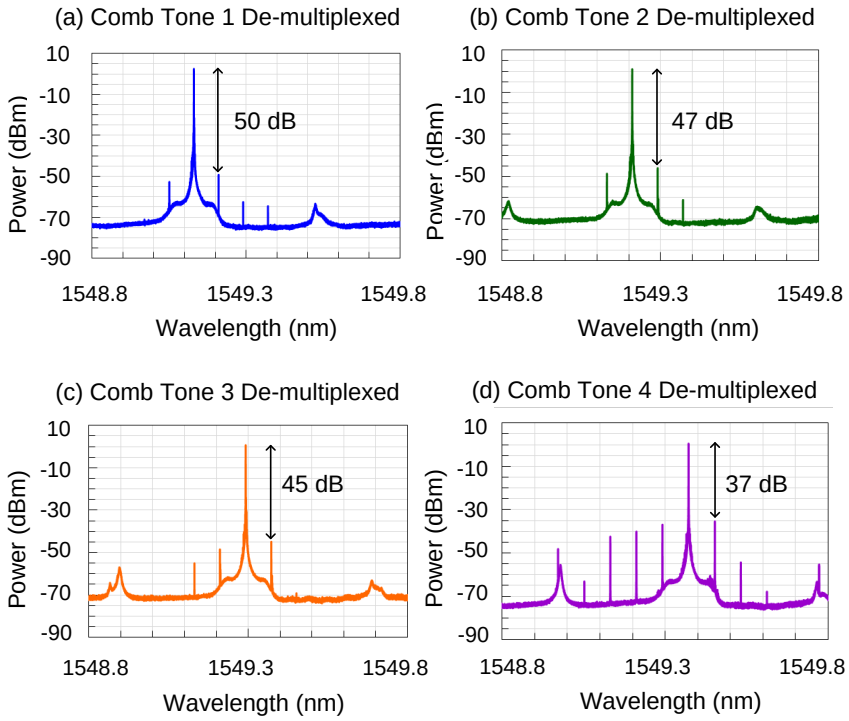

Figure 5.13: Spectrum at each output of the integrated 1x4 comb de-multiplexer: (a) De-multiplexed Comb Tone 1 with a suppression ratio of 50 dB, (b) De-multiplexed Comb Tone 2 with a suppression ratio of 47 dB, (c) De-multiplexed Comb Tone 3 with a suppression ratio of 45 dB, and (d) De-multiplexed Comb Tone 4 with a suppression ratio of 37 dB.

The locking of the de-multiplexer slave laser to specific comb tones is confirmed by observing a narrowing of the optical lineshape of the de-multiplexer outputs, matching with the lineshape of the input comb tones [35], [46] as depicted in Figure 5.14. Consequently, each of the lasers acts as a narrow filter that conserves the phase correlation between the de-multiplexed comb tones from the input comb, and an OCNR of 55 dB as shown in Figure 5.13. The other comb tones are still present at each de-multiplexer output, albeit having experienced some attenuation. The power difference between the selected comb tone and the strongest residual tone is defined as suppression ratio, which corresponds to 37 dB in the worst case, Figure 5.13 (d).

Therefore, salient features of this de-multiplexer have been experimentally demonstrated which include successful comb tone separation with suppression ratio larger than 37 dB, high output power per de-multiplexed comb tone without requiring additional EDFAs, and OCNR, and linewidth preservation from the input OFCS.

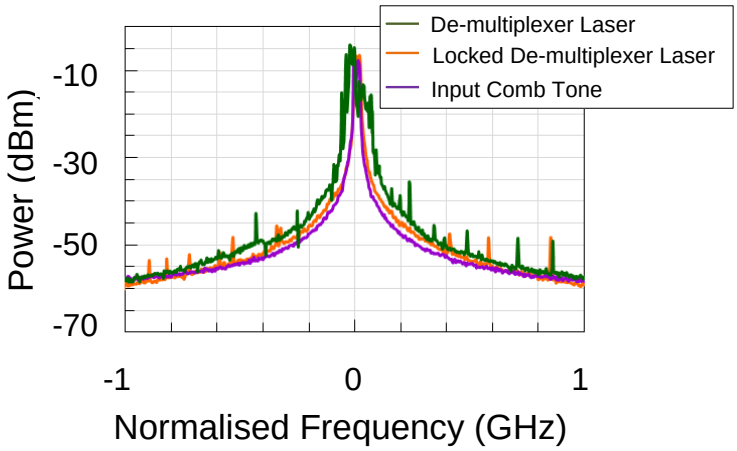

Figure 5.14: Optical lineshape spectrum of a de-multiplexer single mode slave laser (in green), optical lineshape spectrum an input comb tone (in purple), and optical lineshape of a de-multiplexer slave laser locked to the input comb tone (in orange) acquiring the same lineshape of the comb tone.

5.4 Optical Transmission Experiments

The potential of the InP photonic integrated, externally injected GS-OFCS device for spectrally efficient data transmission systems is demonstrated as follows. The GS-OFCS with a 6.25 GHz frequency spacing, 8 comb spectral lines within 3 dB of spectral ripple, and OCNR $>$ 45 dB is employed in these experiments. The influence of the device noise properties (RIN and phase noise) is assessed in two optical transmission systems that employ multi-level amplitude and phase modulation formats. Hence, the integrated GS-OFCS is used in a PAM-4 and in a Nyquist coherent Quadrature Phase Shift Keying (PSK) (QPSK) system transmitting over 3 km and 50 km of Standard Single Mode Fibre (SSMF), respectively. Both systems performed below 7% Forward Error Correction (FEC) limit for all the channels. These experiments highlight the suitability of this integrated device for future communications links that use advanced modulation formats.

5.4.1 PAM-4 System based on the Photonic Integrated GS-OFCS

The experimental set up for the PAM-4 system is illustrated in Figure 5.15. The photonic integrated GS-OFCS was used to generate 8 optical carriers within 3 dB of spectral flatness. As mentioned earlier, all the sections were dc biased accordingly while the slave gain section was also gain switched by employing an amplified RF sinewave (24 dBm). The GS-OFCS was filtered to select the central 8 optical carriers and suppress the outer side comb tones. All the filtered comb tones were subsequently amplified with an EDFA and sent to a single-drive Mach-Zehnder Modulator (MZM)

(SD-MZM) via a Polarization Controller (PC). The SD-MZM was biased at the quadrature point and then used to modulate the filtered comb with an amplified 3.125 GBaud PAM-4 signal waveform. An arbitrary waveform generator (AWG, Tektronix AWG70002A) operating at 6.25 GSa/s was employed to generate the PAM-4 signal which was then amplified and sent through a Low-Pass Filter (LPF) with a passband of 2.5 GHz. The PAM-4 signal waveform was 2^{16} bits long, and pre-distorted to compensate for non-linearities of the data driver and the SD-MZM.

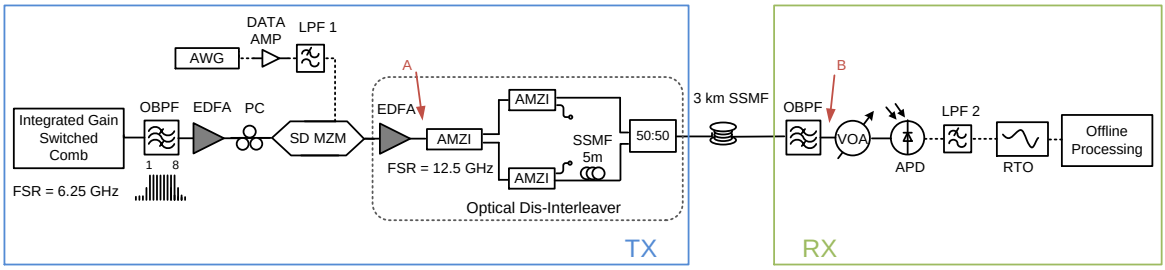

Figure 5.15: Experimental set up schematic of the Nyquist PAM-4 transmission system. FSR: Free spectral range; OBPF: Optical Band-Pass Filter; EDFA: Erbium Doped Fibre Amplifier; PC: Polarization Controller; SD-MZM: Single-drive Mach Zehnder Modulator; AWG: Arbitrary Waveform Generator; Data Amp: Data Amplifier; LPF: Low Pass Filter; AMZI: Asymmetric Mach-Zehnder interferometer; SSMF: Standard Single Mode Fibre; VOA: Variable Optical Attenuator; APD: Avalanche Photodetector; RTO: Real Time Oscilloscope.

Therefore, the bandwidth of the optical 3.125 GBaud PAM-4 signal was 5 GHz and there is a 1.25 GHz guard band between adjacent optical channels. The modulated 8 channel PAM-4 at point *A* in Figure 5.15, with an aggregated data of 50 Gbit/s, is illustrated in Figure 5.16 (a). The 8 channel PAM-4 signal was de-correlated by passing through a 2-stage dis-interleaver based on Asymmetric Mach-Zehnder interferometers (AMZI), with an FSR of 12.5 GHz to separate the comb into odd (Figure 5.16 (b)) and even channels (Figure 5.16 (c)) with an extinction ratio of 30 dB. The even channels were passed through a 5 m fibre patch cord for de-correlation and then, passively combined with the odd channels for transmission over 3 km of SSMF.

At the receiver side, the desired channel was selected with a narrowband tunable Optical Band Pass Filter (OBPF) Yenista STM-50 with an approximate 3 dB bandwidth of 6 GHz. The optical spectrum of a filtered modulated comb tone, at point *B* of Figure 5.15, is shown in Figure 5.16 (d). The filtered channel was detected using a 10 GHz receiver that consists of an avalanche photodetector (APD) and an integrated trans-impedance amplifier. A VOA was used to vary the input power falling on the APD to measure Bit Error Rate (BER) as a function of the received optical power. The detected signal was filtered using a 5 GHz LPF (LPF 2) and captured with a Real Time Oscilloscope (RTO) operating at 25 GSa/s. Digital processing of the received signal (resampling, normalization,

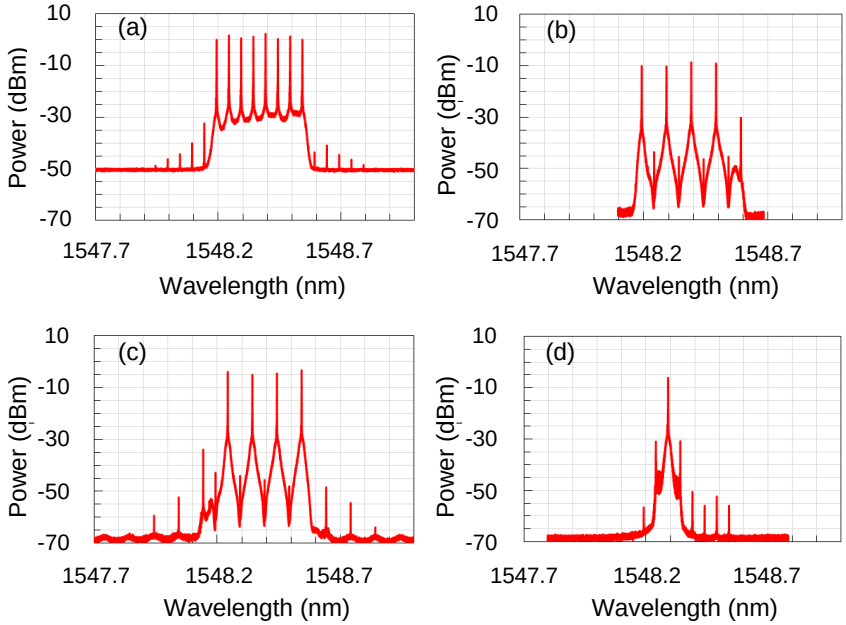

Figure 5.16: (a) Optical spectrum of the 50 Gbit/s PAM-4 signal (b) optical spectrum of odd channels filtered for de-correlation, (c) optical spectrum of even channels filtered for de-correlation and (d) optical spectrum of a filtered channel at the receiver.

adaptive equalization, symbol synchronization, decoding), and BER calculations were performed offline using Matlab. The symbol synchronization was performed with the aid of a 2^5 symbols long training sequence.

5.4.1.1 Results and Discussion

The performance of the 50 Gbit/s PAM-4 system after 3 km SSMF transmission was verified by carrying out BER measurements. Figure 5.17 (a) illustrates the BER achieved (black squares) for a received optical power of ~ -18 dBm, and the corresponding RIN for each channel (blue circles). The performance for all the received filtered channels are below the 7% FEC (BER = 3.8x10^{-3} [47]) limit. It can be observed that the performance tends to degrade for higher channel number due to the reduction of OCNR and increase of the RIN, which are key performance limiting factors of multi-level amplitude modulation formats [17], [19] such as PAM-4. Hence, the best performance with a BER of 1.3x10^{-4} corresponds to Channel 1 that exhibits a low RIN of -128.6 dB/Hz. On the contrary, the worst BER of 2.3x10^{-3} is incurred by Channel 6 that presents the lowest OCNR and highest RIN of -122.5 dB/Hz.

We then analyse the BER as a function of received power for three representative channels. An

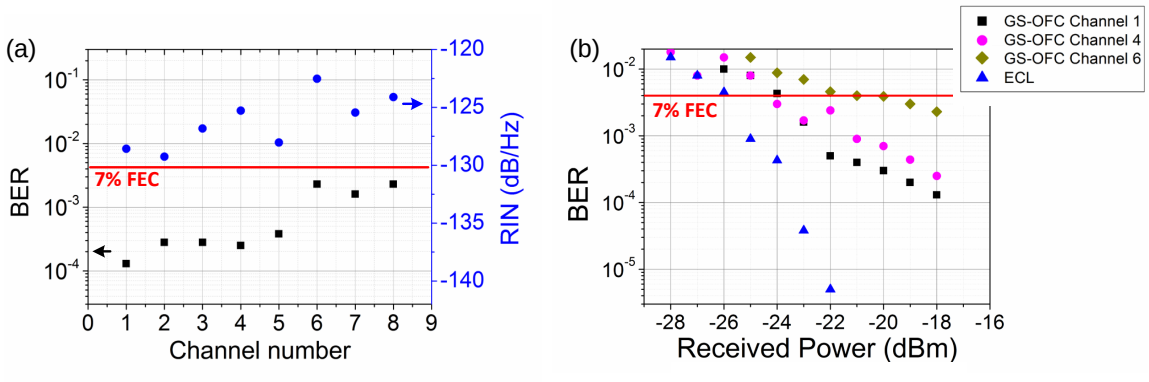

Figure 5.17: (a) Measured BER for selected channels after transmission over 3 km (b) BER as a function of received power after 3 km transmission.

External Cavity Laser (ECL) was used to set a benchmark performance of the system, as shown in Figure 5.17 (b) with blue triangles. The ECL has an average RIN (dc-6 GHz) of ~ -145 dB/Hz, and OCNR in excess of 65 dB (RBW = 0.16 pm). Consequently, the penalty in performance for the GS-OFCS channels is caused by elevated RIN (ranging -122.5 to -129.3 dB/Hz) and inferior OCNR compared to the ECL. Channel 1 to 5 exhibit a similar level of performance yielding a receiver sensitivity of -23 dBm, corresponding to 2 dB power penalty at 7% FEC limit compared to the ECL. Channel 6 to 8 present a receiver sensitivity of -21 dBm at the 7% FEC limit. The additional 2 dB penalty incurred by these channels are mainly attributed to the degradation in RIN values and OCNR of these channels. This is also illustrated in Figure 5.18 where the eye-diagrams detected after transmission for CH1 and the ECL can be observed. Nevertheless, these results have clearly illustrated the feasibility of a PAM-4 system utilizing the proposed photonic integrated GS-OFCS device.

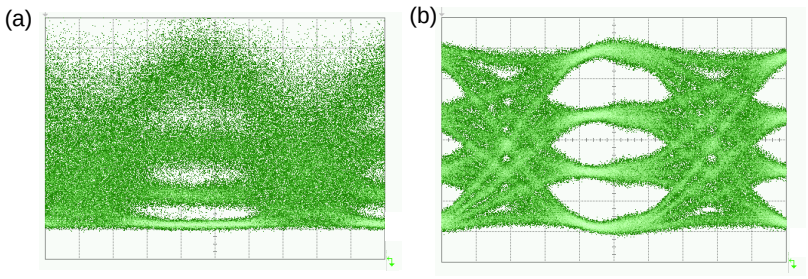

Figure 5.18: (a) Eye-diagram of CH1 after 3 km of transmission and a received power of -18 dBm (b) Eye-diagram of ECL after 3 km of transmission and a received power of - 18 dBm.

5.4.2 Coherent Nyquist-QPSK System based on the Photonic Integrated GS-OFCS

Figure 5.19 illustrates the experimental set up for the Nyquist-QPSK system. The photonic integrated GS-OFCS was used as the multicarrier source. An OBPF and an EDFA were employed to select and amplify the central 8 optical carriers with a 3 dB spectral flatness. All the filtered comb tones were sent to a single IQ MZM (IQ-mod) via a polarization controller (PC). The IQ-mod was biased at null and driven by a 5 GBaud Nyquist-QPSK signal waveform. The waveform was 2^{16} bits long and derived from the same AWG used previously, operating at 25 GSa/s. A digital root raised cosine filter with a roll-off factor of 0.1% was applied to the QPSK signal.

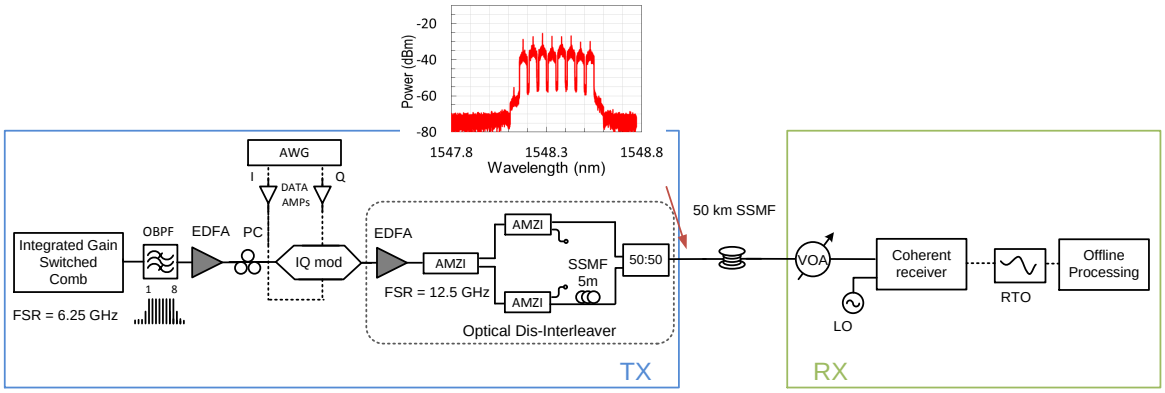

Figure 5.19: Schematic of the Nyquist-QPSK system experimental set up. Inset shows optical spectrum of the modulated superchannel prior transmission. IQ-mod: IQ Mach-Zehnder modulator; LO: Local Oscillator.

The bandwidth of the resulting Nyquist-QPSK signal was 5 GHz with a 1.25 GHz guard band between adjacent optical channels. The 8 channel Nyquist-QPSK signal with an aggregated data rate of 80 Gbit/s was then passed through the de-correlation stage, as explained in detail previously, and transmitted Back-To-Back (B2B) and over 50 km of SSMF. At the receiver side, a phase diversity coherent receiver was used to perform coherent detection. The optical Local Oscillator (LO) was provided by an ECL that had 13 dBm output power and 25 kHz optical linewidth. The LO was tuned to each of the 8 channels for detection. The received signal was captured with a RTO operating at 25 GSa/s. Digital processing of the received signal was performed offline using Matlab. A 2^{nd} order Phase-Locked Loop (PLL) [48], [49] was used for phase recovery and phase tracking. Channel performance was determined using Error-Vector Magnitude (EVM) calculation of the measured constellation diagrams, which defines the distance in the IQ plane between the ideal constellation point and the points received, and also error counting to establish a bit error rate.

5.4.2.1 Results and Discussion

The experimental results obtained are shown in Figure 5.20 (a) and (b), for the total received optical power (received power of the entire 8 channel Nyquist-QPSK signal) of ~ -25 dBm. Figure 5.20 (a) shows the BER measurements for each channel and for B2B (black squares) and for transmission over 50 km of SSMF (magenta circles). We evaluate 2 million samples for each channel to accurately estimate the BER. Channel performance was also analysed through EVM measurements for each channel for B2B case and for transmission over 50 km of SSMF, as illustrated in Figure 5.20 (b). In both cases, all 8 channels exhibit a similar performance far below the 7% FEC limit (BER=4x10^{-3} and EVM=38% [50]). Channels 3 and 4 had the best performance in B2B and 50 km transmission without any errors recorded in the bit length analysed. Rather than omit the corresponding entry on Figure 5.20, these channels have been included at a nominal level of 5x10^{-6} which is intended to represent that no errors were detected. An indicative measured constellation diagram for Channel 7 is shown in Figure 5.20 (c). The constellation diagrams of all channels present a slightly angular spread of the constellation points which is a distinct signature of phase noise. Despite the relatively large linewidth (relative to the employed baud rate), these experimental results demonstrate that this integrated comb source can be used in coherent systems, even at low baud rates where the linewidth requirement is more stringent.

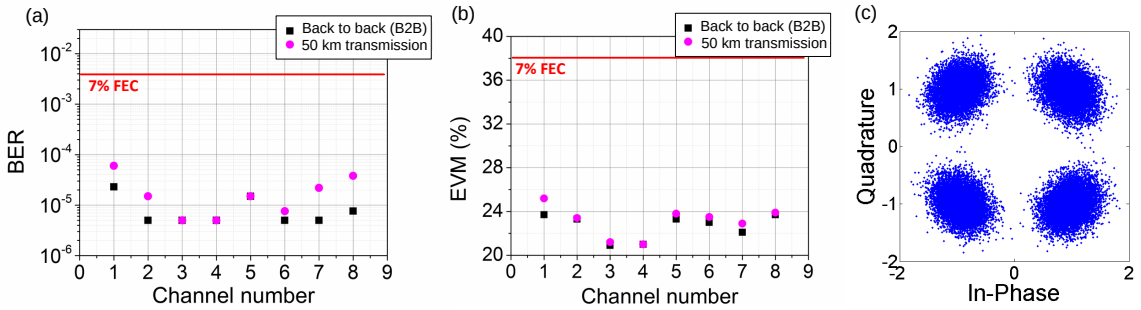

Figure 5.20: (a) Measured BER for selected channels back-to-back (black squares) and after transmission over 50km of SSMF (magenta circles) (b) Measured EVM for selected channels back-to-back (black squares) and after transmission over 3km of SSMF (magenta circles) and (c) QPSK constellation diagram for Channel 7.

5.5 Conclusions

Photonic integrated circuits are key for the development of compact, robust and cost efficient optical devices and systems. Photonic integration provides a perfect platform for mass production as well

as the realization of complex systems, combining otherwise discrete components in a single device and thus, providing reliability, power consumption and cost reductions, low footprint and ease of fabrication.

This chapter has experimentally investigated the operation and presented a detailed characterization of two photonic integrated devices for gain switched comb source generation, and comb de-multiplexing prior to modulation.

The InP photonic integrated externally injected gain switched comb is composed of two lasers with different cavity lengths integrated in a master-slave configuration. The comb spectral enhancement due to optimum external optical injection is first demonstrated, with an increase in the 20 dB bandwidth from 62.5 to 94 GHz caused by an enhancement of the relaxation oscillation frequency. As a result, the generated comb exhibits 8 clearly resolved and highly coherent optical tones within a 3 dB spectral flatness at 6.25 GHz spacing and an OCNR of at least 45 dB. The FSR can be easily adapted from 6 to 10 GHz and the comb noise properties are analysed by characterizing the RIN and phase noise which are key parameters of interest for advanced modulation formats. Average RIN is found to be $\sim$ -125 dB/Hz, an intrinsic optical linewidth of 1.5 MHz is demonstrated and a high degree of phase correlation characterized by a low 10 Hz RF beat tone linewidth. Hence, this GS-OFCS presents exceptional features which clearly highlight its merit for use in numerous applications, including spectrally efficient transmission systems.

The photonic integrated 4-output comb de-multiplexer based on optical injection locking is subsequently characterized. Through experimental results, active comb tone separation (de-multiplexing) with adjacent tone suppression larger than 37 dB is demonstrated which is sufficient to guarantee reliable system operation [42]. The presented de-multiplexer PIC allows selective and power equalized de-multiplexing of the comb tones without OCNR degradation, while maintaining the optical linewidth and strong phase correlation from the input comb source, which is crucial for compensation of non-linear distortion through fibre transmission. Additionally, the de-multiplexed comb tones can be adjacent or separated by multiples of the input FSR, but also equally or unequally spaced, thus allowing for a variety of spectral bandwidth and modulation format arrangements. It is important to note that this 1x4 de-multiplexer PIC could be also used with other comb source techniques, and could be monolithically integrated on a single chip with the comb source for further viability of multicarrier based optical transceivers.

Finally, the photonic integrated GS-OFCS is implemented in two different spectrally efficient optical transmission systems. First, it is employed in a PAM-4 system, where 8 comb tones obtained

from the gain switched device are modulated with a 3.125 Gbaud signal that is subsequently transmitted over 3 km of SSMF. The performance for all the received channels is below the 7% FEC limit but it tends to degrade for high channel number due to inferior OCNR and RIN characteristics, with a 2 dB receiver sensitivity penalty between best and worst performing channels. In the Nyquist-QPSK system, the device phase noise influence is also studied. In the same manner, 8 comb tones are modulated with a 5 GBaud Nyquist-QPSK signal and transmitted over 50 km of SSMF. Successful transmission is achieved with all 8 channels exhibiting a similar performance far below the 7% FEC limit.

The experimental results presented in this Chapter, in conjunction with the compactness and ease of manufacture of the InP monolithically integrated devices, denote the relevance and versatility of the resultant GS-OFCS as a promising multicarrier source for a large variety of future spectrally efficient transmission systems that use advanced modulation formats throughout the network.

References

[1] Cisco V. N. I. Forecast, "Cisco visual networking index: forecast and methodology 2013-2018," 2016 [Online]. Available: http://www.cisco.com/c/en/us/solutions/collateral/service-provider/visual-networking-index-vni/complete-white-paper-c11-481360.html.

[2] R.J. Essiambre and R.W. Tkack, "Capacity trends and limits of optical communication networks," *Proceedings of the IEEE*, vol. 100, no. 5, pp. 1035–1055, May 2012.

[3] S. Gringeri, E. B. Basch, and T. J. Xia, "Technical considerations for supporting data rates beyond 100 Gb/s," *IEEE Communications Magazine*, vol. 50, no. 2, pp. 21–30, Feb. 2012.

[4] A. A. M. Saleh and J. M. Simmons, "Technology an architecture to enable the explosive growth of the Internet," *IEEE Communications Magazine*, vol. 49, no. 1, pp. 126–132, Jan. 2011.

[5] C. Kachris and I. Tomkos, "A survey on optical interconnects for data centers," *IEEE Communications Surveys & Tutorials*, vol. 14, no. 4, pp. 1021–1036, Oct. 2012.

[6] R. P. Davey and D. B. Payne, "The future of optical transmission in access and metro networks – an operator's view," in *Proceedings of European Conference on Optical Communications*, Glasgow, 2005, vol.5, pp. 53–56.

[7] P. Winzer, "Beyond 100G Ethernet," *IEEE Communications Magazine*, vol. 48, no. 7, pp. 26–30, July 2010.

[8] Q. Hu, D. Che, Y. Wang, and W. Shieh, "Advanced modulation formats for high-performance short-reach optical interconnects," *Optics Express*, vol. 23, no. 3, pp. 3245–3259, Feb. 2015.

[9] L. Tao, Y. Ji, J. Liu, A. P. T. Lau, N. Chi, and C. Lu, "Advanced Modulation Formats for Short Reach Optical Communication Systems," in *IEEE Network*, vol. 27, no. 6, pp. 6–13, Nov/Dec. 2103.

[10] M. J. Wale, "Advanced Modulation Formats in Data Centre Communications," in *2nd Sympo-*

sium on Optical Interconnects in Data Centres in European Conference on Optical Communications, Cannes, France, Sep. 2014, pp. 1–13.

[11] F. Karinou, C. Prodaniuc, N. Stojanovic, M. Ortsiefer, A. Daly, R. Hohenleitner, B. Kogel, and C. Neumeyr, "Directly PAM-4 modulated 1530-nm VCSEL enabling 56 Gb/s/λ data-center interconnects," *IEEE Photonics Technology Letters*, vol. 27, no. 17, pp. 1872–1875, Sept. 2015.

[12] D. Sadot, G. Dorman, A. Gorshtein, E. Sonkin, and O. Vidal, "Single channel 112 Gbit/sec PAM4 at 56 Gbaud with digital signal processing for data centers applications," *Optics Express*, vol. 23, pp. 991–997, Jan. 2015.

[13] D. Lavery, E. Torrengo, and S. Savory, "Bidirectional 10 Gbit/s long-reach WDM-PON using digital coherent receivers," in *Proceedings of Optical Fiber Communication Conference/National Fiber Optic Engineers Conference*, paper OTuB4, 2011.

[14] J. Pfeifle, V. Vujicic, R. Watts, P. Schindler, C. Weimann, R. Zhou, W. Freude, L. Barry, and C. Koos, "Flexible terabit/s Nyquist-WDM super-channels using a gain-switched comb source," *Optics Express*, vol. 23, pp. 724–738, Jan. 2015.

[15] V. Ataie, E. Temprana, L. Liu, E. Myslivets, B. P.-P. Kuo, N. Alic, and S. Radic, "Ultrahigh count coherent WDM channels transmission using optical parametric comb-based frequency synthesizer," *IEEE Journal of Lightwave Technology*, vol. 33, no.3, pp. 694–699, 2015.

[16] C. Weimann, P. C. Schindler, R. Palmer, S. Wolf, D. Bekele, D. Korn, J. Pfeifle, S. Koeber, R. Schmogrow, L. Alloatti, D. Elder, H. Yu, W. Bogaerts, L. R. Dalton, W. Freude, J. Leuthold, and C. Koos, "Silicon-organic hybrid (SOH) frequency comb sources for terabit/s data transmission," *Optics Express*, vol. 22, no. 3, pp. 3629–3637, 2014.

[17] V. Vujicic, C. Calo, R. Watts, F. Lelarge, C. Browning, K. Merghem, A. Martinez, A. Ramdane, and L. P. Barry, "Quantum Dash Mode-Locked Lasers for Data Centre Applications," *IEEE Journal of Selected Topics in Quantum Electronics*, vol. 21, no. 6, pp. 53–60, Dec. 2015.

[18] J. Pfeifle, V. Brasch, M. Lauermann, Y. Yu, D. Wegner, T. Herr, K. Hartinger, P. Schindler, J. Li, D. Hillerkuss, R. Schmogrow, C. Weimann, R. Holzwarth, W. Freude, J. Leuthold, T. J. Kippenberg, and C. Koos, "Coherent terabit communications with microresonator Kerr frequency combs," *Nature Photonics*, vol. 8, no.5, pp. 375–380, 2014.

[19] V. Vujicic, A. P. Anthur, A. Saljoghei, V. Panapakkam, R. Zhou, Q. Gaimard, R. Merghem, F. Lelarge, A. Ramdane, and Liam P. Barry, "Mitigation of relative intensity noise of Quantum

Dash mode-locked lasers for PAM4 based optical interconnects using encoding techniques," *Optics Express*, vol. 25, pp. 20–29, 2017.

[20] P. Zhu, J. Li, L. Niu, Y. Xu, Y. Chen, X. Xie, X. Chen, B. Guo, Z. Chen, and Y. He, "Optical Comb-enabled Cost-effective ROADM Scheme for Elastic Optical Networks," in *Proceedings of Optical Fiber Communication Conference*, San Francisco, CA, paper W3B.5, 2014.

[21] M. D. Gutierrez Pascual, P. M. Anandarajah, R. Zhou, F. Smyth, S. Latkowski, and L. P. Barry, "Cascaded Fabry-Pérot lasers for coherent expansion of wavelength tunable gain switched comb," in *Proceedings of European Conference on Optical Communication*, paper Mo.3.4.4, Sept. 2014.

[22] P. M. Anandarajah, R. Maher, Y. Q. Xu, S. Latkowski, J. O'Carroll, S. G. Murdoch, R. Phelan, J. O'Gorman, and L. P. Barry, "Generation of Coherent Multicarrier Signals by Gain Switching of Discrete Mode Lasers," *IEEE Photonics Journal*, vol. 3, no. 1, pp. 112-122, Feb. 2011.

[23] Á R. C. Serrano, C. de Dios Fernandez, E. P. Cano, M. Ortsiefer, P. Meissner and P. Acedo, "VCSEL-Based Optical Frequency Combs: Toward Efficient Single-Device Comb Generation," *IEEE Photonics Technology Letters*, vol. 25, no. 20, pp. 1981-1984, Oct. 2013.

[24] P. Anandarajah, R. Zhou, R. Maher, M. D. Gutierrez Pascual, F. Smyth, V. Vujicic, and L. P. Barry, "Flexible optical comb source for super channel systems," in *Proceedings of Optical Fiber Communication Conference/National Fiber Optic Engineers Conference*, paper OTh31.8, 2013.

[25] M. D. Gutierrez Pascual, R. Zhou, F. Smyth, P. M. Anandarajah, and L. P. Barry, "Software reconfigurable highly flexible gain switched optical frequency comb source," *Optics Express*, vol. 23, no 18, pp. 23225–23235, Aug. 2015.

[26] D. Liang and J. E. Bowers, "Photonic integration: Si or InP substrates?," *Electronics Letters*, vol. 45, no.12, 2009.

[27] C. R. Doerr, "Integrated Photonic Platforms for Telecommunications: InP and Si," *IEICE Transactions on Electronics*, vol. E96–C, no. 7, pp. 950-957, 2013.

[28] R. Piramidowicz, S. T. Stopinski, K. Lawniczuk, K. Welikow, P. Szczepanski, X. J. Leijtens, and M. K. Smit, "Photonic integrated circuits : a new approach to laser technology," *Bulletin of the Polish Academy of Sciences: Technical Sciences*, vol. 60, no. 4, pp. 683-689, 2012.

[29] C. Herbert, D. Jones, A. Kaszubowska-Anandarajah, B. Kelly, M. Rensing, J. O'Carroll, R.

Phelan, P. Anandarajah, P. Perry, L.P. Barry, and J. O'Gorman, "Discrete mode lasers for communication applications," *IET Optoelectronics*, vol. 3, no. 1, pp. 1-17, Feb. 2009.

[30] R. Zhou, P. M. Anandarajah, D. Gutierrez Pascual, J. O'Carroll, R. Phelan, B. Kelly, and L. P. Barry, "Monolithically Integrated 2-Section Lasers for Injection Locked Gain Switched Comb Generation," in *Proceedings of Optical Fiber Communication Conference*, San Francisco, CA, paper Th3A.3, 2014.

[31] B. Jerez, P. Martín-Mateos, E. Prior, C. de Dios, and P. Acedo, "Dual optical frequency comb architecture with capabilities from visible to mid-infrared," *Optics Express*, vol. 24, pp. 14986-14994, 2016.

[32] A. Khodabakhsh, C. Abd Alrahman, and A. Foltynowicz, "Noise-immune cavity-enhanced optical frequency comb spectroscopy," *Optics Letters*, vol. 39, pp. 5034-5037, 2014.

[33] Á. R. Criado, C. de Dios, E. Prior, G. H. Döhler, S. Preu, S. Malzer, H. Lu, A. C. Gossard, and P. Acedo, "Continuous-Wave Sub-THz Photonic Generation With Ultra-Narrow Linewidth, Ultra-High Resolution, Full Frequency Range Coverage and High Long-Term Frequency Stability," *IEEE Transactions on Terahertz Science and Technology*, vol. 3, no. 4, pp. 461-471, 2013.

[34] T. Shao, H. Shams, P. M. Anandarajah, M. J. Fice, C. C. Renaud, F. van Dijk, A. J. Seeds, and L. P. Barry, "Phase Noise Investigation of Multicarrier Sub-THz Wireless Transmission System Based on an Injection-Locked Gain-Switched Laser," *IEEE Transactions on Terahertz Science and Technology*, vol. 5, no. 4, pp. 590-597, 2015.

[35] Eagleyard-Photonics, "Relative Intensity Noise of Distributed Feedback Lasers," 2016, [Online]. Available: http://www.eagleyard.com/fileadmin/downloads/documents/eyP_App_Note_RIN__1-6.pdf

[36] V. Vujicic, P. M. Anandarajah, R. Zhou, C. Browning and L. P. Barry, "Performance Investigation of IM/DD Compatible SSB-OFDM Systems Based on Optical Multicarrier Sources," *IEEE Photonics Journal*, vol. 6, no. 5, pp. 1-10, Oct. 2014.

[37] Kazuro Kikuchi, "Characterization of semiconductor-laser phase noise and estimation of bit-error rate performance with low-speed offline digital coherent receivers," *Optics Express*, vol. 20, pp. 5291-5302, 2012.

[38] T. N. Huynh, L. Nguyen, and L. Barry, "Phase noise characterization of SGDBR lasers using phase modulation detection method with delayed self-heterodyne measurements," *Journal*

Lightwave Technology, vol. 31, no. 8, pp. 1300–1308, 2013.

[39] R. Zhou, T. N. Huynh, V. Vujicic, P. M. Anandarajah, and L. P. Barry, "Phase noise analysis of injected gain switched comb source for coherent communications," *Optics Express*, vol. 22, pp. 8120–8125, March 2014.

[40] D. S. Wu, R. Slavík, G. Marra, and D. J. Richardson, "Direct selection and amplification of individual narrowly spaced optical comb modes via injection locking: Design and characterization," *IEEE Journal of Lightwave Technology*, vol. 31, no. 14, pp. 2287–2295, Jul. 15, 2013.

[41] Z. Liu, S. Farwell, M. Wale, D. J. Richardson, and R. Slavik, "InP-based Optical Comb-locked Tunable Transmitter," in *Proceedings of Optical Fiber Communication Conference*, Anaheim, CA, paper Tu2K.2, 2016.

[42] R. Zhou, T. Shao, D. Gutierrez, F. Smyth, L. P. Barry, "Injection locked wavelength de-multiplexer for optical comb-based Nyquist WDM system," *IEEE Photonics Technology Letters*, vol. 27, no. 24, pp. 2595-2598, 2015.

[43] A. Albores-Mejia, T. Kaneko, E. Banno, K. Uesaka, H. Shoji, H. Kuwatsuka, "Optical-comb-line selection from a low-power/low-OSNR comb using a low-coherence semiconductor laser for flexible ultra-dense short range transceivers," in *Proceedings of Optical Fiber Communication Conference*, Los Angeles, CA, paper W2A.23, 2015.

[44] R. Zhou, M. D. Gutierrez Pascual, P. M. Anandarajah, T. Shao, F. Smyth, and L. P. Barry, "Flexible wavelength de-multiplexer for elastic optical networking," *Optics Letters*, vol. 41, pp. 2241-2244, 2016.

[45] D. Malka, Y. Danan, Y. Ramon, Z. Zalevsky, "A Photonic 1 × 4 Power Splitter Based on Multimode Interference in Silicon–Gallium-Nitride Slot Waveguide Structures," *Materials*, vol. 9, no. 7, pp. 516, 2016.

[46] E. Temprana, E. Myslivets, L. Liu, A. Pejkic, V. Ataie, B. P.-P. Kuo, D. Esman, A. Wiberg, N. Alic, S. Radic, "Transmission reach doubling enabled by transmitter-side digital back propagation and frequency referenced carriers," in *Proceedings of European Conference on Optical Communication*, Valencia, Spain, pp. 1-3, 2015.

[47] N. Eiselt, J. Wei; H. Griesser, A. Dochhan, M. H. Eiselt, J. P. Elbers, J. J. Vegas Olmos, and I. Tafur Monroy, "Evaluation of Real-Time 8x56.25 Gb/s (400G) PAM-4 for Inter-Data center application over 80 km of SSMF at 1550 nm," *IEEE Journal of Lightwave Technology*, vol. 35,

no. 4, pp. 955-962, Feb. 2017.

[48] T.N. Huynh, A. T. Nguyen, W. C. Ng, L. Nguyen, L. A. Rusch, and L. P. Barry, "BER performance of coherent optical communications systems employing monolithic tunable lasers with excess phase noise," *IEEE Journal of Lightwave Technology*, vol. 32, no. 10, pp. 1973–1980, 2014.

[49] V. Vujicic, A. Anthur, V. Panapakkam, R. Zhou, Q. Gaimard, K. Merghem, F. Lelarge, A. Ramdane, and L. Barry, "Tbit/s optical interconnects based on low linewidth quantum-dash lasers and coherent detection," in *Conference on Lasers and Electro-Optics*, paper SF2F.4, San Jose, CA, 2016.

[50] R. Schmogrow, B. Nebendahl, M. Winter, A. Josten, D. Hillerkuss, S. Koenig, J. Meyer, M. Dreschmann, M. Huebner, C. Koos, J. Becker, W. Freude, and J. Leuthold, "Error Vector Magnitude as a Performance Measure for Advanced Modulation Formats," *IEEE Photonics Technology Letters*, vol. 24, no. 1, pp. 61–63, Jan. 2012.

[51] M. D. Gutierrez, J. Braddell, F. Smyth, and L. P. Barry, "Monolithically integrated lasers for comb generation in bandwidth variable transponders," in *Proceedings of European Conference on Integrated Optics*, paper ECIO-O-01, Warsaw (Poland), May 2016.

[52] M. Deseada Gutierrez, Jules Braddell, Frank Smyth, Liam P. Barry, "Monolithically Integrated 1x4 Comb De-multiplexer Based on Injection Locking", in *Proceedings of European Conference on Integrated Optics*, paper p-37, Warsaw (Poland), May 2016.

[53] M. D. Gutierrez, V. Vujicic, J. Braddell, F. Smyth, P. Anandarajah, and L. P. Barry, "InP Photonic Integrated Externally Injected Gain Switched Optical Frequency Comb," *Optics Letters*, vol. 42, pp. 555-558, Jan. 2017.

[54] M. Deseada Gutierrez Pascual, Vidak Vujicic, Jules Braddell, Frank Smyth, Prince M. Anandarajah, and Liam P. Barry, "Photonic Integrated Gain Switched Optical Frequency Comb for Spectrally Efficient Optical Transmission Systems," *IEEE Photonics Journal*, vol. 9, no. 3, pp. 1-8, 2017.

Chapter 6

Conclusions and Future Work

6.1 Conclusions

Externally injected gain switched optical frequency comb sources have been recognised as promising candidates for next generation, flexible and high capacity optical networks due to their spectral efficiency, stability and flexibility while offering simplicity and good noise characteristics for the employment of advanced modulation formats.

As a result, in this thesis, an extensive experimental development and investigation of these sources has been presented with special focus on their enhancement and feasibility for practical applications, as well as the examination of their implementation in transmission systems. The main results are outlined below.

Gain Switched Comb Generation and Development

In Chapter 3, the generation of a software reconfigurable optical frequency comb has been demonstrated, based on the external injection of a temperature tuned and gain switched Fabry-Pérot (FP) laser. The source presents automatic setting of the various parameters required for optimum, low noise comb generation, and allows us to dynamically reconfigure the Free Spectral Range (FSR) and central wavelength, according to traffic conditions and network resources. Furthermore, the performance and noise properties of the software reconfigurable source are examined in detail and presented, highlighting its suitability for employment in next generation flexible optical transmission networks. As a result, a highly coherent optical comb source consisting of 6 clearly resolved

12.5 GHz tones delivering $\sim$ 2 dBm output power per comb line with an Optical Carrier to Noise Ratio (OCNR) in excess of 50 dB is achieved. The FSR can be software reconfigured from 6 to 14 GHz while the wavelength can be continuously tuned along the whole C-band (1535-1565 nm = 30 nm). A stability characterization demonstrates the source robustness over 24 hours with fluctuations of the individual comb tones of less than 0.5dB in power and 5pm in wavelength. Finally, experimental measurements highlight the excellent spectral quality of the comb tones and performance consistency, with Relative Intensity Noise (RIN) of $\sim$ -130 dB/Hz and low phase noise (estimated linewidth of 300 kHz transferred from the master laser), at any operating wavelength across the C-band.

This source has served as a prototype demo unit for the company Pilot Photonics and has been implemented in several research studies, including transmissions of 12 Gbaud Nyquist Polarization Division Multiplexing (PM) Quadrature Phase Shift Keying (PSK) (QPSK) signals over 100 km [1] and the investigation of superchannel switching over the C-band with a micro-ring resonator switch, where 6 comb tones were modulated with 10 Gbaud Nyquist QPSK signals and transmitted over 50 km [2]. Additionally, a second iteration of this prototype which included a simultaneous fine tuning of the FSR with the same microcontroller through a voltage controlled oscillator, has been used as a multiple local oscillator for parallel detection at the receiver [3] as part of an EU FP 7 Project. This is achieved by synchronizing the reconfigurable Gain Switched Optical Frequency Comb Source (GS-OFCS) centre wavelength and FSR with the corresponding parameters of the free-running transmitter comb to compensate for environmental drifts, which allows simultaneous detection of superchannels. The source has also been employed in a spectroscopy application [4] where the comb signal is passed through the gas hydrogen sulphide. The comb tones that overlap with the gas spectral components are absorbed by the gas, and thus the comb tone power gets attenuated and an absorption profile of the target gas can be deduced.

In Chapter 4, two novel techniques for bandwidth expansion of gain switched comb sources are investigated and experimentally demonstrated. Both configurations present expanded gain switched combs with low optical linewidth, excellent phase correlation and continuous central wavelength tunability within the C-band.

The first technique proposed entails the cascading of gain switched FP lasers externally injected by a single low linewidth Tunable Laser (TL). The expansion obtained using this scheme, with two cascaded FP laser diodes, results in 13 clearly resolved comb lines (doubling the bandwidth of the initial source) with a remarkable flatness of 3 dB. The comb tones exhibit strong phase correlation

and low optical linewidth of 80 kHz, transferred from the master laser. Continuous wavelength tunability within a range of 20 nm is also demonstrated. Moreover, the proposed method can be escalated, by cascading more FP lasers, and exhibits potential for integration which would reduce the footprint and power consumption.

The second technique developed stands out due to its simplicity but effective expansion. The configuration provides low complexity, with a low component count and power consumption, while delivering high spectral purity, flexibility, and a broadband comb spectrum. It comprises an externally injected and gain switched FP laser, where the optical injection takes place between two neighbouring FP longitudinal modes. The obtained expanded gain switched comb exhibits 6.25 GHz spaced comb tones spanning over 325 GHz with an OCNR exceeding 30 dB. This corresponds to 52 highly coherent comb tones (in a 6 dB spectral flatness) with good phase correlation and low optical linewidth of 300 kHz, transferred and only limited by the external injection employed. Moreover, continuous wavelength tunability over 30 nm is also demonstrated. However, the irregular flatness obtained may require equalisation techniques for coherent superchannel transmission.

Hence, these two expansion techniques clearly show a trade-off between complexity/power consumption and the obtained spectral flatness.

Photonic Integrated Circuits Testing and Characterization

A Indium Phosphide (InP) photonic integrated device for the generation of externally injected gain switched optical frequency combs is tested and characterized in detail in Chapter 5. The device is composed of two slotted single mode laser diodes with different cavity lengths and integrated in a master-slave configuration. The slave section is optically injected by the master section and simultaneously gain switched. The comb spectral enhancement due to the external optical injection is first demonstrated, with an increase in the 3 dB spectral flatness from 2 to 8 comb tones and 20 dB bandwidth from 62.5 to 94 GHz caused by an enhancement of the relaxation oscillation frequency. Thus, the generated 6.25 GHz gain switched comb presents 8 clearly resolved and highly coherent optical tones within 3 dB of spectral ripple, with an OCNR larger than 45 dB. The FSR tunability is ranging from 6 to 10 GHz by simply changing the Radio frequency (RF) sinewave frequency used to gain switch. The comb noise properties of the individual comb tones are also characterized. The measured averaged RIN (dc-6 GHz) of the selected comb tones was found to vary in the range of -122.5 to -129.3 dB/Hz. The phase noise is characterized by carrying out a detailed analysis of the

Frequency Modulated (FM)-noise spectrum. This analysis can provide more thorough information and understanding of the different noise processes contributing to the overall phase noise. The intrinsic optical linewidth of each comb tone was found to be 1.5 MHz and a significant excess *1/f* noise component at low frequencies (below 20 MHz) was presented. Finally, a high degree of phase correlation is characterized by a low 10 Hz RF beat tone linewidth.

A novel four-output monolithically integrated comb de-multiplexer has also been tested and its performance characterized in Chapter 5. The comb de-multiplexer is based on the optical injection locking of single mode lasers by individual comb tones. As such, each injection locked single mode laser selects an individual comb line and suppresses other comb tones by more than 37 dB. The four outputs are all mutually frequency locked and possess the same OCNR, phase noise properties and correlation as the input comb. Furthermore, the use of this de-multiplexer does not induce insertion losses that reduce the de-multiplexed comb tone power, avoiding the need for optical amplifiers.

Optical Transmission Systems Application

Finally, Chapter 5 verifies the feasibility of employing the integrated gain switched comb source in network scenarios through experimental transmissions. These entail, at the time of writing, the first demonstrations of a photonic integrated gain switched comb source in a four-level Pulse Amplitude Modulation (PAM), and in a Nyquist-QPSK optical transmission systems.

An experimental transmission of a 50 Gbit/s PAM-4 signal operating at 3.125-GBaud per channel and over 3 km of Standard Single Mode Fibre (SSMF) employing the integrated device is presented, for short-reach application as intra-datacentre links. The effect of RIN and OCNR on the system performance is investigated by examining the Bit Error Rate (BER) and receiver sensitivity of all channels, and compared to the performance of a low noise benchmark External Cavity Laser (ECL). All channels successfully performed below the 7% Forward Error Correction (FEC) limit and RIN and OCNR have been recognised as limiting parameters for the system performance as the measured BER tends to degrade for high channel number due to inferior OCNR and RIN. A 2 dB receiver sensitivity penalty between best and worst performing channels is found.

The integrated gain switched comb is also implemented in a Nyquist-QPSK system operating at 5-Gbaud per channel, with a total data rate of 80 Gbit/s and transmitted over 50 km of SSMF, suitable for medium-haul or inter-datacentre optical transmissions. The system performance was examined by measuring BER, and Error-Vector Magnitude (EVM) to study the influence of the device phase

noise. The constellation diagrams of all channels presented a slightly angular spread of the constellation points which is a distinct signature of phase noise. All received channels successfully exhibited a similar performance well below the 7% FEC limit.

The development and investigation presented in this thesis has successfully proved and strengthened the potential of gain switched comb sources to play a key role in future optical communication systems.

6.2 Future Work

The research in this thesis has shown the potential of gain switched comb sources for next generation optical networks. Potential future work in need of further investigation is now described:

• As discussed in Chapter 3, future networks may incorporate flexible features that facilitate network adaptability according to dynamic traffic conditions. This thesis has presented a software reconfigurable gain switched optical frequency comb that could be used in future flexible transponders thanks to its continuous flexibility in FSR and central wavelength that can be software controlled with system demand, and to the low RIN and phase noise that allows the encoding of amplitude and phase modulation formats alike. Future work would see a further development of this source towards a general sliceable bandwidth variable transponder architecture, which is a transponder able to dynamically tune the required optical bandwidth occupancy and slice it in a number of independent superchannels with different destinations.

A proposed architecture is illustrated in Figure 6.1. A similar software reconfigurable source as the one presented in Chapter 3 would form the main block in the multicarrier source. Additionally, an optional expansion block, which could consist of a phase modulator or cascaded lasers as proposed in Chapter 4, could be selected depending on the required number of carriers and the specification for power consumption. A filtering stage would follow to slice the overall bandwidth and to filter the individual carriers for independent modulation, which could be implemented by injection-locked de-multiplexers, proposed in Chapter 5, programmable filters, or micro-ring resonators. Finally, an array of I-Q modulators would need to be incorporated to allow various complex modulation formats to be encoded.

• Chapter 4 presented two techniques for expansion of GS-OFCS, while offering good flexibility and low noise properties. Future work could look at the study of these techniques through modelling in

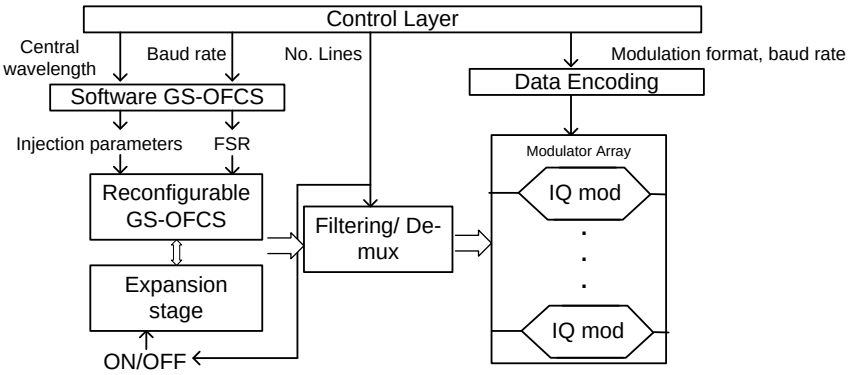

Figure 6.1: Proposed architecture for sliceable bandwidth variable transponder

VPI Transmission Maker and simulation of analytic/numerical modelling against which the output of the experiments could be compared. These simulations could study the cascading of more lasers, for the first technique, and the investigation of its limitations in terms of number of cascaded lasers, overall power consumption and achievable number of comb tones. For the second technique, further increment of the injected power and chirp in the laser to achieve injection in more than two FP longitudinal modes would be of interest as well as the increase of the cavity length which would result in a reduced spacing between longitudinal modes and better overlapping of the generated comb tones with enhanced flatness.

• Future design iterations of the integrated gain switched comb source presented in Chapter 5 could strive to achieve higher FSRs that would be more suitable for future optical transmission systems (i.e. 12.5 to 28 GHz). This could be accomplished through increasing the bandwidth of the slave section with a shorter slave gain cavity design, by reducing the wire-bond length and device parasitics, and improving the high speed submount while also increasing the number of lines through the monolithic integration of phase modulators or cascaded lasers.

Furthermore, wavelength tunability across the C-band would certainly improve the viability of this integrated source in practical systems. The current design allows a narrow-band wavelength tunability (of approximately 1 nm) that can be tuned with the bias in the slotted sections. The development of an integrated gain switched comb capable of full C-band wavelength tunability could be implemented using an array of Discrete Mode Laser Diodes (DMLD) that act as master tunable laser to injection lock a slave FP cavity, identical to the discrete component version presented in Chapter 3.

• In Chapter 5, two integrated devices have been characterized in detail for gain switched comb

generation and de-multiplexing. The logical next step is then the monolithic integration of both devices in a single chip to be employed in next generation optical transceivers. The device could also include electro-absorption modulators after each de-multiplexed carrier for independent data modulation. Another approach could entail hybrid integration to combine the InP integrated comb and de-multiplexer with Silicon-Organic Hybrid (SOH) modulators, which show ultra-low voltage drive requirements. These two integrated components could be then connected on-chip level, through photonic wirebonds to keep compactness.

• Potential future work could also be focused in other disciplines, that could benefit from the use of optical frequency combs and particularly, from the simplicity, compactness and ease and precise control of FSR of the gain switching technology, such as gas spectroscopy or sensing.

Dual optical frequency comb (Dual-OFC) architectures have recently attracted attention due to their wide broadband range, stability and measurement times. In Dual-OFC spectroscopy, two optical combs with slightly different FSRs are down converted (i.e. mapped) into the RF domain where they are detected and the information is quickly processed.

As illustrated in Figure 6.2, a single master laser could be used to injection lock two gain-switched lasers. As such, mutual phase correlation and frequency locking is achieved, and the mapped RF comb presents a frequency spacing corresponding to the optical FSRs difference. The combined optical frequency combs can traverse a gas cell filled with a specific target gas.

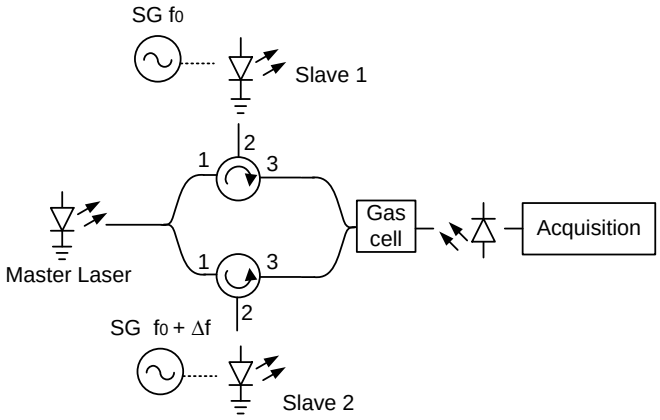

Figure 6.2: Dual optical frequency comb spectroscopy employing external injection and gain switching technologies

The absorption spectral profile caused by the gas is obtained by processing the amplitude of the data in the RF domain. Therefore, externally injected gain switched combs could bring significant advantages to this scheme, such as low component count and possibility of gas detection in a broad-

band wavelength range of the electromagnetic spectrum by selecting lasers to gain switch at the desired wavelengths.

The wavelength range around 2 μm is particularly attractive for gas sensing due to presence of strong absorption lines of many gas species, including atmospheric gases, e.g. nitrous oxide, carbon dioxide, acetone, and ammonia. Furthermore, this wavelength range is called “eye safe”, since laser radiation does not reach the retina, showing great potential for applications in free space. Hence, dual-OFC with gain switched comb sources around the 2 μm wavelength range could be investigated and examined in terms of accuracy, resolution, and measurement time. Furthermore, a prototype could be manufactured, characterised and tested.

References

[1] T. Shao, R. Zhou, V. Vujicic, M. D. Gutierrez Pascual, P. M. Anandarajah and L. P. Barry, "100 km coherent Nyquist ultradense wavelength division multiplexed passive optical network using a tunable gain-switched comb source," *IEEE/OSA Journal of Optical Communications and Networking*, vol. 8, no. 2, pp. 112–117, Feb. 2016.

[2] V. Vujicic, A. P. Anthur, A. Gazman, C. Browning, M. D. Gutierrez Pascual, Z. Zhu, K. Bergman, and L. P. Barry, "Software-Defined Silicon-Photonics-Based Metro Node for Spatial and Wavelength Superchannel Switching," *IEEE/OSA Journal of Optical Communications and Networking*, vol. 9, no. 5, pp. 342–350, May 2017.

[3] J. N. Kemal, J. Pfeifle, P. Marin-Palomo, M. D. Gutierrez Pascual, S. Wolf, F. Smyth, W. Freude, and C. Koos, "Multi-wavelength coherent transmission using an optical frequency comb as a local oscillator," *Optics Express*, vol. 24, no. 22, pp. 25432–25445, Oct. 2016.

[4] S. Chandran, S. Mahon, M. D. Gutierrez Pascual, J. Braddell, F. Smyth, and A. A. Ruth, "Cavity-enhanced absorption detection of H 2S in the near infra-red using a gain-switched frequency comb laser," 13th International Conference on Fiber Optics and Photonics, paper Th2C.5, Kanpur (India), Dec. 2016.

Appendix A

List of Publications

The following is the list of publications included in this work.

A.1 Refereed Journal Papers

M. Deseada Gutierrez Pascual, Rui Zhou, Frank Smyth, Prince M. Anandarajah, and Liam P. Barry, "Software reconfigurable highly flexible gain switched optical frequency comb source," *Optics Express*, vol. 23, pp. 23225-23235, August 2015.

M. Deseada Gutierrez Pascual, Vidak Vujicic, Jules Braddell, Frank Smyth, Prince M. Anandarajah, and Liam P. Barry, "InP photonic integrated externally injected gain switched optical frequency comb," *Optics Letters*, vol. 42, pp. 555-558, January 2017.

M. Deseada Gutierrez Pascual, Vidak Vujicic, Jules Braddell, Frank Smyth, Prince M. Anandarajah, and Liam P. Barry, "Photonic Integrated Gain Switched Optical Frequency Comb for Spectrally Efficient Optical Transmission Systems," *IEEE Photonics Journal*, vol. 9, no. 3, pp. 1-8, June 2017.

A.2 Refereed Conference Papers

M. Deseada Gutierrez Pascual, Prince M. Anandarajah, Rui Zhou, Frank Smyth, Sylwester Latkowski, and Liam. P. Barry, "Cascaded Fabry-Pérot lasers for coherent expansion of wavelength tunable gain switched comb," European Conference on Optical Communication (ECOC),

Cannes (France), paper Mo.3.4.4, September 2014.

M. Deseada Gutierrez Pascual, Rui Zhou, Frank Smyth, and Liam P. Barry, "Coherent Expansion of Gain Switched Optical Frequency Comb by Cascading Fabry-Pérot Lasers," Photonics Ireland, Cork (Ireland), September 2015.

M. Deseada Gutierrez Pascual, Rui Zhou, Frank Smyth, Tong Shao, Prince M. Anandarajah, and Liam P. Barry, "Dual mode injection locking of a Fabry-Pérot laser for tunable broadband gain switched comb generation," European Conference on Optical Communication (ECOC), Valencia (Spain), September 2015.

M. Deseada Gutierrez Pascual, Jules Braddell, Frank Smyth, and Liam P. Barry, "Monolithically integrated lasers for comb generation in bandwidth variable transponders," 18th European Conference on Integrated Optics (ECIO), ECIO-O-01, Warsaw (Poland), May 2016.

M. Deseada Gutierrez Pascual, Jules Braddell, Frank Smyth, and Liam P. Barry, "Monolithically Integrated 1x4 Comb De-multiplexer Based on Injection Locking," 18th European Conference on Integrated Optics (ECIO), ECIO-P-37, Warsaw (Poland), May 2016.

A.3 Other Publications Arisen from the PhD Research

A.3.1 Journal Papers

Tong Shao, Rui Zhou, **M. Deseada Gutierrez Pascual**, Prince M. Anandarajah and Liam P. Barry, "Integrated Gain Switched Comb Source for 100 Gb/s WDM-SSB-DD-OFDM System," *Journal of Lightwave Technology*, vol. 33, no. 17, pp. 3525–3532, Sept. 2015.

Rui Zhou, Tong Shao, **M. Deseada Gutierrez Pascual**, Frank Smyth and Liam P. Barry, "Injection Locked Wavelength De-Multiplexer for Optical Comb-Based Nyquist WDM System," *IEEE Photonics Technology Letters*, vol. 27, no. 24, pp. 2595–2598, Dec 2015.

Tong Shao, Rui Zhou, Vidak Vujicic, **M. Deseada Gutierrez Pascual**, Prince M. Anandarajah and Liam P. Barry, "100 km coherent Nyquist ultradense wavelength division multiplexed passive optical network using a tunable gain-switched comb source," *IEEE/OSA Journal of Optical Communications and Networking*, vol. 8, no. 2, pp. 112–117, Feb. 2016.

Tam N. Huynh, Regan Watts, Vidak Vujicic, **M. Deseada Gutierrez Pascual**, Cosimo Calo, Kamel Merghem, Vivek Panapakkam, Francois Lelarge, Anthony Martinez, Badr-Eddine Benkelfat, Abderrahim Ramdane, and Liam P. Barry, "200-Gb/s Baudrate-Pilot-Aided QPSK/Direct Detection With Single-Section Quantum-Well Mode-Locked Laser," *IEEE Photonics Journal*, vol. 8, no. 2, pp. 1–7, April 2016.

Rui Zhou, **M. Deseada Gutierrez Pascual**, Prince M. Anandarajah, Tong Shao, Frank Smyth, and Liam P. Barry, "Flexible wavelength de-multiplexer for elastic optical networking," *Optics Letters*, vol. 41, no. 10, pp. 2241–2244, May 2016.

Juned N. Kemal, Joerg Pfeifle, Pablo Marin-Palomo, **M. Deseada Gutierrez Pascual**, Stefan Wolf, Frank Smyth, Wolfgang Freude, and Christian Koos, "Multi-wavelength coherent transmission using an optical frequency comb as a local oscillator," *Optics Express*, vol. 24, no. 22, pp. 25432–25445, Oct. 2016.

Vidak Vujicic, Aravind P. Anthur, Alexander Gazman, Colm Browning, **M. Deseada Gutierrez Pascual**, Ziyi Zhu, Keren Bergman, and Liam P. Barry, "Software-Defined Silicon-Photonics-Based Metro Node for Spatial and Wavelength Superchannel Switching," *IEEE/OSA Journal of Optical Communications and Networking*, vol. 9, no. 5, pp. 342–350, May 2017.

A.3.2 Conference Papers

Prince M. Anandarajah, Rui Zhou, Robert Maher, **M. Deseada Gutierrez Pascual**, Frank Smyth, Vidak Vujicic, and Liam P. Barry, "Flexible Optical Comb Source for Super Channel Systems," in Optical Fiber Communication Conference/National Fiber Optic Engineers Conference (OFC/NFOEC), paper OTh3I.8, Anaheim, CA, March 2013.

Prince M. Anandarajah, Rui Zhou, Robert Maher, **M. Deseada Gutierrez Pascual**, Frank Smyth, Vidak Vujicic, and Liam P. Barry, "Injection locked lasers for flexible optical comb sources," in 15th International Conference on Transparent Optical Networks (ICTON), pp. 1-2, Cartagena (Spain), July 2013.

Rui Zhou, Prince M. Anandarajah, **M. Deseada Gutierrez Pascual**, John O'Carroll, Richard Phelan, Brian Kelly, and Liam P. Barry, "Monolithically Integrated 2-Section Lasers for Injection Locked Gain Switched Comb Generation," in Optical Fiber Communication Conference (OFC),

paper Th3A.3, San Francisco, CA, March 2014.

Prince M. Anandarajah, Rui Zhou, Vidak Vujicic, **M. Deseada Gutierrez Pascual**, Eamonn Martin, and Liam P. Barry, "Long Reach UDWDM PON with SCM-QPSK Modulation and Direct Detection," in Optical Fiber Communication Conference (OFC), paper W2A.42, San Francisco, CA, March 2014.

Prince M. Anandarajah, Rui Zhou, Vidak Vujicic, **M. Deseada Gutierrez Pascual**, Liam P. Barry, "Multi-Carrier Transmitters in Next Generation Access Networks," in Applications of Optics and Photonics (AOP), Mo.1.A, Aveiro (Portugal), May 2014.

Prince M. Anandarajah, Rui Zhou, Vidak Vujicic, **M. Deseada Gutierrez Pascual**, Robert Maher, Domanic Lavery, Milen Paskov, Benn Thomsen, Seb Savory, and Liam P. Barry, "Long reach UDWDM PON with direct and coherent detection," in 16th International Conference on Transparent Optical Networks (ICTON), pp. 1-1, Graz (Austria), July 2014.

Tam N. Huynh, Vidak Vujicic, **M. Deseada Gutierrez Pascual**, Prince M. Anandarajah, and Liam P. Barry, "Digital Coherent Communications With a 1550 nm VCSEL," in Optical Fiber Communication Conference (OFC), paper M2D.7, Los Angeles, CA, March 2015.

Prince M. Anandarajah, Tong Shao, Rui Zhou, **M. Deseada Gutierrez Pascual**, and Liam P. Barry, "100Gb/s WDM-SSB-DD-OFDM using a Gain Switched Monolithically Integrated Passive Feedback Comb Source," in Conference on Lasers and Electro-Optics (CLEO): Science and Innovations 2015, paper SF2K.1, San Jose, CA, May 2015.

Prince M. Anandarajah, **M. Deseada Gutierrez Pascual**, Tong Shao, Rui Zhou, Vidak Vujicic, Frank Smyth, and Liam P. Barry, "Reconfigurable optical frequency comb and its applications," in 17th International Conference on Transparent Optical Networks (ICTON), pp. 1-1, Budapest (Hungary), July 2015.

Juned N. Kemal, Joerg Pfeifle, Pablo Marin-Palomo, **M. Deseada Gutierrez Pascual**, Stefan Wolf, Frank Smyth, Wolfgang Freude, and Christian Koos, "Parallel multi-wavelength intradyne reception using an optical frequency comb as a local oscillator," in European Conference on Optical Communication (ECOC), pp. 1-3Valencia (Spain), September 2015.

Aleksandra Kaszubowska, Luis Jacobo Alvarez Ruiz de Ojeda, **M. Deseada Gutierrez Pascual**,

Christian Blumm, Jules Bradell, Frank Smyth, and Prince M. Anandarajah, “Flexible optical networking employing integrated frequency combs,” 18th International Conference on Transparent Optical Networks (ICTON), pp. 1-1, Trento (Italy), July 2016.

Satheesh Chandran, Stephen Mahon, **M. Deseada Gutierrez Pascual**, Jules Braddell, Frank Smyth, and Albert A. Ruth, “Cavity-enhanced absorption detection of H 2S in the near infra-red using a gain-switched frequency comb laser,” 13th International Conference on Fiber Optics and Photonics, paper Th2C.5, Kanpur (India), December 2016.

Yanni Ou, Fanchao Meng, Prince M. Anandarajah, Shuangyi Yan, Alejandro Aguado, **M. Deseada Gutierrez Pascual**, Reza Nejabati, and Dimitra E. Simeonidou, “Investigation of Optical Impacts on Virtualization using SDN-enabled Transceiver and Optical Monitoring,” in Optical Fiber Communication Conference (OFC), paper Th1J.5, Los Angeles, CA, March 2017.

Mohammad Al-Khateeb, Mary E. McCarthy, **M. Deseada Gutierrez Pascual**, Frank Smyth, Andrew D. Ellis, “Optimization of Parametric Comb Generation Using Interferometric Wavelength Selective Switch,” in Conference on Lasers and Electro-Optics (CLEO), paper JW2A, San Jose, CA, May 2017.

Appendix B

Turn-on dynamics of semiconductor lasers

The dynamic behaviour of a semiconductor laser is given by a set of non-linear rate equations, which define the relationship between carrier and photon densities inside a laser cavity. The basic rate equations for a single mode laser can be written as:

$$\frac{\partial N}{\partial t} = \frac{I(t)}{eV} - \frac{N}{\tau_e} - g(N - N_0)S \tag{B.1}$$

$$\frac{\partial S}{\partial t} = \Big[g(N - N_0) - \frac{1}{\tau_p}\Big]S + \beta\frac{N}{\tau_e} \tag{B.2}$$

where N is the carrier density, $I(t)$ is the time dependent injected bias current, e is the electron charge, V is the volume of the laser active region, τ_e, denotes the carrier lifetime, g is the gain constant, N_0 is the carrier density at transparency, S is the photon density, τ_p is the photon lifetime and β is the spontaneous emission coupling factor.

The dynamics involved during the turn-on of a semiconductor laser diode are here considered, where a step current $I(t)$ is applied and, consequently, the carrier and photon densities can be considered to be disturbed around their steady state value, which is mathematically described as:

$$N = \bar{N} + \delta N \tag{B.3}$$

$$S = \bar{S} + \delta S \tag{B.4}$$

where $\bar{N}$ and $\bar{S}$ are the steady state values, and δN and δS are the transient perturbations around the steady states for the carrier and photon densities, respectively. Substituting these expressions in the rate equations B.1 and B.2, neglecting second order terms (ie. $\delta N \delta S$) and assuming that the

spontaneous emission is negligible:

$$\frac{\partial(\bar{N}+\delta N(t))}{\partial t} = \frac{I}{eV} - g(\bar{N}+\delta N(t)-N_0)(\bar{S}+\delta S(t)) - (\frac{\bar{N}+\delta N(t)}{\tau_e}) \tag{B.5}$$

$$\frac{\partial(\bar{S}+\delta S(t))}{\partial t} = g(\bar{N}+\delta N(t)-N_0)(\bar{S}+\delta S(t)) - (\frac{\bar{S}+\delta S(t)}{\tau_p}) \tag{B.6}$$

As the semiconductor laser is turned on, biased above threshold reaches the steady state with a small perturbation around it:

$$\frac{\partial \bar{N}}{dt} = \frac{I(t)}{eV} - \frac{\bar{N}}{\tau_e} - g(\bar{N}-N_0)S = 0 \tag{B.7}$$

$$\frac{\partial \bar{S}}{\partial t} = \Big[g(\bar{N}-N_0) - \frac{1}{\tau_p}\Big]\bar{S} = 0 \tag{B.8}$$

Taking into account equations B.7, B.8, and neglecting the second order terms (i.e. $\delta N(t)\delta S(t)$):

$$\frac{d(\delta N)}{dt} = -\delta N(g\bar{S}+\frac{1}{\tau_e}) - g(\bar{N}-N_0)\delta S \tag{B.9}$$

$$\frac{d(\delta S)}{dt} = g(\bar{N}-N_0)\delta S - \frac{\delta S}{\tau_p} + g\delta N\bar{S} \tag{B.10}$$

Additionally, the threshold condition can be obtained from equation B.2:

$$\frac{\partial \bar{S}}{\partial t} = \Big[g(\bar{N}-N_0) - \frac{1}{\tau_p}\Big]\bar{S} = 0 \tag{B.11}$$

$$g(\bar{N}-N_0)\bar{S} - \frac{1}{\tau_p}\bar{S} = 0 \tag{B.12}$$

$$g(\bar{N}-N_0) = \frac{1}{\tau_p} \tag{B.13}$$

By substituting B.13 in B.9 and B.10:

$$\frac{\partial(\delta N)}{\partial t} = -\delta N(g\bar{S}+\frac{1}{\tau_e}) - \frac{\delta S}{\tau_p} \tag{B.14}$$

$$\frac{\partial(\delta S)}{\partial t} = \delta N g\bar{S} \tag{B.15}$$

The transient response of the photon density can be obtained by differentiating B.15 with respect to time, and substituting $\frac{\partial(\delta N)}{\partial t}$ with the expression in 2.8 and δN with $\delta N = \frac{\partial(\delta S)}{\partial t}\frac{1}{g\bar{S}}$ from B.15.

$$\frac{\partial^2\delta S}{\partial t^2} + \frac{\partial \delta S}{\partial t}(g\bar{S}+\frac{1}{\tau_e}) + \frac{\delta S}{\tau_p}g\bar{S} = 0 \tag{B.16}$$